ALPHA FOUNDATION FOR THE IMPROVEMENT OF MINE SAFETY AND HEALTH

Final Technical Report

Project Title: A practical, mechanics based approach to pillar design

Grant Number: AFC719-15

Organization: West Virginia University, Morgantown, WV

Principal Investigator: Ihsan Berk Tulu, PhD
Department of Mining Engineering
Benjamin M. Statler College of Engineering and Mineral Resources
West Virginia University
395 Evansdale Drive| PO Box 6070
Morgantown, WV 26506-6070
P: (304)293-3883 | Fax: (304)293-2307
E-mail: **itulu@mail.wvu.edu**

Graduate Students: Deniz Tuncay (Ph.D. Student)
Haochen Zhao (Ph.D. Student)

Period of Performance: July 1, 2018 - December 31, 2019

Acknowledgement/Disclaimer: Final Report must include the following disclaimer language: "This study was sponsored by the Alpha Foundation for the Improvement of Mine Safety and Health, Inc. (ALPHA FOUNDATION). The views, opinions and recommendations expressed herein are solely those of the authors and do not imply any endorsement by the ALPHA FOUNDATION, its Directors and staff."

1.0 Executive Summary:

Traditional pillar stability analysis methods; Analysis of Longwall Pillar Stability (ALPS) and Analysis of Retreat Mine Pillar Stability (ARMPS) use simple geometric conceptualizations/simplications like "tributary area theory", "pressure arch theory" and "abutment angle theory" to calculate overburden loading. "The pressure arch theory" has been implemented into the ARMPS program to recognize the inherently greater stability of narrow panels at depth. Although the pressure arch loading approach indirectly accounts for the generally stiffer overburden response of narrow and deep panels, the actual mechanics of the overburden and the effects of the pillar system on the overburden response are not included in these computations. The recent ARMPS-LAM program developed at West Virginia University (WVU) was an initial step towards incorporating mechanistic overburden behavior into pillar design. However, the overburden in this original version of the program was automatically calibrated to simulate the loading assumptions of ALPS and ARMPS. The objective of this research is to develop a practical approach for quantifying overburden loading that incorporates the mechanical response, specific geology and structural competence of the overburden, and the in situ stresses.

This objective was accomplished by the analysis of a database of 40 field monitoring case studies using two different methods. The first method was the displacement-discontinuity (DD) variation of the boundary element method (BEM), LaModel. The second method was the finite volume method (FVM), Fast Lagrangian Analysis of Continua (FLAC3D). After case history analysis and parametric runs, results were analyzed statistically to develop relationships between overburden stiffness, panel depth-to-width ratio and overburden loading.

The research presented in this report has produced a number of significant results that will undoubtedly raise the quality of mine design in the United States in the future, particularly for deep cover, pillar retreat and longwall mines. Analysis of the large database of field measurements with analytical laminated overburden and FVM modeling approaches produced the following abutment angle equation for the mines deeper than 650 ft:

Overburden Depth (H) / Panel Width (PW)	*Abutment Angle (deg.)*
H/PW ≤ 1.66	21°
H/PW > 1.66	$\beta = 34.51 \times \left(\frac{H}{PW}\right)^{-0.96}$

The ARMPS-LAM program developed at WVU was used as the practical mechanical overburden tool and the new abutment angle equation was programmed into ARMPS-LAM. 215 deep cover cases from the ARMPS database were used to conduct a detailed comparison between ARMPS2010 and ARMPS-LAM. The results of this comparison show that the new loading equation with ARMPS-LAM improves the successful classification accuracy by 19%.

The research presented in this report also offers a rational explanation for the lower abutment angles (compared to default 21^0) observed in mines deeper than 650 ft and with overburden depth-to-panel-width ratio larger than 1.66. Remnant structures (gob, barrier pillars or gateroad pillar systems) of prior panels provide considerable support to the response of the overburden strata in deep mines. Support provided by remnant structures of the prior panels keep the percentage of overburden loads transferred to the abutments of the active panel constant when the depth to panel width ratio is larger than a threshold value (in this study, the threshold value is estimated as 1.66).

Findings of this research also indicates the importance of the size of the barrier pillars on global stability during the design of deep panels, as Mark (2010) suggested previously. However, results of this study also implies that it is possible to develop safe and economical panel design by including support provided by remnant structures of the prior panels into the design of deep cover panels rather than only increasing the barrier pillar sizes. Finally, the practical design tool and methods developed during this research are immediately available to the mining industry, Mine Safety and Health Administration (MSHA) and National Institute for Occupational Safety and Health (NIOSH) to evaluate and consider for application in ground control analysis process.

2.0 Problem Statement and Objective:

This project focuses on underground coal mining industry and addresses the Topical Area "*Health and Safety Interventions*" with a specific emphasis on Alpha Foundation Priority Area Ground Control - *Prevention of unstable ground conditions that result in collapses, ventilation disruption, and miner entrapment; roof and rib falls; and injuries due to insufficient support coverage*. Despite the major progress in reducing ground control related fatalities and injuries in the US underground mining sector, fall of ground related accidents are still one of the major causes of the fatalities and injuries. According to MSHA, between 2013 and 2018, fall of ground related accidents caused 28.2% of the occupational fatalities in underground mines. In the same time period, 1,082 of the 9,249 nonfatal lost-time injuries were due to fall of ground accidents (MSHA, 2019).

Past and recent research has suggested that very little attention is being paid to specific overburden mechanics and its' interaction with pillar system (van der Merwe, 2006; Esterhuizen et al., 2010; Frith and Reed 2017). Frith and Reed (2017) stated that current state-of-the-art pillar design methods ignore the overburden mechanics and use estimated dead-weight of overburden to compute pillar sizes. In the USA and around the World, overburden loading is typically estimated by simple geometric rules, while the specific overburden mechanics, structural competence of the overburden strata, specific geology, in situ stresses and overburden/pillar interactions are typically ignored. However, these important mechanical factors affect the stability of the mine pillars and openings; and therefore, the mine safety. National Institute for Occupational Safety and Health (NIOSH) research conducted after the Crandall Canyon mine disaster (Esterhuizen et al., 2010) showed that small panel width-to-depth ratios and stiff-strong overburden result in a reduction of the observed pillar loads, much smaller than tributary area theory estimate. In fact, as a response to the Crandall Canyon disaster, Mark (2010) implemented a pressure arch loading approach (Figure 1) into the latest ARMPS program to recognize the inherently greater stability of narrow panels at depth. Although the pressure arch loading approach indirectly accounts for the generally stiffer overburden response of narrow and deep panels, it doesn't include the effect of specific geology on the specific mechanics of the overburden. The recent ARMPS-LAM program developed at WVU was an initial step towards incorporating mechanistic overburden behavior into pillar design. However, the overburden in this original version of the program was calibrated to simulate the loading assumptions used in the traditional pillar stability analysis methods.

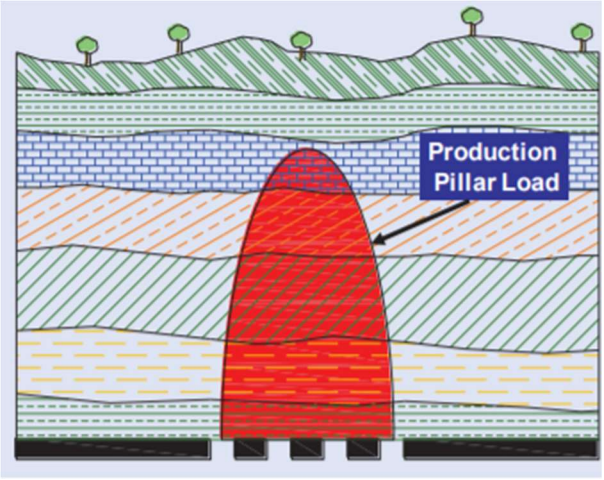

Figure 1. Pressure arch loading concept (after, Mark, 2010).

The objective of this research was to develop a practical approach for quantifying overburden loading that incorporates the mechanical response, specific geology and structural competence of the overburden, and the in situ stresses. Specific aims were to: (i) understand how the critical parameters (overburden geology, structural competence of overburden and in situ stresses) affect the overburden stiffness, stability and overburden/pillar interactions; and (ii) develop a practical mechanics-based approach to determine the optimal ARMPS-LAM structural input given the geology, in situ horizontal stresses and overburden competence.

3.0 Research Approach:

The complex behavior of the sedimentary overburden strata during the mining of the coal seam is affected by the physiographic province of the mine, geologic formation of the seam, in situ stress state of the formation and operational parameters of the mine (mining height, panel width, depth, pillar design etc.), and can change drastically from one coal basin to another. Surface to seam extensometers might provide direct measurement on relative movements of the overburden strata in one dimension, but widespread spatial and temporal measurements of relative movements and stress changes aren't practical, economical or perhaps possible. Therefore, it is fair to state that there isn't any cost-effective method to directly measure or observe complex overburden behavior, but surface subsidence, and near seam deformation and stress measurements are presently the best sources to interpret the mechanical response of the overburden indirectly. The research strategy followed in this project consisted of (i) a fundamental research phase that aimed to understand the mechanism of how the response of overburden is affected by changing geological and operational parameters; (ii) an applied research phase that aims to translate the knowledge gained from the first phase to a practical approach that can be directly transferred to the design tools available to the US underground coal mining industry.

The fundamental research phase consisted of database development, model development and analysis tasks. During the database development task, a field monitoring database with a total of 40 case histories from 40 mines was developed. Cases in the database were categorized into three datasets based on available information. The first dataset consists of 12 longwall mine case histories that have the full side abutment measurements and geological logs from 11 different mines (10 Australian and 1 US mines). The second dataset consists of 12 cases from 12 different US longwall mines that have either stress measurements, subsidence measurements or both, along with detailed geological logs, overburden maps, mine maps and other operational parameters. The third dataset consists of 18 supplementary cases from 6 US and 12 Australian mines that only have the magnitude of the measured loads and basic operational parameters. During the model development task, two different methods were developed for the analysis of the datasets based on the available information. The first method was an analytical method derived from the fundamental equations of the laminated overburden model. The second method was finite volume analysis (FVM) with a systematic procedure to estimate the model's mechanical inputs. During the analysis task, the analytical laminated overburden method was used to back calculate the magnitude of the loads transferred to the abutments for the first dataset with 10 AU and 1 US mines; and the FVM used to study the mechanical response of the overburden for the 12 US mines from the second dataset.

The analytical laminated overburden method is used to analyze first dataset (with 10 AU and 1 US cases) due to the nature of the available information for each case in this dataset. Heasley recommended two different methods for calibrating the overburden stiffness and gob stiffness for best simulating stress distribution (Heasley et al, 2010) or best simulating surface subsidence (Jian and Heasley, 2016) accurately. In addition, the laminated overburden model simulates realistic flexibility for stratified sedimentary geologies very efficiently with two overburden stiffness input parameters: elastic modulus and lamination thickness. Therefore, the laminated overburden model only requires stress profile measurements and not the detailed mechanical properties of the geological layers or subsidence profile for load analysis. Since the first data set consists of case studies with only abutment stress measurements and limited information about the mechanical properties of the geologic layers, the laminated overburden method is used to analyze this set.

The FVM modeling methodology detailed in *section 3.2.2* works best when detailed overburden geology and mechanical properties of layers are known. In addition, verification of the method requires both subsidence and stress measurements (or at least one is measured and other should be predicted reliably). Cases in the first dataset don't have sufficient required information to use FVM approach reliably, but the second dataset has detailed geologic information is suitable to use the FVM modeling methodology.

The applied research phase included the development of practical loading models based on the laminated overburden model to allow rapid calculation of overburden load distributions for the specific geologic input without the need to conduct a full finite-difference numerical model analyses. Complex rock mass response was approximated by simplified relationships developed from the statistical analysis of field monitoring case histories

and the controlled numerical model experiments. The new loading models were implemented into ARMPS-LAM and the accuracy and effectiveness was tested with case studies from ARMPS database. The specific research tasks are described in more detail in the following sections.

3.1 Task 1: Database development

The geologic formation of the coal seam plays an important role in the design of a mine, and mines in the same physiographic and geologic province tend to have similar panel designs. The complex response of the sedimentary overburden strata to mining in the same geological formations is generally similar, but affected from the changes in topography and operational parameters (mining height, panel width, overburden depth and pillar design etc.) at the mine. Therefore, the true understanding of the mechanism of overburden response to mining requires the study of this complex response under a variety of loading, operational and most importantly geologic conditions as encountered by operating mines. In this task, we focused on developing a database of field monitoring cases from mines operating in different physiographic provinces and different geological formations.

Each case study in the database was characterized based on local geology, structural competence of overburden, in-situ stress and panel depth-to-width ratio. The following methodologies were used to characterize each case studies:

a) *Overburden geology* was characterized based on seam, geologic formation, and physiographic province.
b) *Overburden competence* was characterized based on the percent of hardrock in the overburden. The same approach used in Surface Deformation Prediction System (SDPS) was used to compute percent of hard rock. In SDPS, the percentage of hardrock is defined as the sum of the strong rocks (e.g., sandstone, limestone), having minimum thickness of 5ft (Agioutantis and Karmis, 2017). Available mechanical property tests, Ferm numbers and/or geologic definitions of the rock layers (detailed on the geologic log) were used to define a hardrock.
c) *In-situ stresses* were characterized based on the regional tectonic horizontal stress and overburden depth of the case study mine.
d) *Panel depth-to-width* ratio and its' impact on overburden response was characterized based on the mine geometry and subsidence profile of the case study mine (subcritical, critical or supercritical).

3.1.1 Australian mine sites

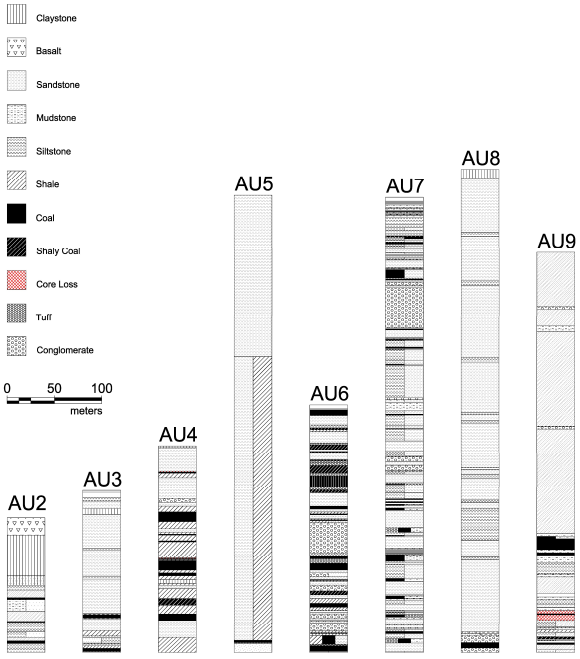

Figure 2. Generalized stratigraphic column representation of the Australian mines.

In the first dataset there are 10 cases from different Australian longwall mines. Geologic core logs were available for 8 of the mines and more information on the geology was gathered from confidential consulting reports. Figure 2 shows the generalized stratigraphic columns of the case study sites, where enough information was present about the geology. Layers with more than one rock type represent interbedded or intermixed components, but the percentages may vary. Also, thick layers do not necessarily represent massive rock formations. Adjacent thin layers of the same rock types were combined for easier representation.

Available core logs and descriptions of the geologies from the reports were used to determine the hard rock percentage (HR) of the overlying strata for each case. Hard rock percentage is calculated considering the total thickness of hard rock (sandstone and limestone) layers that are more than 5 ft thick from the core log (Agioutantis and Karmis, 2017). The HR is the ratio of the length of hard rock core that is longer than 5 ft to the total length of the core log above the coal seam. This methodology for defining the hard rock percentage was originally developed by Agioutantis and Karmis (2017) and used successfully in predicting subsidence magnitude and profile for U.S. coal mines. The list of the case studies with the mine geometries and available geologic information can be found in the Appendices section 9.1.1. Table 1 shows the summary of the cases.

Table 1. Summary of mine geometries for the Australian cases.

Case	***Depth (ft)***	***Panel Width (ft)***	***Seam Thickness (ft)***	***Entry Width (ft)***	***HR%***	***Depth / Panel Width***
AU-1	*870*	*673*	*8.2*	*16.7*	-	1.29
AU-2	*410*	*920*	*11.8*	*16.4*	*48%*	0.45
AU-3	*427*	*673*	*10.2*	*17.0*	*57%*	0.63
AU-4	*590*	*444*	*10.5*	*16.4*	*33%*	1.33
AU-5	*1,560*	*673*	*8.2*	*15.7*	*71%*	2.32
AU-6	*787*	*492*	*21.3*	*16.0*	*23%*	1.60
AU-7	*1,330*	*820*	*8.2*	*17.0*	*21%*	1.62
AU-8a	*1,683*	*745*	*18.0*	*16.4*	*72%*	2.26
AU-8b	*1,673*	*778*	*18.0*	*20.0*	*95%*	2.15
AU-9	*1,197*	*820*	*22.0*	*16.4*	*61%*	1.46

3.1.2 Appalachian basin mine sites

The Appalachian case study mines are in the Northernand Central Appalachian basins (Figure 3). In the database, there are 7 cases from 6 Northern Appalachian basin mines and 4 cases from 3 Central Appalachian basin mines.

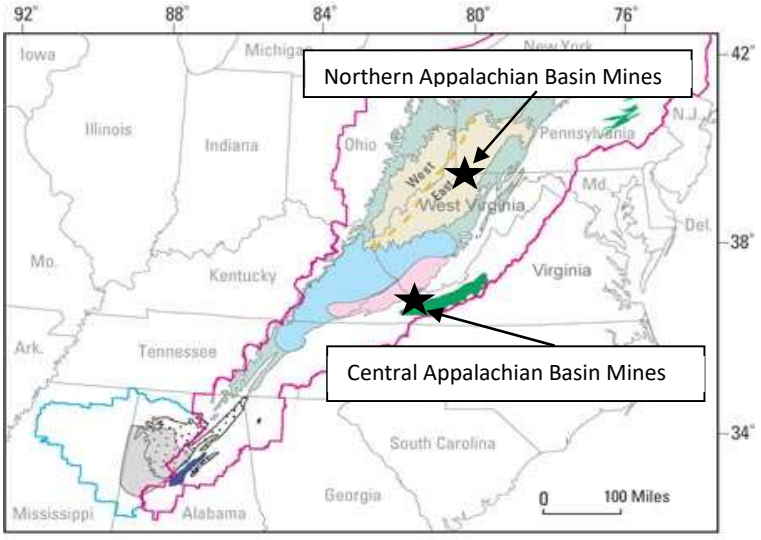

Figure 3. Locations of the studied mines from Appalachian Basin (modified from USGS, 2004).

Geologic core logs were available for all of the mines and more information on the geology was gathered from confidential reports available to the PI. Figure 4 shows the generalized stratigraphic columns of the Northern Appalachian case study sites. The list of the case studies with the mine geometries and available geologic information can be found in the Appendices section 9.1.2, and Table 2 show the summary of the Northern Appalachian cases.

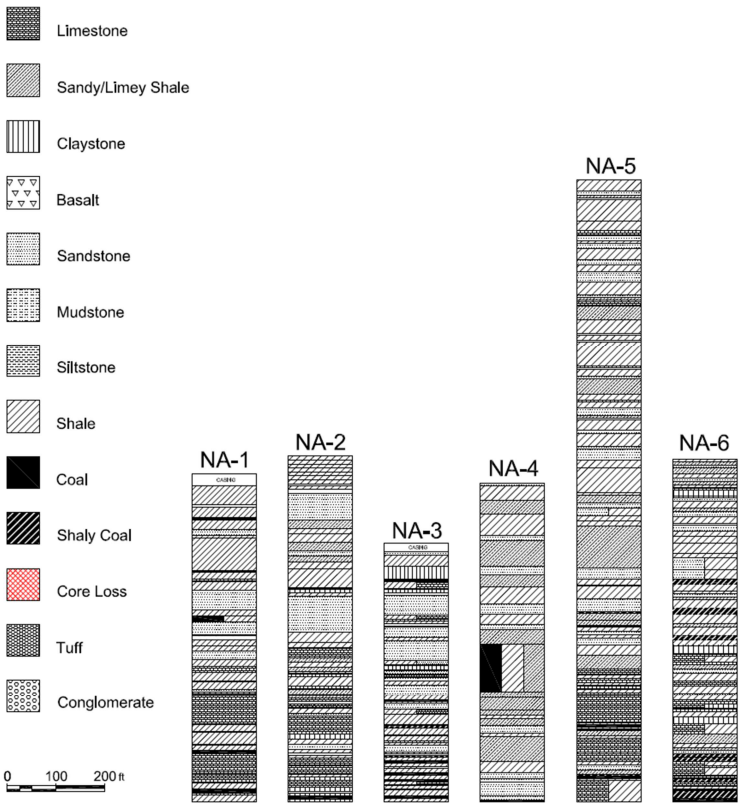

Figure 4. Generalized stratigraphic column representation of the Northern Appalachian mines.

Table 2. Summary of case study characterization for the Northern Appalachian longwall mines.

Case	***Seam Name***	***Seam Height (ft)***	***Geologic Formation***	***HR%***	***In situ Stress Region***	***Depth / Panel Width***
NA-1	*Pittsburgh*	*6.5 ft.*	*Pittsburgh*	*Case 1: 37%* *Case 2: 25%*	*Eastern U.S., Northern Appalachia*	*Case 1: 0.48* *Case 2: 0.91*
NA-2	*Pittsburgh*	*7.5 ft.*	*Pittsburgh*	*42%*	*Eastern U.S., Northern Appalachia*	*0.60*
NA-3	*Middle Kittaning*	*7ft.*	*Allegheny*	*28%*	*Eastern U.S., Northern Appalachia*	*0.44*
NA-4	*Lower Kittaning*	*7ft.*	*Allegheny*	*22%*	*Eastern U.S., Northern Appalachia*	*1.10*
NA-5	*Pittsburgh*	*7 ft.*	*Pittsburgh*	*25%*	*Eastern U.S., Northern Appalachia*	*1.22*
NA-6	*Pittsburgh*	*6.5 ft.*	*Pittsburgh*	*28%*	*Eastern U.S., Northern Appalachia*	*0.69*

Figure 5 shows the generalized stratigraphic columns of the Central Appalachian case study mines. The list of the case studies with the mine geometries and available geologic information can be found in the Appendices section 9.1.2, and Table 3 show the summary of the Central Appalachian cases.

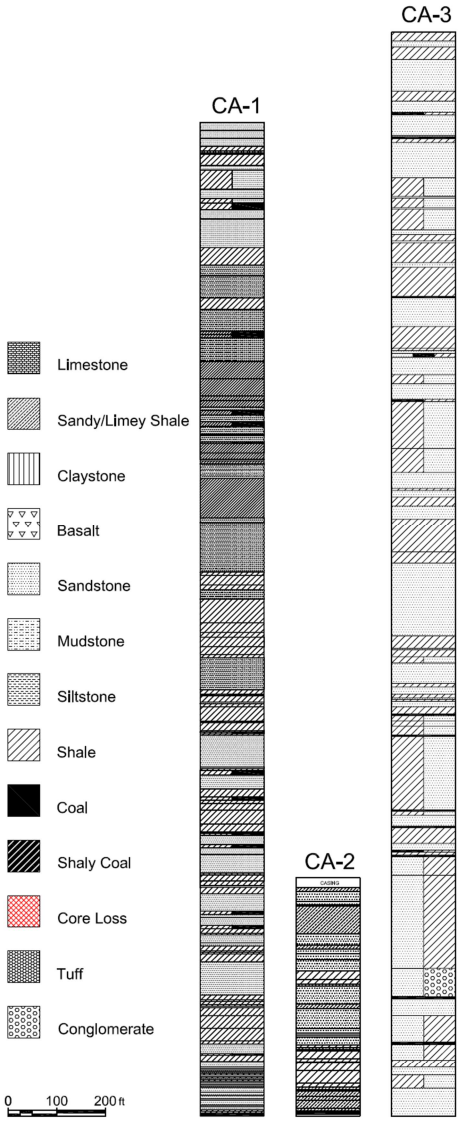

Figure 5. Generalized stratigraphic column representation of the Central Appalachian mines.

Table 3. Summary of case study characterization for the Central Appalachian longwall mines.

MINE CODE	***Seam Name***	***Seam Height (ft)***	***Geologic Formation***	***HR%***	***In situ Stress Region***	***Depth / Panel Width***
CA-1	*Pocahontas No.3*	*5.5 ft.*	*Pocahontas*	*Case 1: 48% Case 2: 46%*	*Eastern U.S., Central App.*	*Case 1: 2.94 Case 2: 1.82*
CA-2	*Pocahontas No.3*	*4.2 ft.*	*Pocahontas*	*53%*	*Eastern U.S., Central App.*	*0.61*
CA-3	*Pocahontas No.3*	*5.5 ft.*	*Pocahontas*	*32%*	*Eastern U.S., Central App.*	*3.45*

3.1.3 Black Warrior basin mine site

There is only one mine from Black Warrior Basin in Southern Appalachia and its location is shown in Figure 6. Figure 7 shows the generalized stratigraphic columns of the case study mine. Mine BW-1 is a moderately deep mine with average overburden depth of 1450 ft and panel width of 1000 ft. Overburden HR percentage is around 32%. The case study with the mine geometry and available geologic information can be found in the Appendices section 9.1.2.

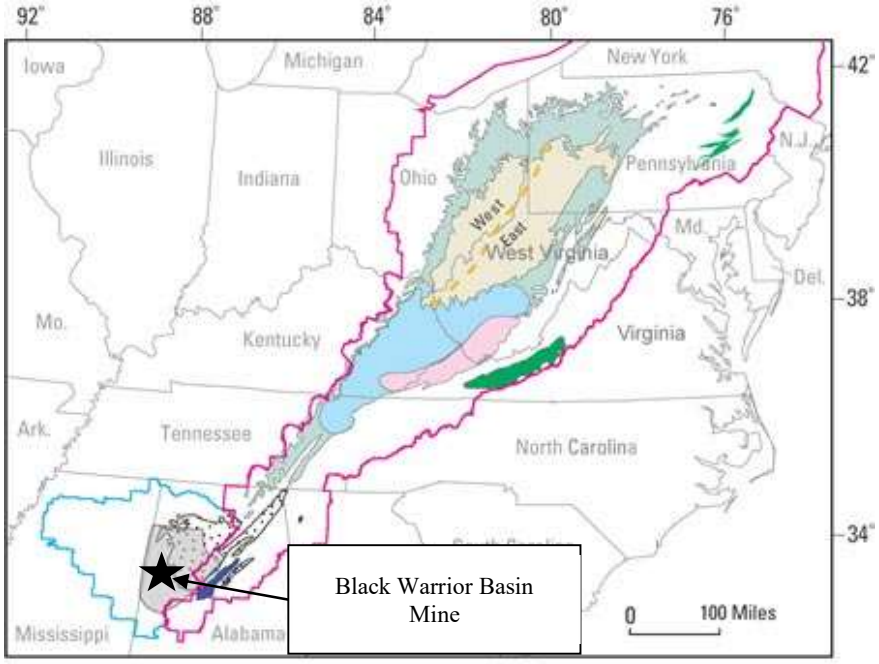

Figure 6. Locations of the studied mine from Black Warrior Basin (modified from USGS, 2004).

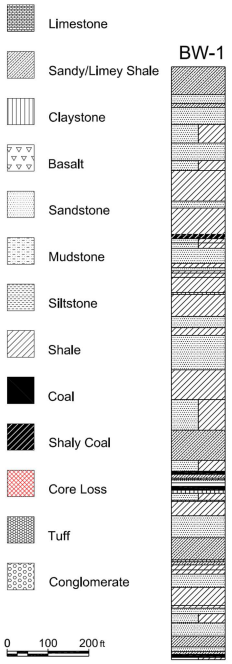

Figure 7. Generalized stratigraphic column representation of the Black Warrior Basin mine.

3.1.4 Western US mine sites

The Western US case study mines are in the coalfields of Utah and Colorado. In the database, there are 3 cases from 2 Utah mines and 1 case from a Colorado mine. Figure 8 shows the location of the mines.

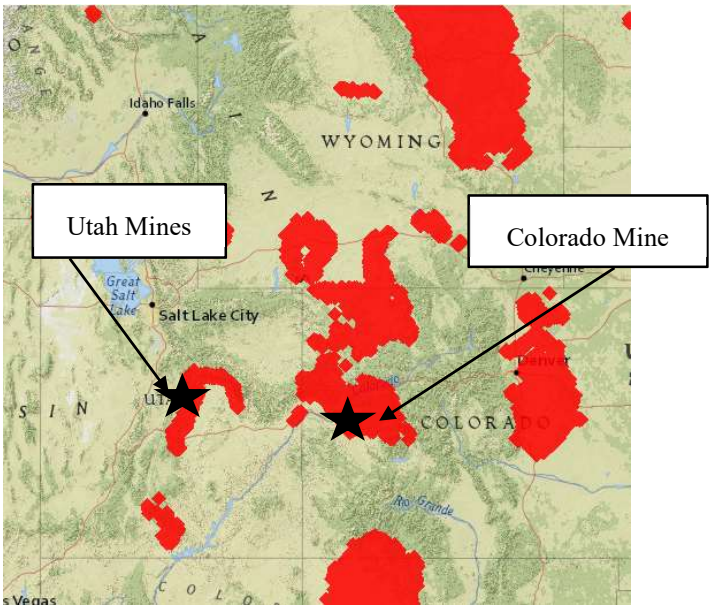

Figure 8. Locations of the studied mines from Western US (USGS, 2020)

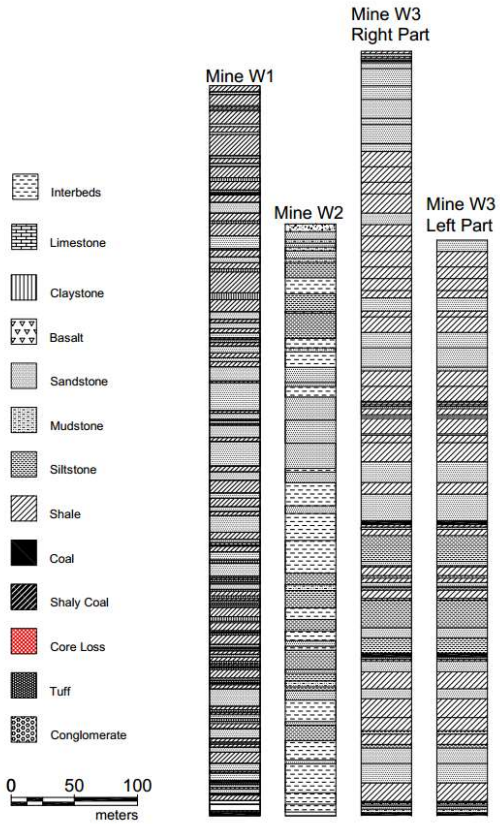

Figure 9. Generalized stratigraphic columns representation of the Western US mines.

Figure 9 shows the generalized stratigraphic columns of the Western US case study sites. The list of the case studies with the mine geometries and available geologic information can be found in the Appendices section 9.1.2, and Table 4 show the summary of the western USA cases.

Table 4. Summary of case study characterization for the Western USA mines.

Mine Name	***Seam Name***	***Seam Height (ft)***	***Overburden Competence (% of HR)***	***In situ Stress Region***	***Depth / Panel Width***
W1	*Hiawatha*	*8 ft.*	*44%*	*Western U.S. (Utah)*	*2.38*
W2	*Blind Canyon*	*10 ft.*	*44%*	*Western U.S. (Utah)*	*3.23*
W3	*D coal seam*	*10 ft.*	*Case W3-L: 49%* *Case W3-R: 49%*	*Western U.S. (Colorado)*	*Case W3-L: 1.89* *Case W3-R: 2.38*

3.1.4 Supplementary cases

In addition to Australian and the US cases detailed above, there are 18 supplementary cases where only the total side abutment load was known and not the exact stress profile or geological information. These cases were used during the analysis stage to help the development of the loading models. Table 5 shows the summary of the supplementary cases used in this project. Abutment angles listed in Table 5 are taken from Mark (1992) and Colwell et al. (1999).

Table 5. Supplementary field measurement data (Mark, 1992; Colwell et al., 1999).

Case	***Depth of Cover (ft)***	***Panel Width (ft)***	***Mining Height (ft)***	***Entry Width (ft)***	***Pillar Width(ft) (c-c)***	***Location***	***Abutment Angle (Deg.)***
D-1	*760*	*1,000*	*5.0*	*18*	*60, 60*	*US*	*18*
A-2	*520*	*470*	*6.5*	*16*	*50, 110*	*US*	*25*
E-3	*630*	*500*	*11.0*	*18*	*90, 90*	*US*	*20*
B-2	*650*	*600*	*6.5*	*18*	*63, 63*	*US*	*23*
B-3	*600*	*600*	*6.5*	*18*	*98, 38*	*US*	*10*
B-4	*455*	*600*	*6.5*	*18*	*98, 76*	*US*	*19*
AU-11	*853*	*676*	*8.0*	*16*	*115*	*AU*	*5*
AU-12	*476*	*656*	*8.0*	*16*	*82*	*AU*	*25*
AU-13	*525*	*640*	*10.0*	*16*	*82*	*AU*	*35*
AU-14	*1,312*	*492*	*10.0*	*16*	*246, 82*	*AU*	*18*
AU-15	*1,312*	*492*	*10.0*	*16*	*82*	*AU*	*10*
AU-16	*427*	*656*	*10.0*	*16*	*82*	*AU*	*45*
AU-17	*558*	*837*	*11.0*	*16*	*82*	*AU*	*29*
AU-18	*525*	*656*	*10.0*	*16*	*82*	*AU*	*33*
AU-19	*1,181*	*344*	*9.0*	*16*	*217*	*AU*	*9*
AU-20	*1,476*	*466*	*9.0*	*16*	*92, 43*	*AU*	*6*
AU-21	*853*	*738*	*8.0*	*16*	*79*	*AU*	*5*
AU-22	*591*	*640*	*10.0*	*16*	*98*	*AU*	*8*

3.2 Task 2: Model development

In this task, we developed the methods to analyze the detailed case history database. Case studies in the database were divided into three datasets based on the available information. The first dataset consisted of 12 cases from 10 AU and 1 US longwall mines with only abutment stress measurements and geological logs with rough information. The second dataset consisted of 12 cases from 12 US longwall mines with very detailed measurements, geologic and operational parameters. The third dataset consists of the 18 supplementary cases with solely geometry and measured abutment loading.

Two different methods were developed for the analysis of these datasets. The first method is an analytical method derived from the fundamental equations of the laminated overburden model (Heasley, 1998). The second method is a finite volume method (FVM) with a systematic procedure to estimate the model's mechanical inputs (Tulu et al., 2018).

3.2.1 Analytical laminated overburden model

Figure 10 shows a sample stress profile plotted using the measured values from one of the Australian cases in Table 1. The figure represents the stress change profile of a two-entry system where the measurements are taken from the pillars and the adjacent solid coal. The area L_A represents the abutment load on the gateroad pillar, and the area L_B represents the abutment load on the adjacent solid coal. The areas L_A and L_B were numerically calculated by integrating the load under the curve. Tulu and Heasley (2012) have explained the back-calculation method for the laminated overburden stress distribution approach in detail, and the same procedure is used for calculating the abutment loads in this study.

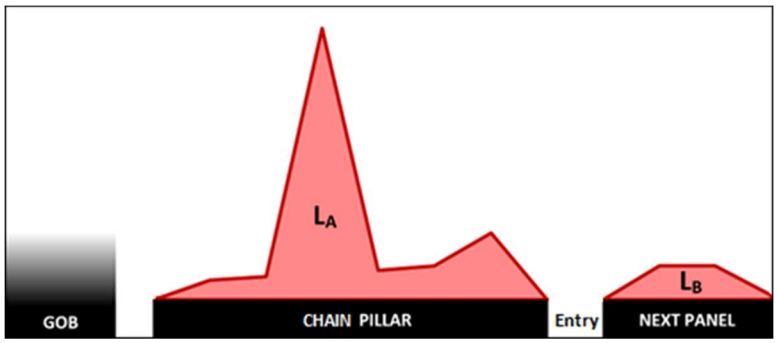

Figure 10. Sample stress profile from a two-entry Australian mine.

For the laminated overburden stress distribution approach, Equation 1 gives the abutment stress magnitude (σ_1) as a function of the distance from the panel rib (x) (Heasley, 1998).

$$\sigma_1(x)=q\frac{P}{2}\sqrt{\frac{2E_s}{E\lambda h}}e^{-\sqrt{\frac{2E_s}{E\lambda h}}x} \quad (1)$$

where;

σ_1 = the abutment stress magnitude.

q = the in situ stress.

P = the width of the panel.

E_s = the elastic modulus of the seam.

E = the elastic modulus of the overburden.

λ = a parameter of the laminated model.

h = the seam thickness.

x = distance from the panel rib.

In this equation, the in situ stress (q) is determined as:

$$q = \gamma H \quad (2)$$

where:

γ = the overburden density.

H = the seam depth.

and

$$\lambda = \frac{t}{\sqrt{12(1-\upsilon^2)}} \tag{3}$$

where:

t = lamination thickness (During this study, it is calculated as proposed by Heasley et al. (2010)).

υ = Poisson's Ratio of the rock mass.

The percentage of the total measured load on the abutment pillar (n) for the two entry gate road in Equation 4 is calculated from the stress measurements as:

$$n = \frac{L_A}{L_A + L_B} \tag{4}$$

To determine the lamination thickness which gives the same load percentage (n) of the side abutment load as measured in the field, first, the stress defined by the Equation 1 is integrated over the x_1 distance to calculate the load on abutment pillar (see Equation 5).

$$L_A = \int_0^{x_1} \sigma_l(x)dx = -mq\frac{p}{2}\left(e^{-\sqrt{\frac{2E_S}{E\lambda h}}x_1} - 1\right) \tag{5}$$

Second, Equation 1 is also integrated over the x_2 distance to calculate the total abutment load on the abutment pillar and solid coal (see Equation 6).

$$L_A + L_B = \int_0^{x_2} \sigma_l(x)dx = -mq\frac{p}{2}\left(e^{-\sqrt{\frac{2E_S}{E\lambda h}}x_2} - 1\right) \tag{6}$$

Then the percentage of the abutment load on the abutment pillar can be determined by dividing Equation 5 by Equation 6 as:

$$n = \frac{-mq\frac{p}{2}\left(e^{-\sqrt{\frac{2E_S}{E\lambda h}}x_1} - 1\right)}{-mq\frac{p}{2}\left(e^{-\sqrt{\frac{2E_S}{E\lambda h}}x_2} - 1\right)} \tag{7}$$

Simplifying, and substituting back in for λ, we get:

$$0 = ne^{-\sqrt{\frac{2E_S\sqrt{12(1-\upsilon^2)}}{Eht}}x_2} - e^{-\sqrt{\frac{2E_S\sqrt{12(1-\upsilon^2)}}{Eht}}x_1} - n + 1 \tag{8}$$

In order to back calculate the observed abutment angle, the ratio of the total abutment load over the total panel load (qp/2) needs to be known. This ratio can be estimated by looking at the measured load on pillar A (L_A) versus the amount of load on pillar A without any gob loading (see Equation 9).

$$m = -\frac{L_A}{q\frac{p}{2}\left(e^{-\sqrt{\frac{2E_S}{E\lambda h}}x_1} - 1\right)} \tag{9}$$

Finally, the value of the abutment angle can be back calculated from the ratio "m" according to the subcritical or supercritical panel formulas.

3.2.2 Finite Volume Method

Overburden stiffness, stability and overburden/pillar interactions are affected by many parameters such as overburden geology, structural competence of overburden, in situ stresses and extraction geometry. The relative importance of each of these parameters needs to be understood to develop a true understanding of the overburden mechanics on pillar design. The critical parameters affecting overburden stiffness and stability were investigated by the analysis of field monitoring case studies with well calibrated numerical models building on a recently developed modeling approach (Tulu et al., 2018). In this approach, a systematic procedure is used to estimate the model's mechanical inputs.

Pillar Strength Modeling: The coal is modeled with a Hoek-Brown coal model based on the model developed in 2010 at NIOSH by (Esterhuizen et al., 2010) with the following updated input parameters:

Bulk modulus	: 290,000 psi
Shear Modulus	: 174,045 psi
m-value	:1.47 (residual: 1.17)
s-value	:0.07 (residual: 0.03)
a-value	:0.67
Interface friction angle	:20°
Interface cohesion	:54 psi
Interface tensile strength	:0.0
Interface normal stiffness	:4.42 10^6 psi/ft
Interface shear stiffness	:2.21 10^6 psi/ft

The peak pillar strengths simulated by the numerical models are compared with the empirical Bieniawski pillar strength equation in Figure 11. The results show good agreement between the model calculations and the empirical equation.

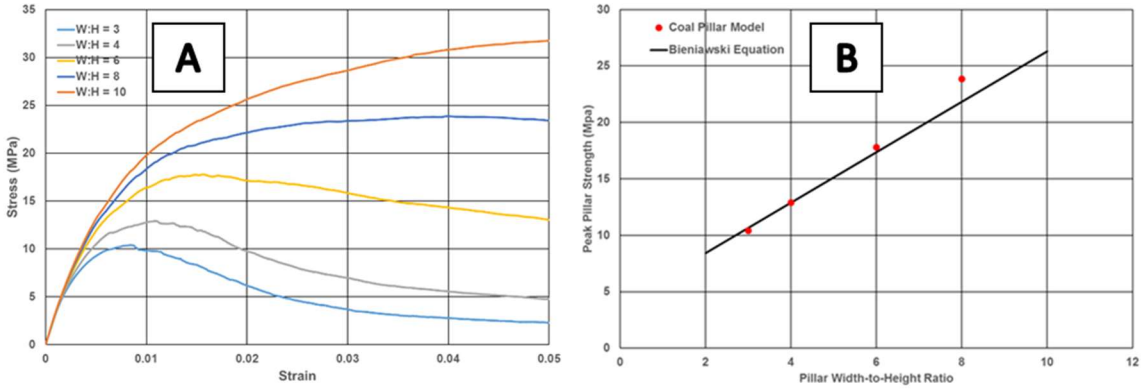

Figure. 11. a) Stress-strain curves, b) Pillar strength results calculated by the model.

Gob Response Modeling: As indicated by Pappas and Mark (1993) laboratory tests on shale and sandstone fragments showed that the stress strain response of caved material should follow a strain hardening curve. Pappas and Mark (1993) used the hyperbolic function derived by Salamon (1990) to fit test results, and they found that this function sufficiently simulates the strain-hardening gob response.

$$\sigma = \frac{a \times \varepsilon}{b - \varepsilon} \tag{10}$$

where:

σ = vertical gob stress (psi).

ε = vertical gob strain.

b = maximum strain parameter related to void ratio.

a = gob stress (psi) where ε = b/2.

In this project, the gob represents only the caved material and excludes fractured rock above the caved zone. Based on the above discussions and the calibration of the gob response curve with subsidence data, the gob parameters proposed by Esterhuizen et al. (2010) were modified by assuming the gob was formed under an initial bulking factor of 1.5, which represents a maximum strain of 33% and a caving height equal to three times the mining height measured from the floor. This approach also provides reasonable estimates of the subsidence. Two types of gob parameters are suggested for strong overburden and weak overburden. Figure 12 shows the stress-strain behavior of these two gob types and a comparison to the tests results of Pappas and Mark (1993). Table 6 shows the gob parameters for these two curves. In the model, strain-hardening gob behavior is simulated by updating the elastic modulus of each zone with the expected tangent modulus. The expected tangent modulus can be calculated by taking the derivative of Equation 10 with respect to vertical strain. This task is performed by using the FISH option of the FLAC3D software.

Table 6. Input parameters for Gob material model.

Rock Type	***a (psi)***	***b***
Weak	*435*	*0.33*
Strong	*1,305*	*0.33*

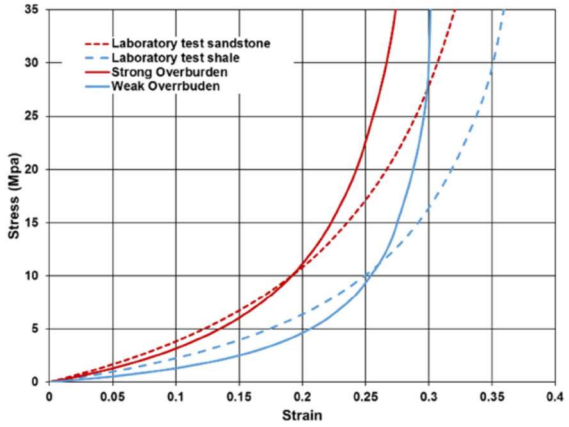

Figure. 12. Stress-strain behavior of the Gob.

Overburden strata rock properties: In 2010, Esterhuizen et al. (2010) published suggested overburden rock parameters to be used in large-scale models. Those parameters were later modified by Tulu et al. (2018) and presented in Table 7. The UCS values in Table 7 are laboratory scale values, and the field UCS values are estimated by reducing the laboratory scale value to 58% (Esterhuizen et al., 2010; Hoek and Brown, 1980).

For sandstone and shale, the elastic modulus (E) is estimated from Equation 11, and for limestone, the elastic modulus is estimated from Equation 12. These equations were driven from the regression analysis of a large number of UCS tests. In Equation 11 and 12, the *UCS* is the laboratory scale value in psi and the resultant elastic modulus is in also psi.

$$E = 0.143 \times UCS + 893.43 \quad (11)$$

$$E = 0.1162 \times UCS + 2210.4 \quad (12)$$

The friction angles are determined from the database of tri-axial tests (Esterhuizen et al., 2010). The friction values are also assumed to be the same in the laboratory and field scales. The cohesion values listed in Table 7 are field scale values and calculated by using Equation 13.

$$C = \frac{UCS_{field} \times (1 - \mathrm{Sin}(\emptyset))}{2 \times Cos(\emptyset)} \quad (13)$$

Where;

C = field scale cohesion.

ϕ = friction angle.

Table 7. Suggested rockmass input properties.

	UCS$_{lab}$ (psi)	***E (psi)***	***Friction Angle (°)***	***Cohesion (psi)***	***Tensile Strength (psi)***
Limestone	20,305	4,570,147	42	2,622	1,178
	14,504	3,895,721	42	1,872	841
	11,603	3,559,233	40	1,569	673
Sandstone	17,405	3,382,286	42	2,247	1,009
	14,504	2,967,477	40	1,961	841
	11,603	2,552,669	37	1,678	673
	8,702	2,137,860	35	1,314	505
	5,802	1,723,051	30	9,72	336
Shale	11,603	2,552,669	32	1,865	673
	8,702	2,137,860	30	1,458	505
	5,802	1,723,051	25	1,072	336
	4,351	1,515,647	20	883	252
	2,901	1,308,243	20	589	168
	1,450	1,100,838	20	294	84
	725	99,7861	20	148	42

Bedding strength parameters summarized in Table 8 were derived by Esterhuizen et al. (2010). Bedding tensile strength was set to 10% of the field-scale UCS. Esterhuizen et al. (2010) indicated that bedding friction angles may seem to be small compared to small-scale laboratory strength tests, but the presence of weak clay materials, especially in the shale beds, can have a significant impact on the overall shear resistance of a bedding plane. The matrix cohesion and tensile strength decreased from their peak values given in Table 7 to a residual value of 10% of peak over 5 millistrains of plastic strain (Zipf, 2007). The matrix friction angle remains constant at the values shown in Table 7. The stress-strain behavior of the bedding planes is assumed to be elastic perfectly plastic.

Table 8. Suggested bedding strength input properties.

	UCS$_{lab}$ (psi)	***Cohesion (psi)***	***Friction Angle (°)***	***Tensile Strength (psi)***
Limestone	*20,305*	*1374*	*32*	*117*
	14,504	*1095*	*30*	*84*
	11,603	*972*	*28*	*67*
Sandstone	*17,405*	*1176*	*30*	*102*
	14,504	*980*	*30*	*84*
	11,603	*876*	*27*	*67*
	8,702	*657*	*25*	*51*
	5,802	*486*	*20*	*33*
Shale	*11,603*	*429*	*10*	*67*
	8,702	*354*	*7*	*51*
	5,802	*258*	*7*	*33*
	4,351	*73*	*7*	*25*
	2,901	*43*	*5*	*17*
	1,450	*29*	*5*	*9*
	725	*14*	*5*	*4*

3.3 Task 3: Analysis of case history databases with two different methods

3.3.1 Analysis of first dataset with a*nalytical laminated overburden model*

ALPS and ARMPS programs utilize the abutment angle concept for the abutment stress calculations. The abutment angle (β) is used to calculate the magnitude of abutment loading adjacent to a gob area. It considers an angle between the vertical plane and the panel roof in order to calculate the transferred load to the abutments when the panel is mined (Figure 13). If the total area above the mined-out panel is considered as the total load to be transferred, the hatched areas in Figure 13 constitutes the load that is transferred to the side and the remaining load is carried by the gob. The total load to be transferred is calculated using as the dead weight of the overburden directly above the mined-out panel. Mark (1992) analyzed the abutment stress measurements collected from five different mines and concluded that an average abutment angle of 21° would yield a conservative estimate of the side abutment load, and implemented 21° as a default value to ALPS and ARMPS.

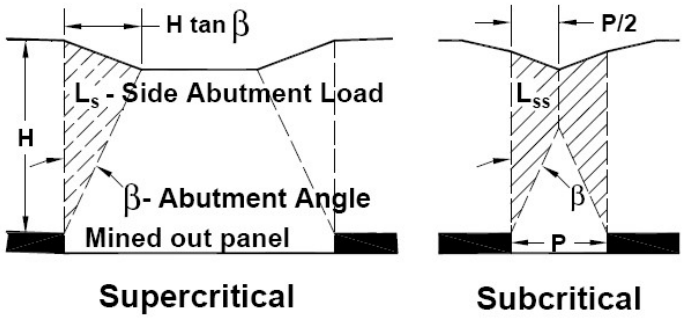

Figure 13. Abutment angle concept (Mark, 1992.)

The abutment angles were back calculated by using the analytical laminated overburden method discussed in section 3.2.1 from the first dataset of the database. Results of the back calculated abutment angles can be seen in Table 9. The results of these calculations for deeper mines do not match the average 21° abutment angle used in ALPS and ARMPS programs.

Table 9. Back calculated abutment angles

Case	*Abutment Angle*	*Overburden Depth (ft)*	*Panel Width (ft)*
AU-1	*23.39*	*870*	*673*
AU-2	*19.30*	*410*	*920*
AU-3	*17.24*	*427*	*673*
AU-4	*16.03*	*590*	*444*
AU-5	*6.33*	*1,560*	*673*
AU-6	*11.79*	*787*	*492*
AU-7	*12.48*	*1,330*	*820*
AU-8a	*13.62*	*1,683*	*745*
AU-8b	*8.85*	*1,673*	*778*
AU-9	*10.00*	*1,197*	*820*
US-1a	*9.51*	*1,950*	*640*
US-2b	*8.74*	*2,050*	*600*

3.3.2 Analysis of second dataset with Finite Volume *Method (FVM)*

In Section 3.2.2, we described the FVM that uses a systematic methodology to compute input parameters for overburden, pillar and gob material-models to simulate mining induced overburden loads and deformations. In this task, we used the FVM to carry out analysis of the 12 US cases in the second dataset to study the mechanism of the overburden response under variable overburden geologies, in situ stresses and panel designs. Analysis of each case study was performed in three steps. First, stresses and deformations approximated by the FVM were compared with

the field measurements; then loads transferred to the abutments, chain pillars, gobs and barrier pillars were computed; and finally overburden ground response curve was computed.

FVM Model Development: For each case, the mine scale FVM analysis was conducted on a two-dimensional cross-section of the instrumented sections of the mine. Model geometry for each mine was developed from actual stratigraphy, using all the geological layers with a minimum layer thickness of 1 ft, from a core hole near by the instrumented sections. Stress-strain behavior of the overburden strata was modelled with strain-softening ubiquitous-joint material, pillars were modeled with Hoek-Brown material and gob was modeled with strain-hardening material, and input parameters for each material model were assigned by the systematic procedure explained in section 3.2.2 of this report.

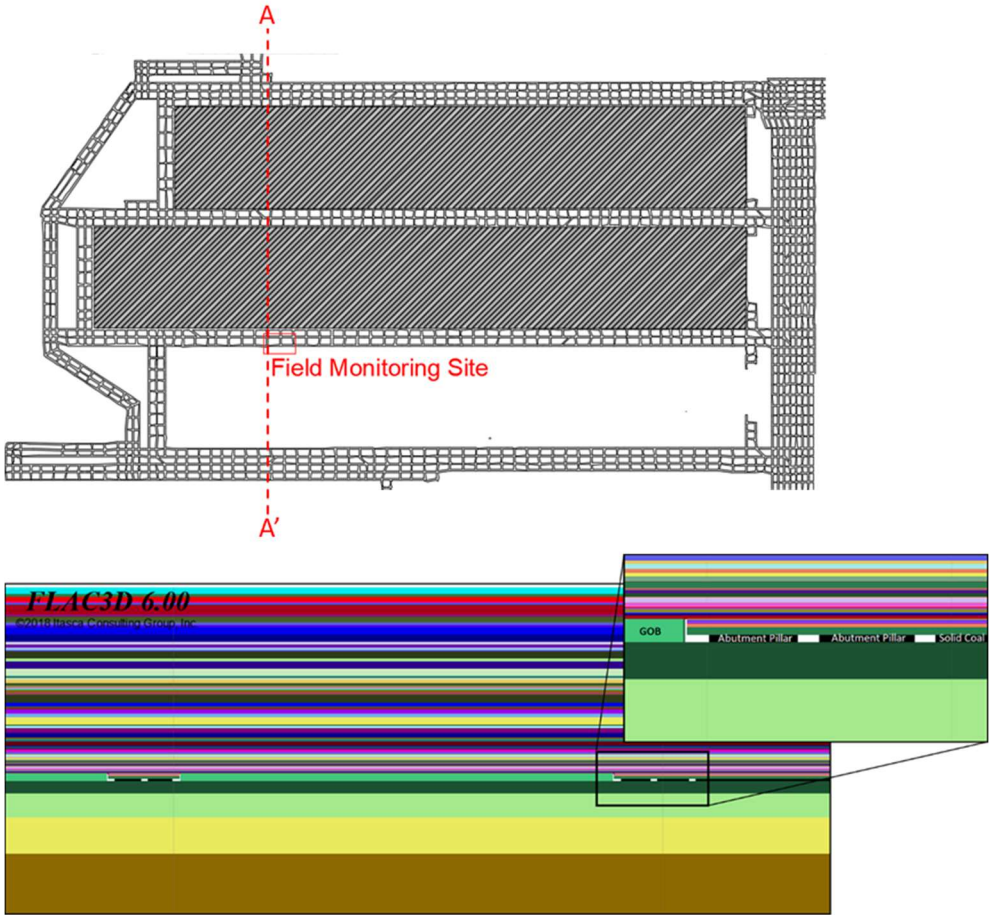

Figure 14. FVM model geometry for mine NA-3.

After grid generation and material model assignment, each model was solved in successive loading stages simulating different face positions relative to the instrumented site. For all the cases, the first stage was simply the development-mining scenario when all the entries in the model were mined. The consecutive stages for each case were determined uniquely to simulate the influence of the consecutive panel mining on instrumented sections. Figure 14 and Figure 15 show two of the field measurement case studies from Northern and Central Appalachia, and model geometries used to approximate these cases. Mine NA-3 (Figure 14) is a shallow mine with typical overburden depth of 520 ft and panel width of 1200 ft. To simulate the subsidence and mining induced stress distribution, cross-section AA' was approximated with the FVM model geometry shown in Figure 14, and total of 100 layers were modeled including the seam level and the bottom filler layers, resulting in 860,000 total number of elements. Three mining steps were simulated for Mine NA-3; development, Panel-2 mining and Panel-3 mining. Since the Panel-1 is more than 1300 ft away from the instrumented portions, influence of Panel-1 mining on measurements is negligible. Mine CA-3 (Figure 15) is a deep mine with overburden depth of 2085 ft and panel

width of 600 ft. Cross-section BB' was approximated with the FVM model geometry shown n Figure 15, and total of 142 layers were modeled including the seam level and the bottom filler layers, resulting in almost 1 million total number of elements. Since CA-3 is a deep mine with relatively strong overburden and narrow panels, surface deformation and mining induced stresses were influenced up to five consecutive panel mining. Therefore, six mining steps were simulated for CA-3 mine case.

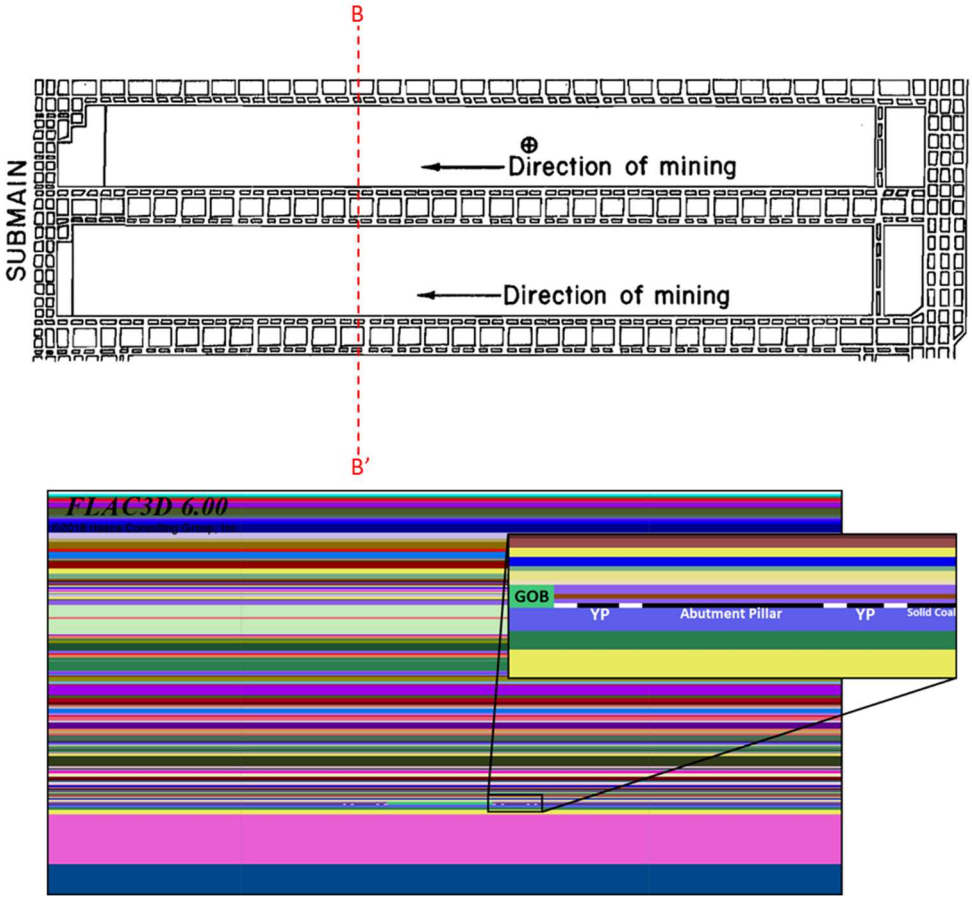

Figure 15. FVM model geometry for Mine CA-3.

FVM Model Results and Verification with Field Monitoring: After each case study mine model was solved, stresses and displacements computed by the model at the instrument locations were queried and compared with the field monitoring results, initially for model verification. Figure 16 shows the surface subsidence approximated by the model and measured in the field for the mine NA-3. The model approximated maximum subsidence of the first panel to be 3.85 ft compared to the measurements of 3.84 – 3.93 ft.

Figure 17 shows the abutment stress distribution approximated by the FVM model and measured by the Borehole Pressure Cells (BPC) for case study mine NA-3. The model computed the vertical stresses within 2%-10% of the field values. Although there are inconsistencies between the measured and modeled stresses, the general trend is similar and within reasonable accuracy. Some of the variations could be accounted for the installation of the instrumentation, local coal composition/strength and calibration errors. Section 9.2 (*in Appendices*) of this report summarizes the verification of FVM models for all the other case study mines in the database.

After the model verification stage, overburden load distributions computed by FVM and ALPS/ARMPS were compared. Then, mechanical response of the overburden was investigated by the ground response curve approach (GRC). Finally, parametric studies were performed to study the effect of changing panel depth-to-width ratio on standard loading parameters and mechanical response of the overburden.

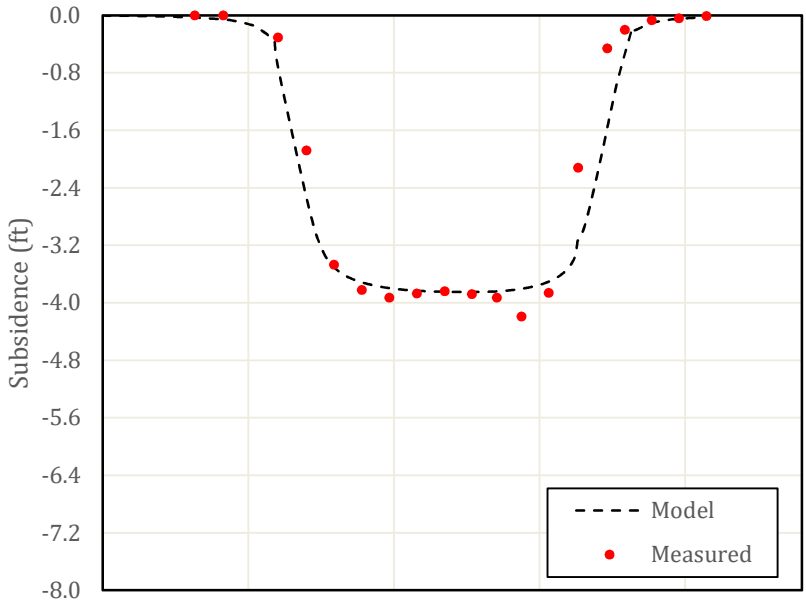

Figure 16. Comparison of modeled and measured surface subsidence for Mine NA-3.

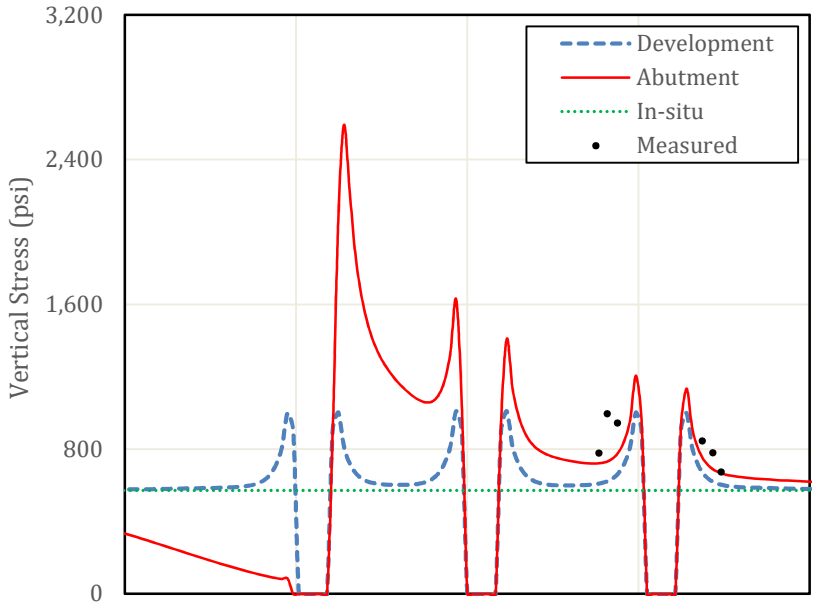

Figure 17. Comparison of the modeled and measured stresses in the abutment pillars for Mine NA-3.

Mining induced load distribution: ALPS and ARMPS use simple geometric conceptualizations like "tributary area theory", "pressure arch theory" and "abutment angle theory" to estimate mining induced load distribution. In this section, mining induced load distributions were back calculated for each case study by using the FVM, and results were compared with the values estimated by the traditional methods.

Extent of the abutment zone: The ALPS and ARMPS programs assume that abutment extent is proportional to the square root of overburden depth (H, in feet), Equation 14 (Peng, 2008) calculates extent (D, in feet) of the abutment zone and Equation 15 calculates extent of 90% ($D_{0.9}$, in feet) of total abutment load zone from the edge of the panel.

$$D = 9.3\sqrt{H} \tag{14}$$

$$D_{0.9} = 5\sqrt{H} \tag{15}$$

Mark (1992) implemented a square decay stress function (Equation 16) to represent load distribution curve in ALPS and ARMPS as a function of abutment extent. Where, "Ls" is total side abutment load, "D" is the extent of abutment (from Equation 14) and "x" is distance from the center of the entry that is adjacent to gob (Mark, 1992).

$$\sigma_a(x) = \frac{3L_s}{D^3}(D - x)^2 \tag{16}$$

Both FVM method and LaModel approximate mining induced load distributions based on solution of governing equations of mechanics, and assigned input parameters. Heasley et al. (2010) also used Equation 15 to calibrate the rockmass lamination thickness in Equation 3 so that 90% of the total abutment load falls into the $D_{0.9}$ distance as calculated by the Equation 16. The best way to assess the impact of the difference between abutment extents calculated by FVM, LaModel and ALPS under deep cover is by comparing the stress distributions of all three methods with field measurements from one of the deep case study mines.

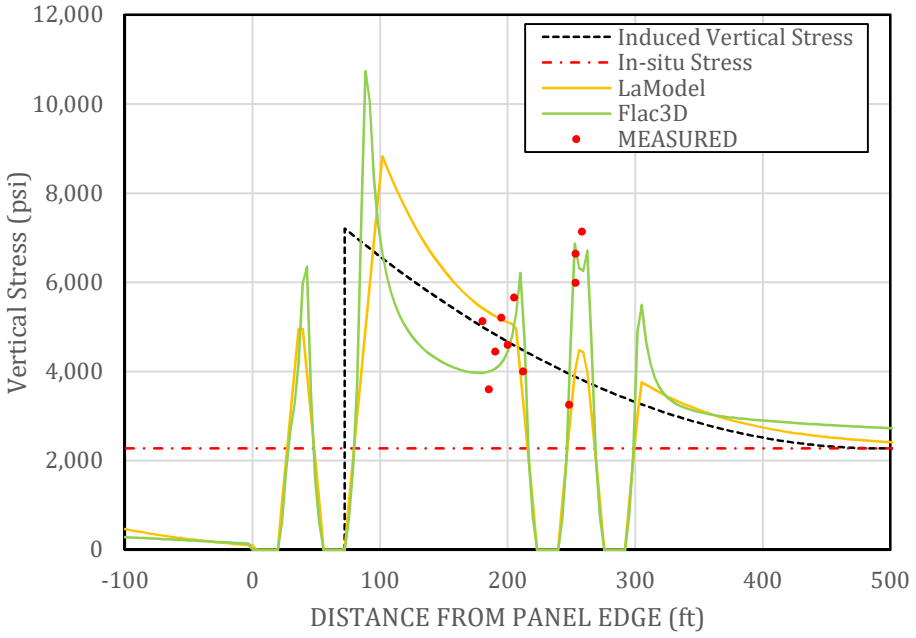

Figure 18. Measured stress data compared for CA-3 mine with stress profiles from different methods.

CA-3 case study mine is a deep mine with an overburden depth of approximately 2085 ft, and Figure 18 compares the three stress distribution curves with field measurement results from this case study mine. The black line represents the stress profile assumed by the ALPS method, the orange line represents the stress profile calculated by LaModel with the calibration method proposed by Heasley et al. (2010), the green line represents the stress profile calculated by FVM and the red-dots represent the BPC measurements. Although both FVM and LaModel show some inconsistencies compared with the measurements, both approximates the general trend and stresses reasonably accurate. The FVM stress profile shows higher peeks near the ribs and lower stresses in the middle of the large abutment pillar. LaModel shows lower peaks near the ribs compared to FVM, but larger stresses in the middle of abutment pillar. These differences are due to the different assumptions used during the derivation of the governing equations for pillar the material-models for FVM and LaModel. In LaModel, seam elements are modelled as one-dimensional springs, and the stress-strain behavior of each element is the function of vertical stress, and replicates the linear Mark-Bieniawski pillar strength formula. The FVM model input parameters are also calibrated to replicate the Bieniawski pillar strength formula (*see, section 3.2.2*), but the stress-strain behavior of each element is the function of three-dimensional stress tensor; nonetheless, the failure criterion is only the function of maximum

and minimum principal stresses. When the extent of the abutments are compared, ALPS has the shortest, LaModel has the intermediate and FVM has the largest abutment extent. When the magnitude of the abutment and in situ stress difference at the tail ends of FVM and LaModel stress profiles compared with the average pillar stresses, they are minor.

Pillar system and gob stress distributions: ALPS use a simple geometric conceptual model, "abutment angle theory," to estimate the magnitude of overburden loads transferred to the gob and abutments, and an empirical stress distribution function (Equation 16) to distribute loads within the extent calculated by Equation 14. There are five loading conditions in ALPS (Mark, 1992):

(i) *Development loading*: The loading on the pillar system before any longwall retreat mining.
(ii) *Headgate loading*: The pillar loading adjacent to headgate corner of the longwall face, which is equal to the development load plus the first front abutment.
(iii) *Bleeder loading*: The loading on a pillar system adjacent to a mined-out panel, which equals the development load plus the first side abutment.
(iv) *Tailgate loading:* The loading on a double-use gate entry system when it is adjacent to the tailgate corner of the longwall face, equal to the development load plus the first side abutment plus the second front abutment.
(v) *Isolated loading:* The loading on a pillar system located between two mined-out panels, equal to the development load plus two side abutments.

In this section, abutment loads calculated by FVM and ALPS are compared for each case study mine. Bleeder and isolated loading conditions are compared because these two loading conditions are analogous with two-dimensional cross-section models. In order to provide a consistent abutment load comparison between the deep and shallow panels, dimensionless (normalized) loads rather than absolute loads were used to calculate overburden loads transferred to abutments and gobs for each case.

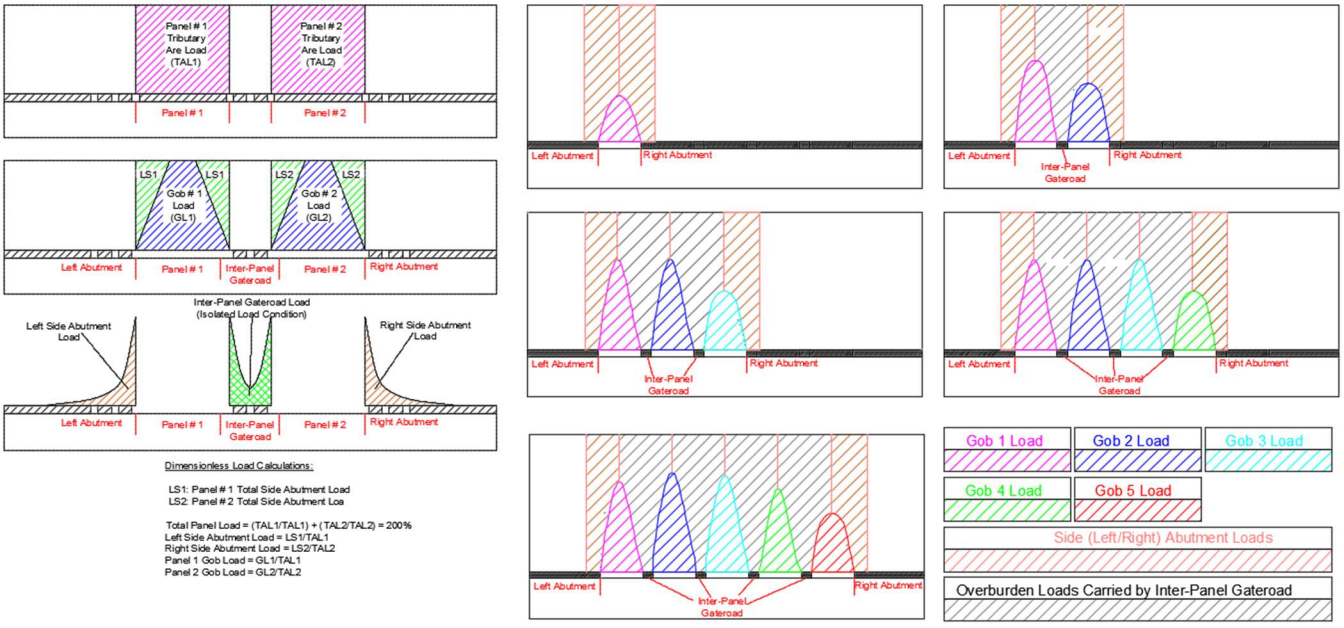

Figure 19. Dimensionless (normalized) overburden load calculations used to compare FVM and ALPS methods and the definition of left/right abutment, inter-panel gateroad.

Figure 19 shows step by step procedure used in this report for calculating the dimensionless loads on gob, gateroads and abutments. The tributary area loading (TAL) method is used to estimate the total overburden load disrupted due to excavation of the panels. For each case, the stress distribution calculated by FVM was numerically integrated to compute the absolute magnitude of the overburden loads transferred to gobs, gateroads and abutments. Later,

dimensionless overburden loads were calculated by normalizing the absolute loads on each structure by TAL as shown in Figure 19.

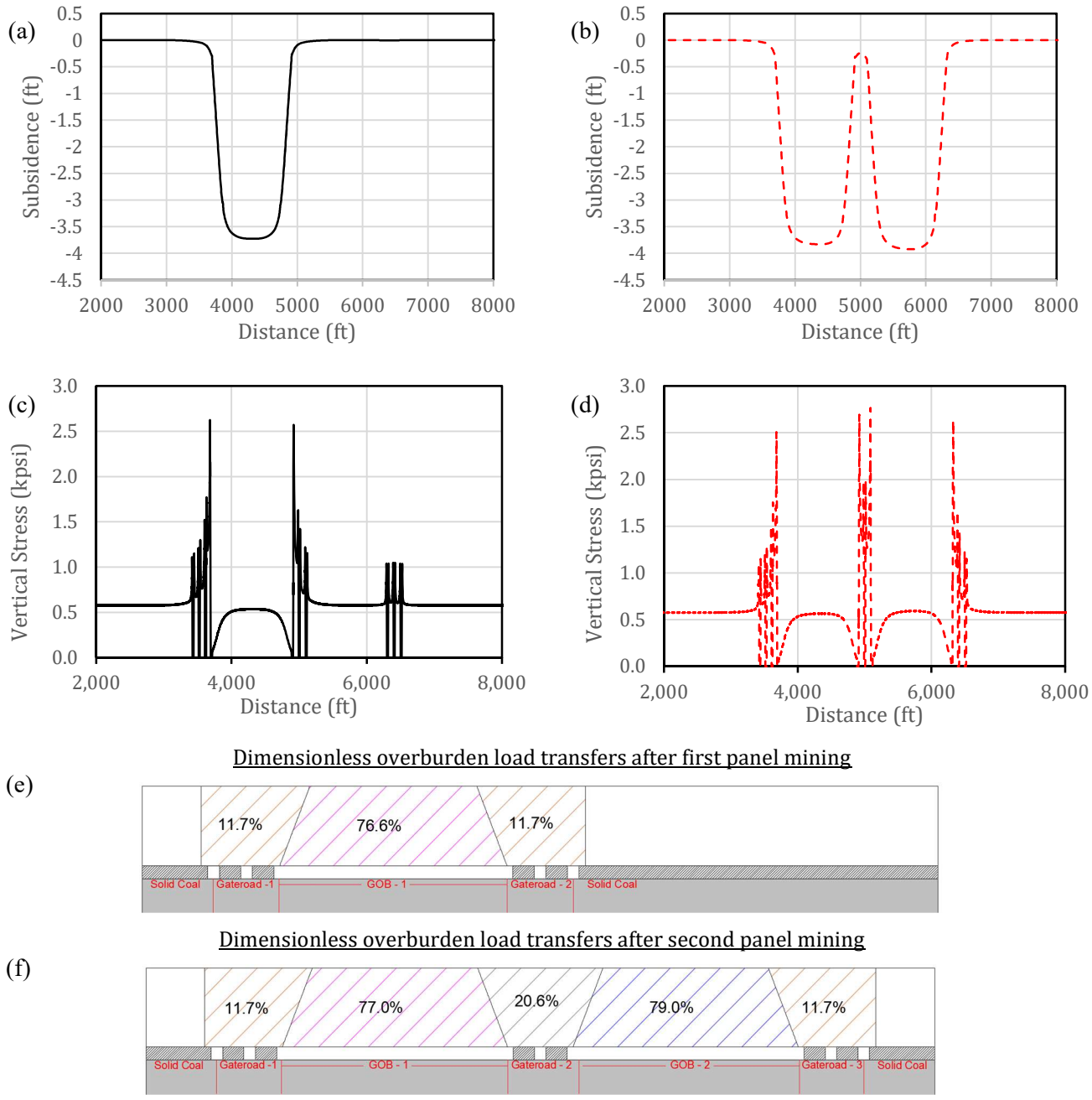

Figure 20. For case NA-3 (a) Subsidence profile after 1st panel mining, (b) subsidence profile after 2nd panel mining, (c) stress profile after 1st panel mining, (d) stress profile after 2nd panel mining, (e) dimensionless overburden load distribution after 1st panel mining and (f) dimensionless overburden load distribution after 2nd panel mining.

Figure 20 shows the subsidence profiles, stress profiles and dimensionless mining induced overburden load distributions approximated by FVM for case study mine NA-3 after the first and the second panels were excavated. Mine NA-3 is a shallow mine with typical overburden depth of 520 ft and panel width of 1200 ft (*see section 9.1.2*). Subsidence profiles of the first and the second panels are supercritical and nearly symmetric, meaning that

subsidence profiles of the first and the second panels are nearly identical (Figures 20a and 20b). This nearly symmetric subsidence profile implies the independent response of overburden strata over the adjacent panels. Galvin (2016) indicated that this independent response is seen when panel width-to-depth ratio is higher than or near 1.2. Stress profiles are also estimated nearly symmetric by the FVM (Figures 20c and 20d). Figures 20e and 20f show the dimensionless mining induced overburden load distribution on abutments and gobs. After the first panel mining, dimensionless overburden loads transferred to the abutments and Gob-1 are equal to 11.7% and 76.6% (Figure 20e). After the second panel mining, load carried by the Gob-1 increased by 0.4% to 77.0% and load carried by the Gob-2 is 79.0%. These slight increases of gob loads are due to the extra compression of the gobs near the inter-panel gateroad (Gateroad-2) after the second panel mining. Overburden loads transferred to the abutments are equal to 11.7%, same as after first panel mining, and loads on inter-panel gateroad (Gateroad-2) is equal to 20.6%.

Dimensionless load distributions were also computed by using the ALPS method. After the first panel mining, load on the abutments and Gob-1 are equal to 8.4% and 83.1%, and after second panel mining, load on the inter-panel gateroad (Gateroad-2) is equal to 16.9%. Although there are some differences between the loads estimated by ALPS and approximated by FVM, the differences (2% after first panel and 4% after second panel) are negligible for shallow overburden depths. ALPS assumes perfectly symmetric isolated loading condition which means that abutment loads transferred on the gateroad from neighboring panels are equal and independent of adjacent panel mining. This assumption is generally correct for the cases like NA-3 where panel width-to-depth ratio is near or larger than 1.2. However, as indicated by Galvin (2016), response of the overburden strata is quite different for deep and narrow panels.

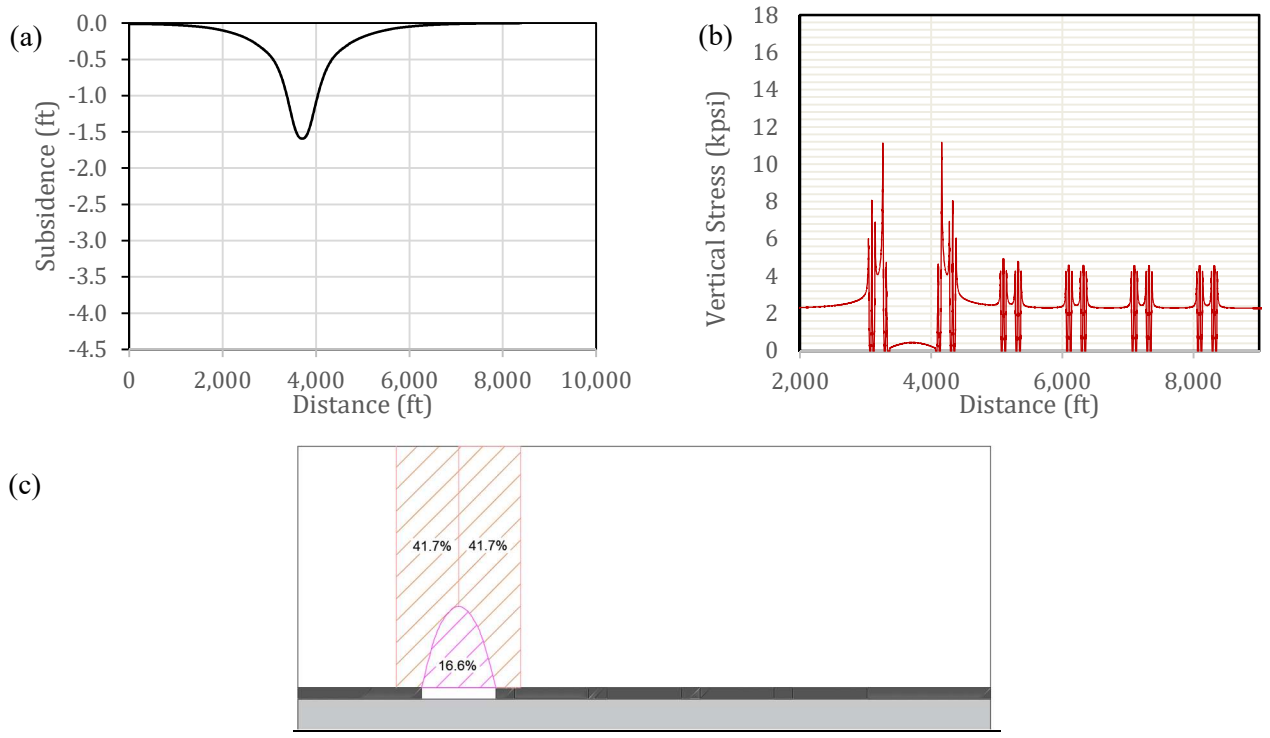

Figure 21. For case CA-1 (a) Subsidence profile after 1st panel mining, (b) stress profile after 1st panel mining, (c) dimensionless overburden load distribution after 1st panel mining.

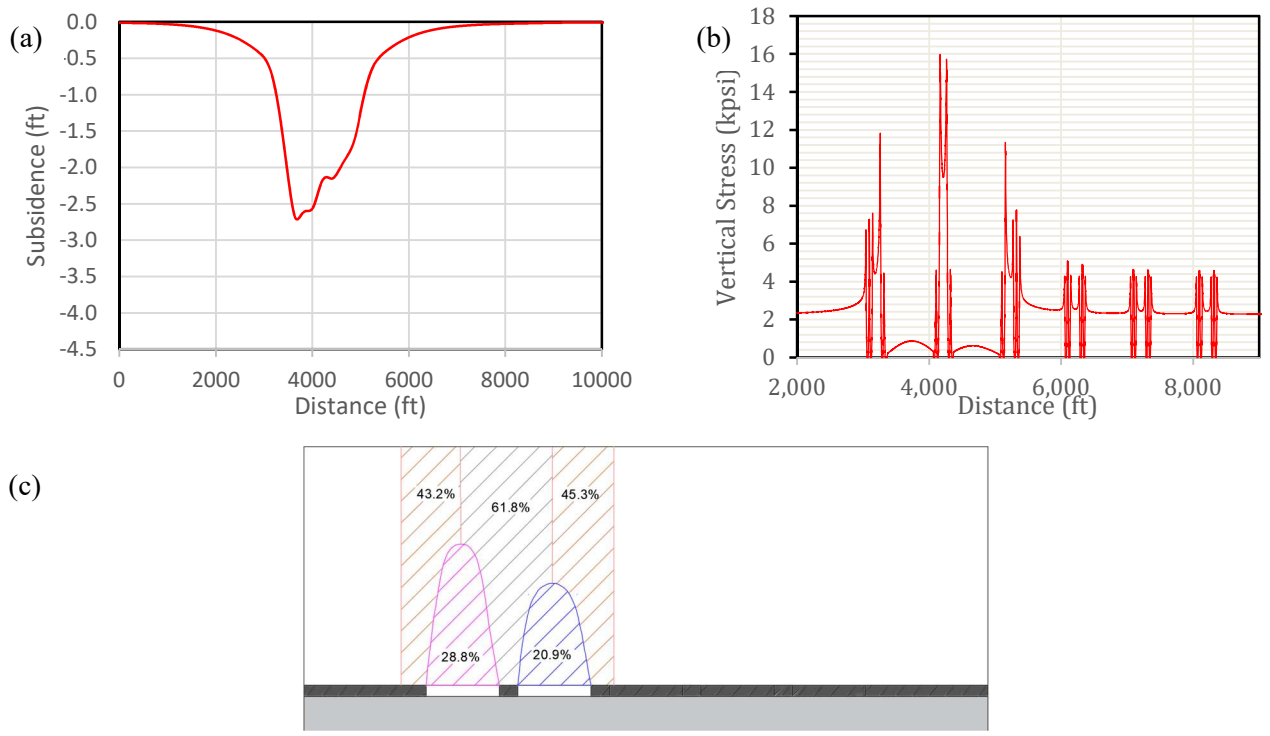

Figure 22. For case CA-1 (a) Subsidence profile, (b) stress profile, (c) dimensionless overburden load distribution after 2nd panel mining.

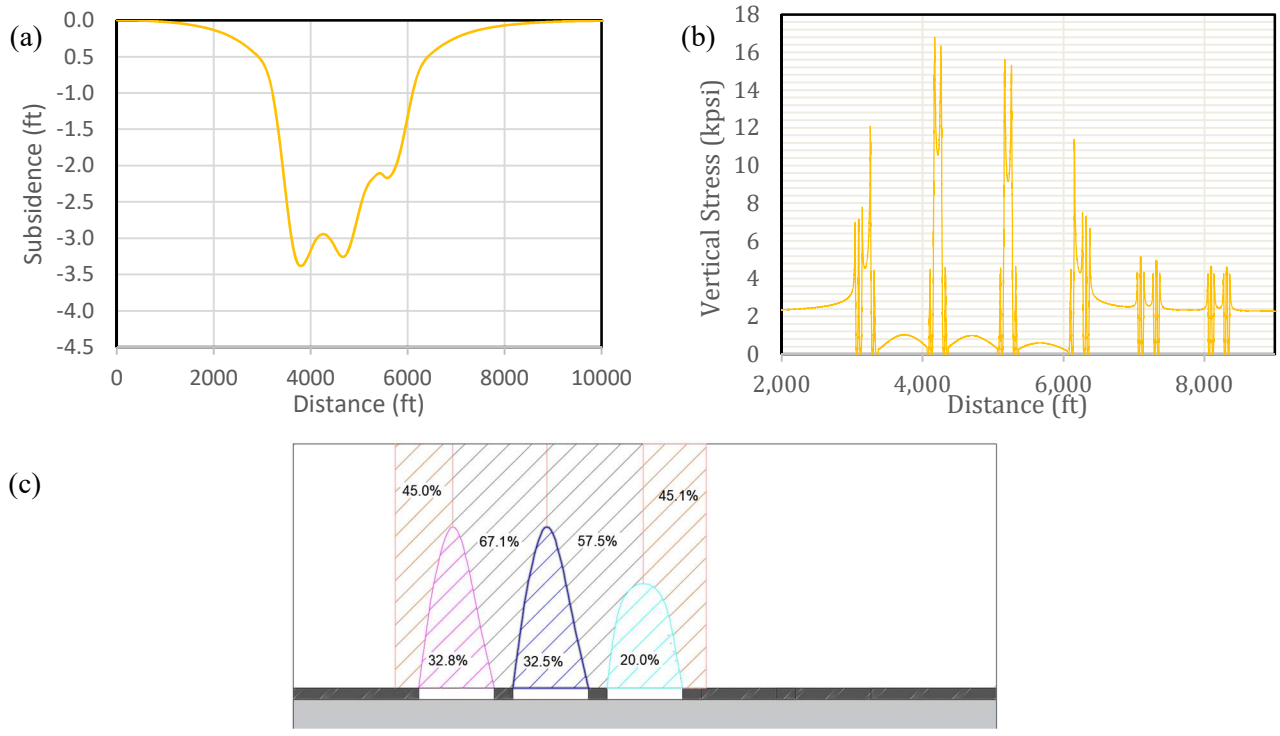

Figure 23. For case CA-1 (a) Subsidence profile, (b) stress profile, (c) dimensionless overburden load distribution after 3rd panel mining.

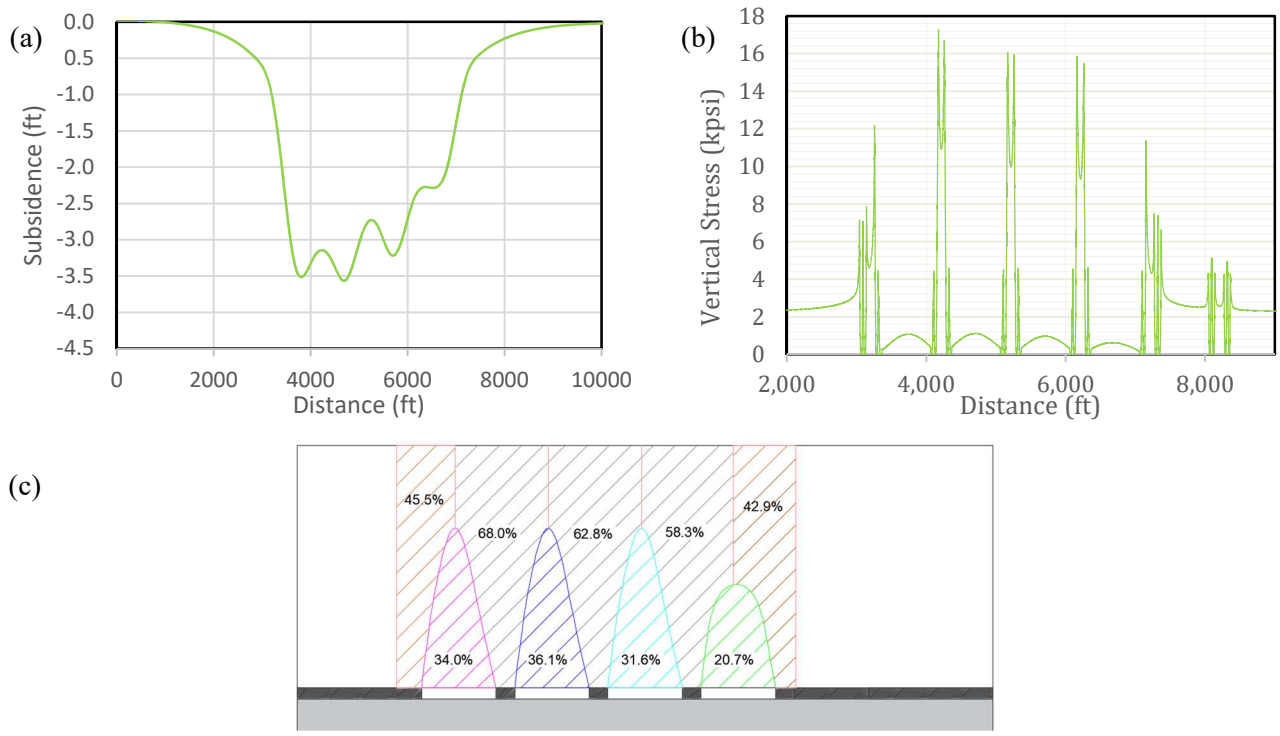

Figure 24. For case CA-1 (a) Subsidence profile, (b) stress profile, (c) dimensionless overburden load distribution after 4th panel mining.

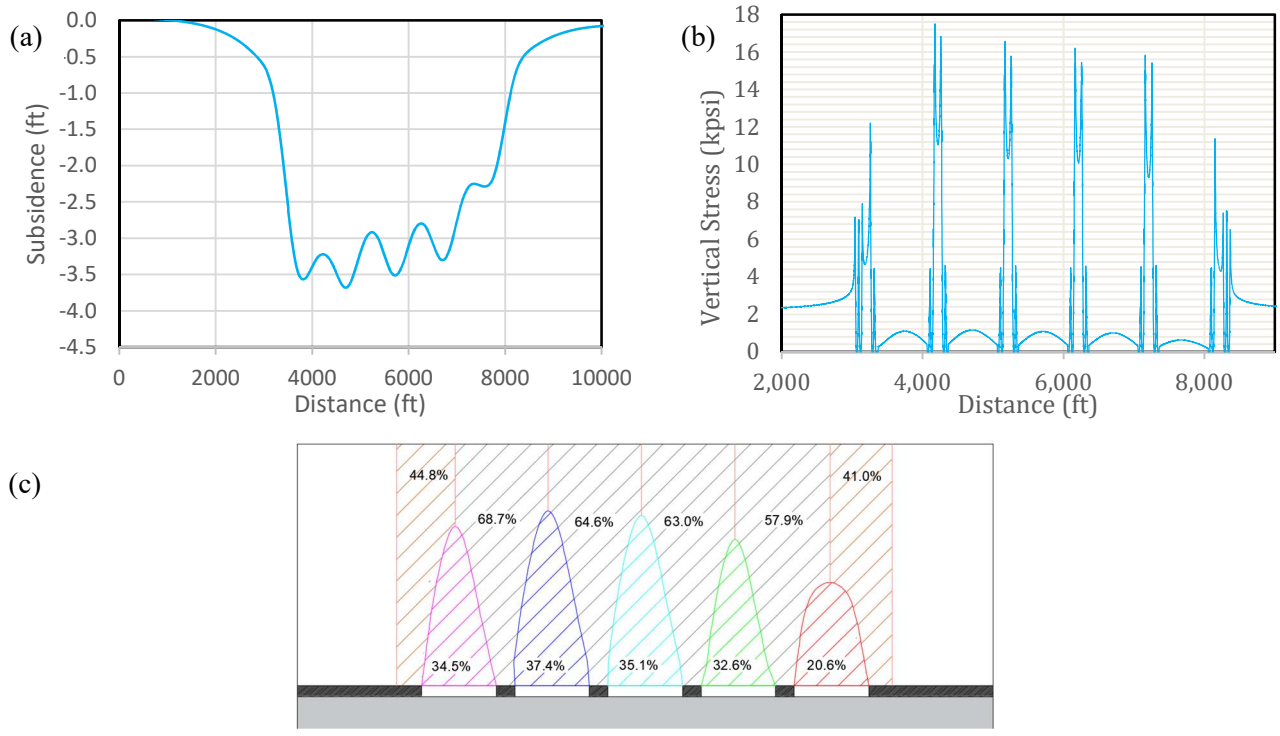

Figure 25. For case CA-1 (a) Subsidence profile, (b) stress profile, (c) dimensionless overburden load distribution after 5th panel mining.

Figures 21, 22, 23, 24 and 25 show the subsidence profiles, stress profiles and dimensionless overburden load distributions approximated by FVM for case study mine CA-1 for five consecutive panel mining. Mine CA-1 is a deep mine with an overburden depth of 2058 ft and a panel width of 700 ft (*see section 9.1.2*). Figure 21a shows that limited vertical displacement occurred over the first longwall panel when it was extracted. Figure 21b shows the symmetric vertical stress profile and Figure 21c shows the dimensionless overburden load distribution. First panel gob carries the 16.6% of the mining induced overburden loads and remaining 83.4% of the loads are carried by the abutments equally divided (41.7%) in between each side. After the first panel mining, ALPS method calculates 22.3% of the loads on the Gob and 77.7% of the loads on the abutments (38.85% on each side). Therefore, ALPS method calculated loads on abutments 2.9% less than the FVM.

Extraction of the second panel resulted in a large step increase in subsidence over the first panel (Figure 22a). Subsidence over the first panel increased from 1.6 ft to 2.7 ft after second panel mining. Galvin (2016) referred to this additional subsidence as incremental subsidence. This incremental subsidence over the first panel increased the load on the first gob from 16.6% to 28.8%. After second panel mining, the load carried by the second panel gob is 20.9%. In addition to higher gob loads, the loads carried by each side of the abutments increased slightly (to 43.2% and 45.3%) and FVM approximated the inter-panel gateroad load as 61.8% (Figure 22c). Excavation of the second panel resulted with an asymmetric subsidence profile, stress profile and load distribution. Incremental subsidence and asymmetric profiles imply that response of the overburden above the adjacent panels are influenced from consecutive mining of the adjacent panels. Since the ALPS method assumes perfectly symmetric isolated loading condition, load on each gob is still calculated as 22.3% and load on the inter-panel gateroad is calculated as 77.8%. Therefore, FVM approximated the load on the inter-panel gateroad significantly lower than the ALPS method.

Extraction of the third panel also resulted in a large step increase in subsidence over the first and second panels (Figure 23a). Subsidence over the first panel increased from 2.7 ft to 3.3 ft and over the second panel increased from 2.1 ft to 3.2 ft. This incremental subsidence also increased the loads carried by the first gob from 28.8% to 32.8% and the second gob from 20.9% to 32.5%. Thee load carried by the third gob is 20.0% at this stage. Loads carried by the left abutment increased slightly to 45.0% and, the load carried by the first inter-panel gateroad also increased from 61.8% to 67.1%. The load on the second inter-barrier gateroad is 57.5%, again significantly lower than the ALPS estimate (77.8%).

Extraction of the fourth and fifth panels also resulted in similar trends in subsidence and loads as explained above (Figure 24 and 25). Incremental subsidence above the first panel continue at a diminishing rate until after the excavation of the fifth panel. Gobs and inter-panel gateroads of the previous panels continue to carry more and more load with subsequent panel extraction. Load carried by the gob of the active panel stayed relatively constant during the consecutive panel mining around 20%. Similarly, load carried by the inter-panel gateroad of the active panel also stayed relatively constant around 60%.

Figure 26 shows the dimensionless overburden load distribution approximated by FVM and ALPS for case study mine CA-3 for five consecutive panel mining. Mine CA-3 is a deep mine with hard rock ratio of 32%, overburden depth of 2080 ft and panel width of 600 ft (*see section 9.1.2*). It is the deepest mine with narrowest panels in the database with overburden depth to panel width ration of 3.47. After the first panel mining, FVM estimated that gob and abutments carry 9.5% and 45.2% of the overburden loads (Figure 26a), and ALPS estimated that gob and abutments carry 18.2% and 40.6% of the loads (Figure 26f). After the second panel mining, FVM estimated that the load carried by the abutments increase to 53.3% and 58.5%, the load carried by the first gob increased to 18%, the load carried by the second gob was 15.4% and the load carried by inter-panel gateroad was 54.9% (Figure 26b). ALPS estimated inter-panel gateroad load as 81.3% (Figure 26f) significantly higher than that estimated by FVM. The extraction of the third, fourth and fifth panels resulted in progressive increase in first panel gob load up to 25.5%, second panel gob load up to 33.5%, third panel gob load up to 32.6% and fourth panel gob load up to 27.9% (Figure 26c, 26c and 26e). After the fifth panel mining, its' gob load was 18.7%. During the consecutive mining of third, fourth and fifth panels, left and right abutment loads ranged between 52% to 58.5%. The load carried by the inter-panel gateroad of the active panel progressively increased from 54.9% to 58.9% (Figure 26b – Figure 26e), significantly lower than the ALPS estimate (Figure 26f).

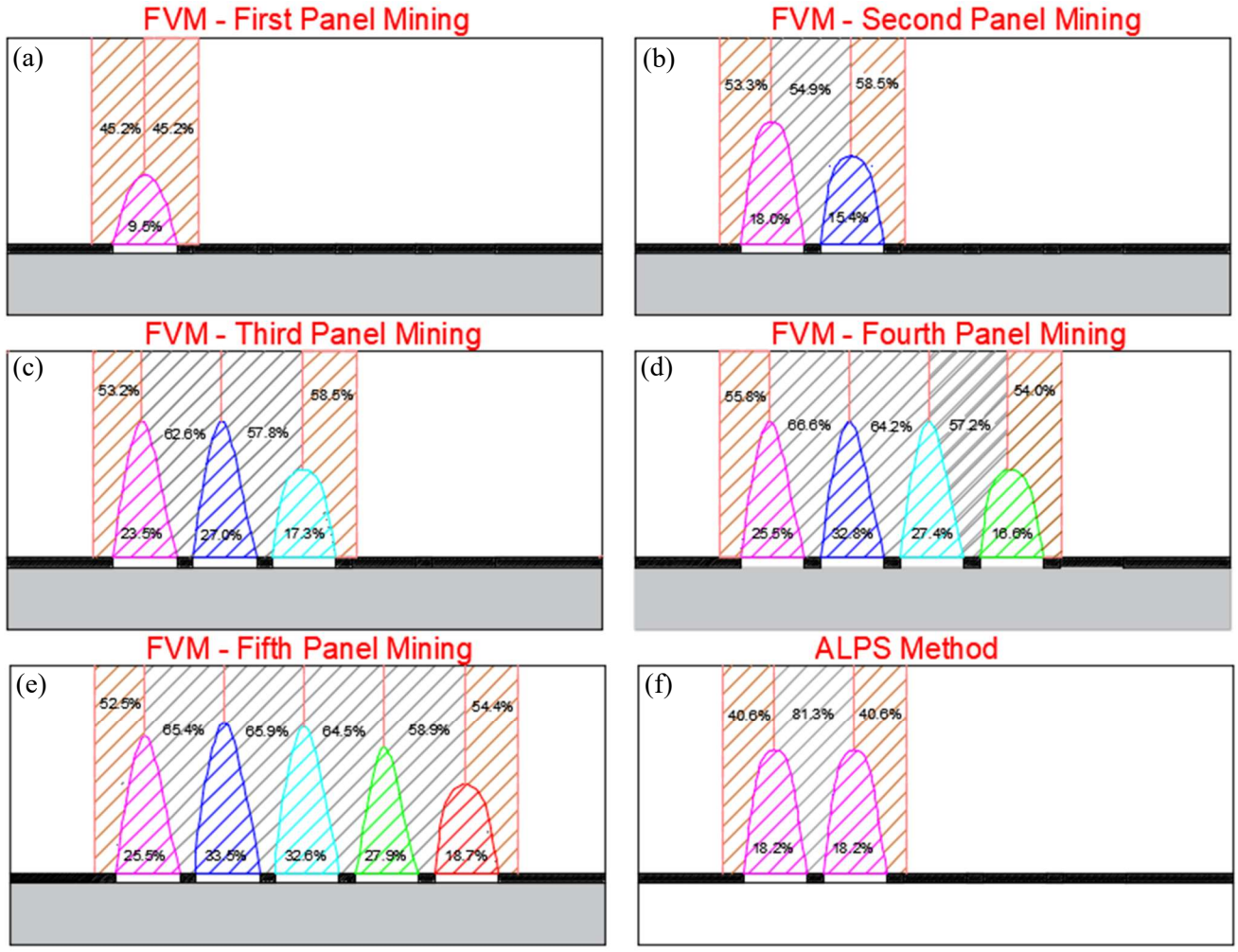

Figure 26. For case CA-3 dimensionless overburden load distribution calculated by FVM after (a) first, (b) second, (c) third, (d) fourth, (e) fifth panel mining and (f) calculated by ALPS method.

Figure 27 shows the dimensionless overburden load distribution approximated by FVM and ALPS for case study mine W3-R for four consecutive panel mining. Mine W3-R is a deep mine with hard rock ratio of 49%, overburden depth of 1978 ft and panel width of 830 ft (*see section 9.1.2*). Overburden depth to panel width ration for W3-R is 2.37. After the first panel mining, FVM estimated that gob and abutments carry 25.7% and 37.1% of the overburden loads (Figure 27a), and ALPS estimated that gob and abutments carry 27.4% and 36.3% of the loads (Figure 27e). After the second panel mining, FVM estimated that load carried by abutments increase slightly to 39.4% and 37.6%, load carried by first gob increased to 31.6%, load carried by second gob was 26.6% and load carried by inter-panel gateroad was 64.9% (Figure 27b). ALPS estimated inter-panel gateroad load as 72.6% significantly higher than the one estimated by FVM. Extraction of the third and fourth panels resulted in progressive increase in first panel gob load up to 32.8%, second panel gob load up to 32.4% and third panel gob load up to 31.1%. After the fourth panel mining, its' gob load was 26.2%. During the consecutive mining of third and fourth panels, left and right abutment loads ranged between 38.6% to 39.2%. Load carried by the inter-panel gateroad of the active panel reduced to 62.9% after third panel mining and then increased to 63.5% after fourth panel mining.

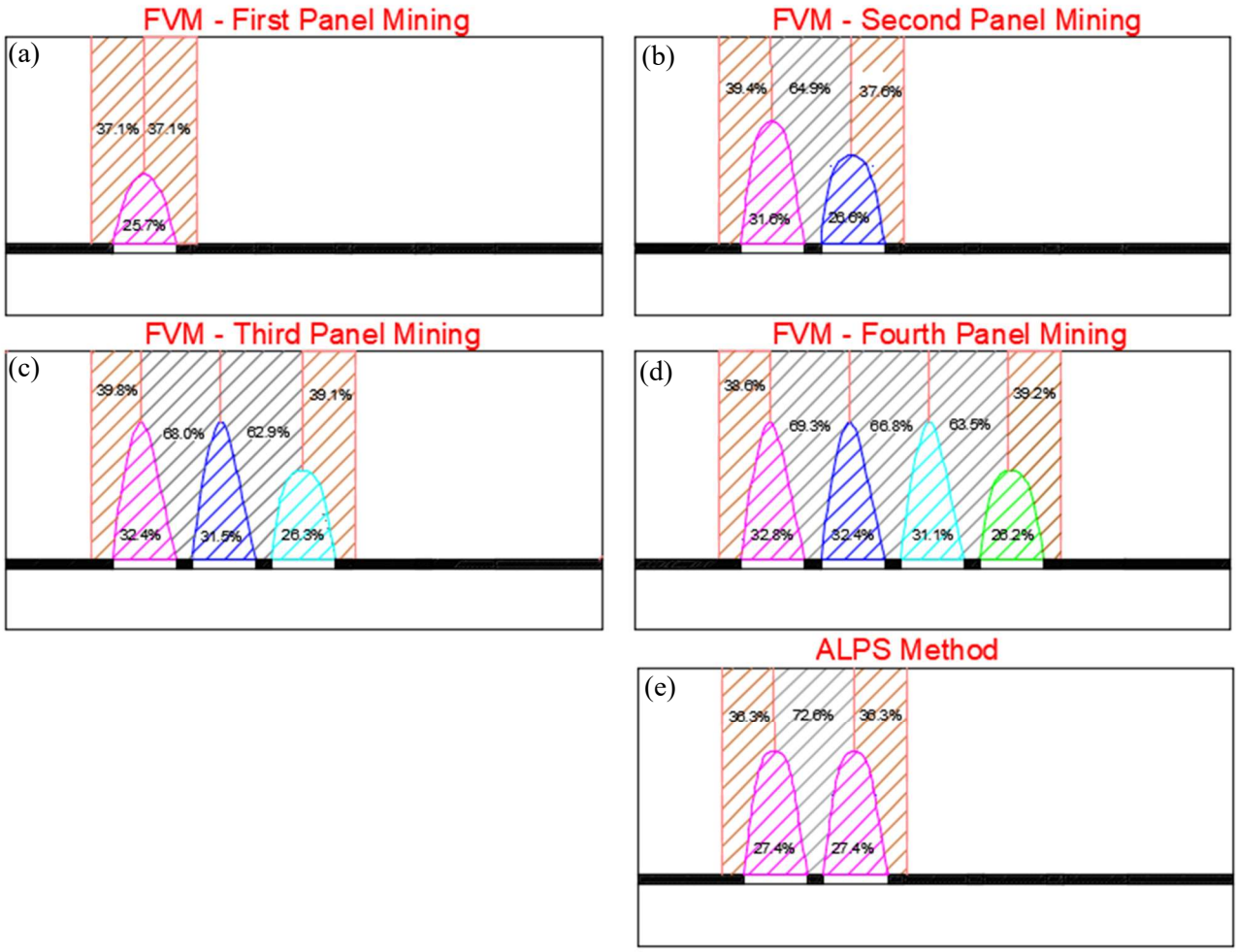

Figure 27. For case W3-R dimensionless overburden load distribution calculated by FVM after (a) first, (b) second, (c) third, (d) fourth and (e) calculated by ALPS method.

Figure 28 shows the dimensionless overburden load distribution approximated by FVM and ALPS for case study mine W3-L for four consecutive panel mining. Mine W3-L is a moderately deep mine with hard rock ratio of 49%, overburden depth of 1487 ft and panel width of 780 ft (*see section 9.1.2*). Overburden depth to panel width ration for W3-R is 1.90. After the first panel mining, FVM estimated that gob and abutments carry 27.1% and 36.4% of the overburden loads (Figure 28a), and ALPS estimated that gob and abutments carry 34.6% and 32.7% of the loads (Figure 28e). After the second panel mining, FVM estimated that load carried by abutments increase slightly to 38.1% and 38.2%, load carried by first gob increased to 35.4%, load carried by the second gob was 27.9% and the load carried by inter-panel gateroad was 60.3% (Figure 28b). ALPS estimated inter-panel gateroad load as 65.4% slightly higher than the one estimated by FVM. Extraction of the third and fourth panels resulted in progressive increase in first panel gob load up to 36.8%, second panel gob load up to 37.2% and third panel gob load up to 36.0%. After the fourth panel mining, its' gob load was 28.2%. During the consecutive mining of the third and fourth panels, the left and right abutment loads ranged between 35.8% to 39.1%. The load carried by the inter-panel gateroad of the active panel stayed at 60.3%.

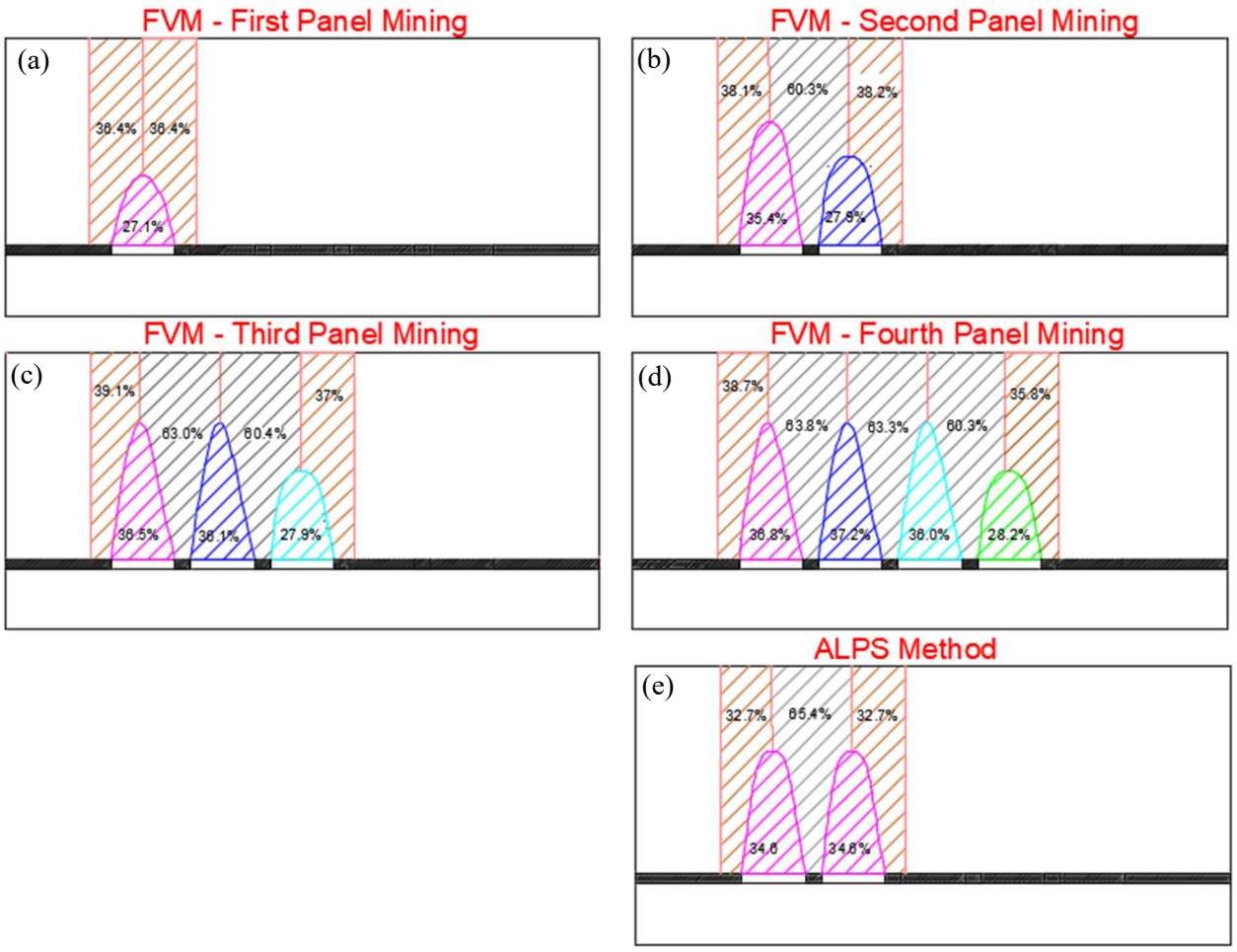

Figure 28. For case W3-L dimensionless overburden load distribution calculated by FVM after (a) first, (b) second, (c) third, (d) fourth and (e) calculated by ALPS method.

Figure 29 shows the dimensionless overburden load distribution approximated by FVM and ALPS for case study mine BW-1 for three consecutive panel mining. Mine BW-1 is a moderately deep mine with hard rock ratio of 32%, overburden depth of 1450 ft and panel width of 1000 ft. Overburden depth to panel width ration for BW-1 is 1.45. After the first panel mining, FVM estimated that gob and abutments carry 35.0% and 32.5% of the overburden loads (Figure 29a), and ALPS estimated that gob and abutments carry 45.0% and 27.5% of the loads (Figure 29d). After the second panel mining, FVM estimated that load carried by abutments change slightly to 32.1% and 33.0%, load carried by first gob increased to 48.2%, load carried by second gob was 34.8% and load carried by inter-panel gateroad was 51.9% (Figure 29b). ALPS estimated inter-panel gateroad load as 48.2% slightly lower than the one estimated by FVM. Extraction of the third panel resulted in increase in first panel gob load up to 48.8% and second panel gob load to 47.6%. After the third panel mining, its' gob load was 35.5%, left abutment load was 30.6%, right abutment load was 32.5% and inter-panel gateroad load was 51.2%.

Figure 30 shows the dimensionless overburden load distribution approximated by FVM and ALPS for case study mine NA-5 for three consecutive panel mining. Mine NA-5 is a moderately deep mine with hard rock ratio of 25%, overburden depth of 1220 ft and panel width of 1000 ft. Overburden depth to panel width ration for BW-1 is 1.22. After the first panel mining, FVM estimated that gob and abutments carry 43.2% and 28.4% of the overburden loads (Figure 30a), and ALPS estimated that gob and abutments carry 54.0% and 23.0% of the loads (Figure 30d). After the second panel mining, FVM estimated that load carried by abutments change slightly to 27.1% and 27.8%, load carried by first gob increased to 50.6%, load carried by second gob was 46.3% and load carried by inter-panel

gateroad was 48.2% (Figure 30b). ALPS estimated inter-panel gateroad load as 46.0% very close to the one estimated by FVM. Extraction of the third panel resulted increase in first panel gob load slightly up to 51.3% and second panel gob load to 52.6%. After the third panel mining, its' gob load was 46.2% and inter-panel gateroad load was 46.8%.

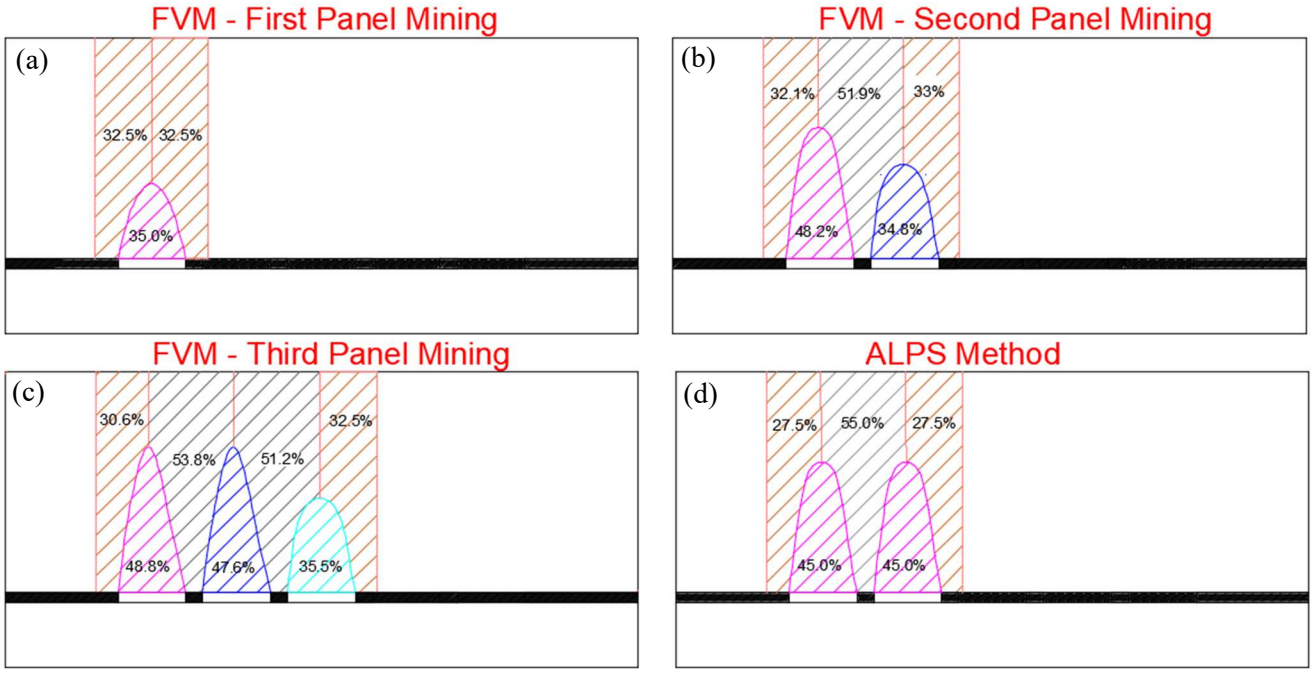

Figure 29. For case BW-1 dimensionless overburden load distribution calculated by FVM after (a) first, (b) second, (c) third and (d) calculated by ALPS method.

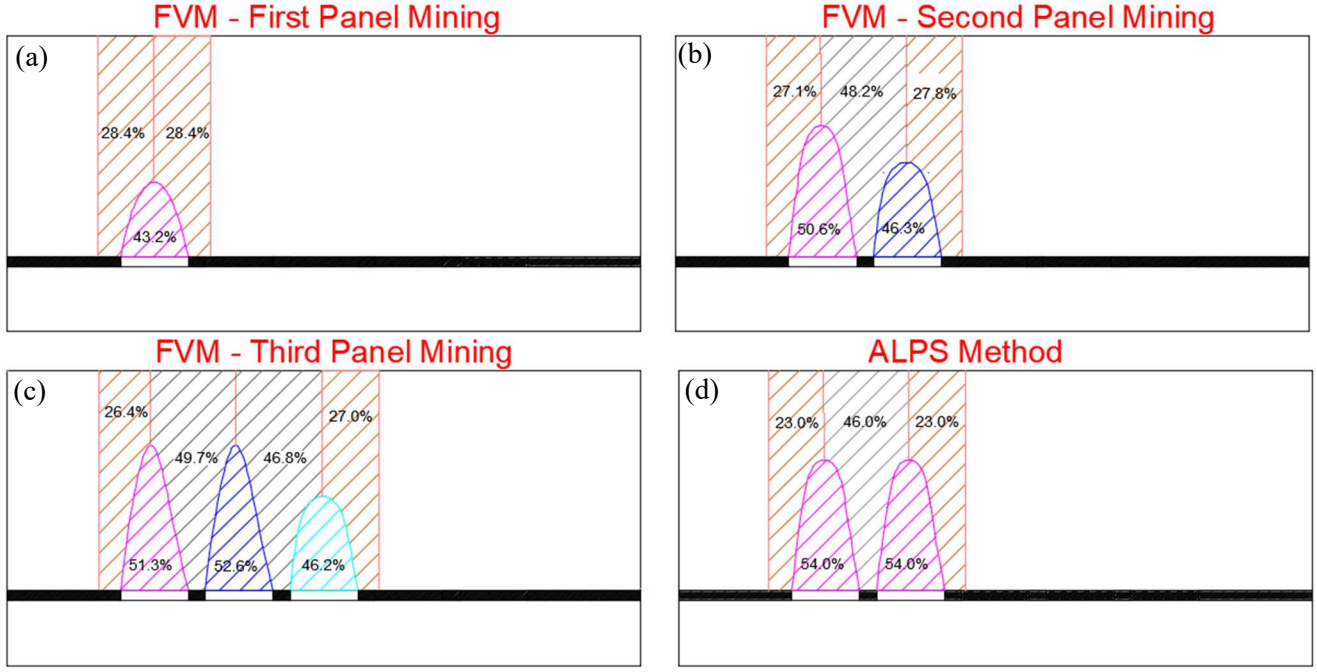

Figure 30. For case NA-5 dimensionless overburden load distribution calculated by FVM after (a) first, (b) second, (c) third and (d) calculated by ALPS method.

Figure 31 shows dimensionless left/right abutment loads estimated by FVM and ALPS methods. The horizontal axis shows the mine name, the vertical axis shows the dimensionless abutment load, and labels show the overburden hard rock ratio (HR) and depth-to-panel width ratio (H/PW) for each mine. In this plot, the dimensionless abutment load is the average of the left and right side abutments, and calculation of the left and right side abutment loads are shown in Figure 19. The red bar represents the abutment load calculated by ALPS and black, orange, green, blue and purple bars represent abutment loads calculated by FVM after each mining step. Mines NA-3, NA-1, NA-2 and NA-6 have supercritical subsidence profiles and they are relatively shallow mines. Other mines have subcritical subsidence profiles and they are moderately deep (H>1200 ft) or deep mines (H >1850 ft). When abutment loads estimated by ALPS (red bar) are compared with the ones estimated by FVM after first panel mining (black bar), FVM results are slightly higher. The average difference of all the cases is 4.44%, and highest differences are seen in two shallow cases; 8.16% for NA-2 and 7.10% for NA-1. Both of these mines have relatively thick and strong limestone/sandstone layers in their overburden (*see, Figure 4*), and HR ratio of NA-2 is 42% and NA-1 is 37%. These results imply that strong units in the overburden of a shallow mine might also affect the abutment loads. However, in this study there are not enough cases to effectively support this argument statistically.

Since the response of the overburden over the supercritical panels are independent of adjacent panel mining, only the abutment loads after the first panel mining are shown in Figure 31 for them. For the subcritical panels, the change of abutment loads with consecutive panel mining is also shown (orange, green, blue and purple bars in Figure 31). The influence of consecutive panel mining on abutment loads is almost negligible except case CA-3. CA-3 mine has deepest and narrowest panels in the database, and after the second panel mining, loads carried by left and right abutments increase nearly 10%.

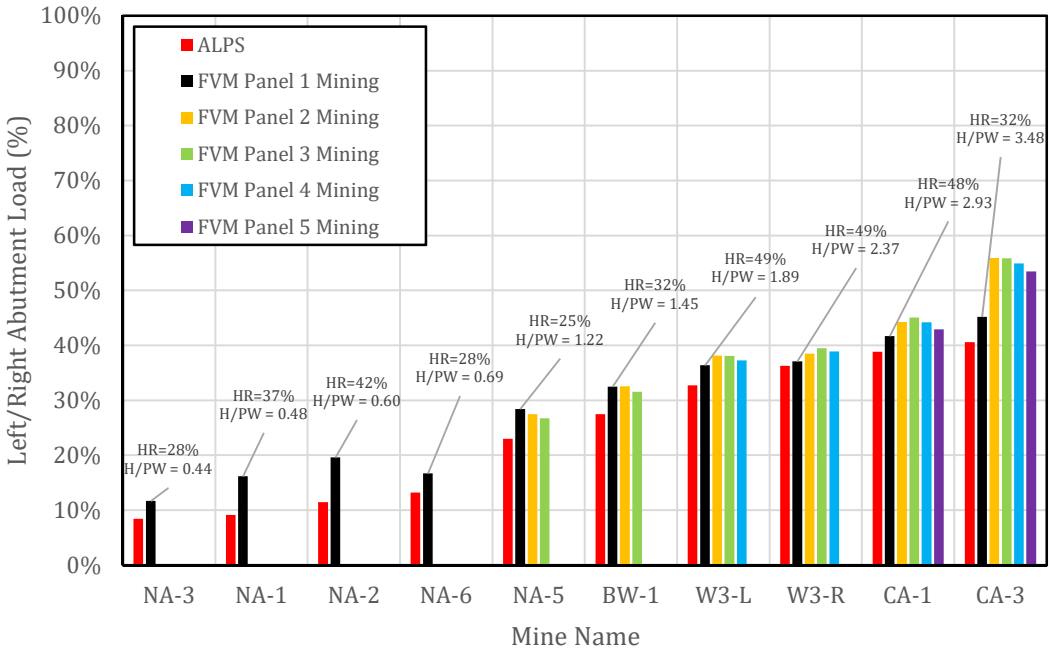

Figure 31. Left/Right abutment load (bleeder loading condition) calculated by FVM and ALPS.

Although Figure 31 shows some trends on the effect of geology in shallow mines and the effect of consecutive panel mining in deep mines on the magnitude of abutment loads, difference between the the ALPS method and FVM aren't significant when the stability of the pillars in the left and right abutment zones are considered. In these zones, gateroad pillars are adjacent to thick barriers pillars and load on these pillars are generally lower than the inter-panel gateroads or barriers (in ARMPS).

Figure 32 shows the inter-panel gateroad of the active panel for four consecutive panel mining to clarify the term "active panel" used in the text. Figure 33 shows a comparison of the dimensionless load on the inter-panel gateroad pillar system calculated by FVM (for the active panels) and ALPS during isolated loading condition. The vertical and horizontal axes represent the load percentage and the panel depth-to-width ratio. The green line shows the critical panel depth-to-width ratio of 0.83 where the subsidence profile translates from super-critical to sub-critical (Agioutantis and Karmis, 2017). While black dots show the loads calculated by FVM, the red dots are the loads calculated by ALPS. Each data point has a label showing case history identifier and overburden hard-rock percentage (HR).

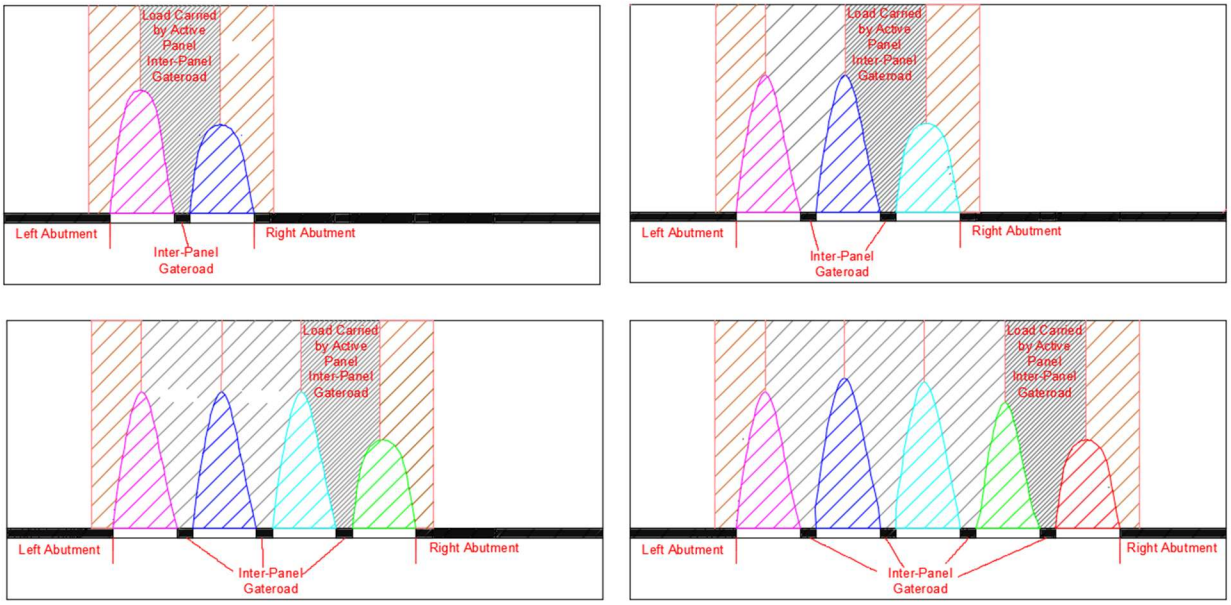

Figure 32. Schematic showing the inter-panel gateroad of the active panel.

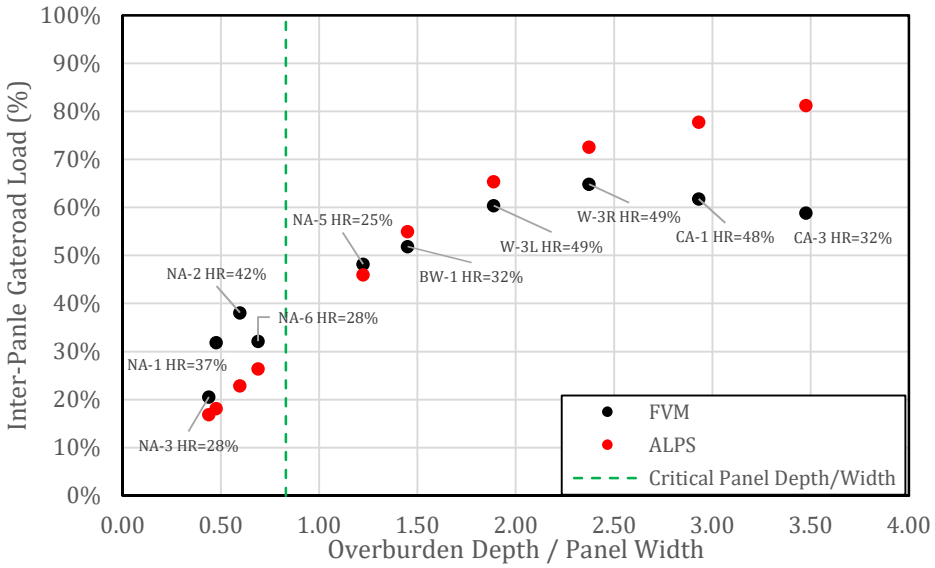

Figure 33. Inter-Panel Gateroad loads (isolated loading condition) calculated by FVM and ALPS methods.

When HR percentages are compared in the supercritical region (left of the green line in Figure 33), it is clear that for lower HR percentage cases (NA-3 and NA-6) the difference in gateroad loads between FVM and ALPS is smaller, but for the higher HR percentage cases (NA-1 and NA-2) the difference increases. For cases with HR percentages of 28% (NA-3 and NA-6), FVM calculate inter-panel gateroad loads approximately 4% higher than ALPS. For case NA-1 with HR percentage of 37%, FVM calculates inter-panel gateroad loads 14% higher and for case NA-2 with HR percentage of 42%, FVM calculates inter-panel gateroad loads 16% higher than the ALPS method. In the subcritical region (right of the green line), we can see that for two case study mines (NA-5 and BW-1), between the depth-to-width ratios of 0.83 (critical ratio) to 1.66, FVM and ALPS methods calculated similar load magnitudes. After the depth-to-width ratio of approximately 1.66, inter-panel gateroad loads calculated by the FVM method converge to approximate a value of 60.0%. Australian stress measurement cases presented in section 3.1.1 and other reported cases in the USA also verify the results of this study (Colwell et al., 1999; Su et al., 2014). To the PI's knowledge there has been only one hypothesis proposed to explain this behavior (Heasley, 2000). In his study Heasley used the analytical laminated overburden model and showed that the percentage of overburden load carried by the strain-hardening gob increases with increasing depth which results in a constant or even decreasing percentage of load carried by the abutments.

It is also important to note that during the comparison of overburden load distributions calculated by the FVM and ALPS methods only 10 of the 12 US cases were used. Two of the Western USA cases, W-1 and W-2 mines, applied two-entry yield pillar gateroad system. Since the support mechanism provided by the two-entry yield pillar systems can only be simulated by the mechanical models, and results of the load analysis aren't comparable with the ALPS method, these two cases are excluded from this section.

Mechanical response of the overburden:

The mechanical response of the overburden strata for the case study mines was studied by the ground response curve (GRC) approach. Both LaModel and FVM can be used to derive GRC. The laminated overburden model, LaModel, simulates realistic flexibility for stratified sedimentary geologies very efficiently with two overburden stiffness input parameters: elastic modulus and lamination thickness, and these overburden parameters represent the average behavior of the overburden. This is a practical and valid approach considering the extremely complex nature of the overburden geology and should be used during the design stages. However, the objective of the analysis in this section is to observe the influence of thick and strong layers in the overburden strata to the mechanical response of the overburden, and FVM is more suitable to demonstrate the influence of individual layers since it can explicitly simulate each geological layer in the overburden.

GRC for a particular panel was determined by applying internal pressure within the modelled panel and reducing this internal pressure gradually. The pillars and gob were kept inside the excavation during the gradual reduction of the internal pressure. During the gradual reduction of the pressure, average strain across the panel gob was computed. During the GRC development only the single panel configuration (not the real-world panel configuration during the field measurement) was modeled.

Three case study mines selected from the second dataset to demonstrate the influence of panel Depth-Width ratio, HR percentage and influence of strong beds on GRC. Figure 34 shows the GRC results for the three case study mines. The vertical axis in the graph is normalized internal load (internal load/in situ load), and the horizontal axis is the average convergence along the gob. The black line indicates the ground reaction curve for case NA-3 with Panel Depth-Width ratio (H/PW) of 0.4 and HR of 28%. The red line represents the ground reaction curve for BW-1 with H/PW ratio of 1.4 and HR of 32%. The orange line is the ground reaction curve for CA-3 with H/PW ratio of 3.5 and HR of 32%. Initially, all three curves are steep and nearly linear. This behavior embodies the elastic response of the overburden (Barczak, 2017). As the internal pressure is reduced, the ground reaction curve becomes nonlinear and begins to flatten, indicating that the overburden is failing (Barczak, 2017). The difference between the normalized internal pressure and normalized in situ pressure (100%) indicates the percentage of in situ load transferred to the abutments. Figure 34 shows that as H/PW ratio increases, the elastic part of the ground response curve's slope increases. In addition, load transferred to the abutments also increases with increasing H/PW ratio.

When similar HR cases (CA-3 and BW-1) with different H/PW are compared, the elastic part of the GRC's slope is steeper and load transferred to abutments are larger for larger H/PW ratios.

GRC analysis provides some useful information on the behavior of the overburden. However, it isn't possible to understand the mechanical response of the overburden without investigating the relative deformation of the strata in the overburden during the consecutive panel mining. Unfortunately, GRC analysis during multiple panel mining couldn't be performed due to the difficulty of incorporating the loads transferred from the previous panels into the GRC.

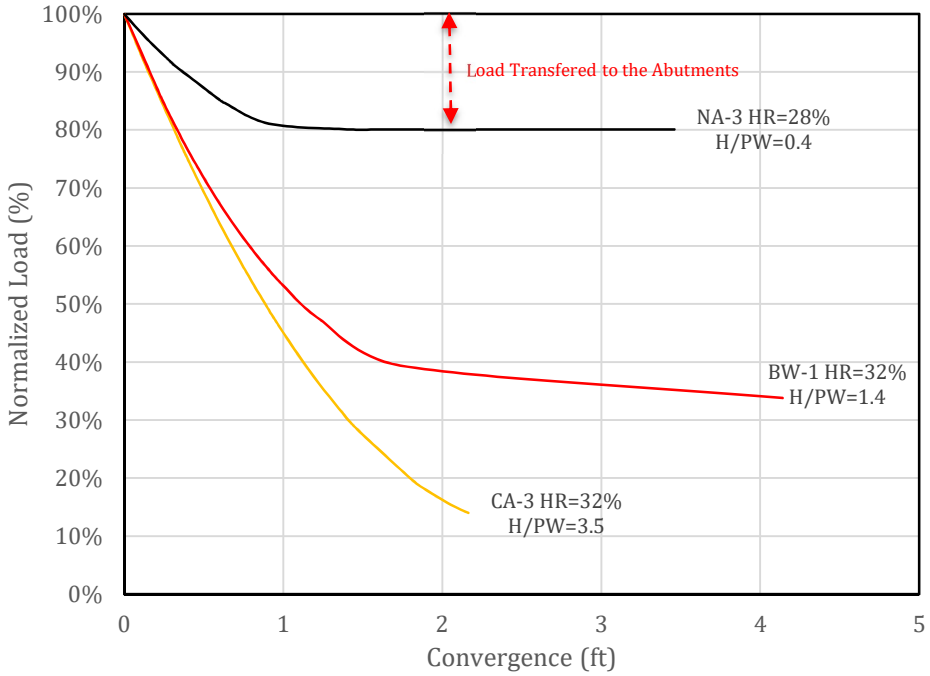

Figure 34. Comparison of GRC for three case study mines.

Figure 35 shows the separation of the overburden layers for the three case study mines. The vertical axis is the overburden depth and the horizontal axis is the layer separation. In order to calculate layer separation, first, displacements of the grid points from the surface to the seam were queried at the midpoint of the panel. Then, the difference in vertical displacements of the grid points located adjacent to each other was calculated. The layer separation is essentially the relative displacement of each geological layer relative to neighboring layers. In Figure 35, the black line represents the NA-3 mine, the red line represents the BW-1 mine and the orange line represents the CA-3 mine. Layer separation depends on the thickness of the strong layers, the location of the strong layers relative to both the seam and the surface, and the width of the panel. Sudden increases in the layer separation indicates the existence of a strong layer and the amplitude of each jump depends on the strong layer thickness, panel width and total weight above the layer. NA-3 is a shallow mine with a low HR ratio and a large panel width, and although overburden strata include strong layers, there isn't any separation. The BW-1 mine is a deep mine with a HR of 32% and a depth-to-width ratio of 1.4. Although it is a deep mine, the panel width cannot be categorized as narrow. Its overburden has strong sandstone layers, due to the large panel width (compared to CA-3), the separation of the layers is not prominent. CA-3 is a deep mine with a narrow panel and a HR percentage the same as BW-1. In Figure 35, we can see that multiple strong layers are separated from each other after first panel mining and we can observe that there are two prominent thick layers 80 ft and 330 ft above the coal seam.

Figure 35 might also explain the difficulty of finding a correlation between overburden loads and HR percentage. Both CA-3 and BW-1 mines have 32% HR percentages. However, we can see from Figure 35 that there are considerable differences between the behavior of the strong units between these two cases. CA-3 is deeper and its'

panels are narrower, and these parameters have a prominent effect on the behavior of the strong units. However, it is also seems reasonable that quantifying the overburden with an average value of HR percentage might not be sufficient for accurately relating overburden geology to pillar loads and deformations. Accurately quantifying overburden strength/stiffness might require more complex input that can incorporate the relative location and thickness of strong units with respect to seam, and the width of the panel.

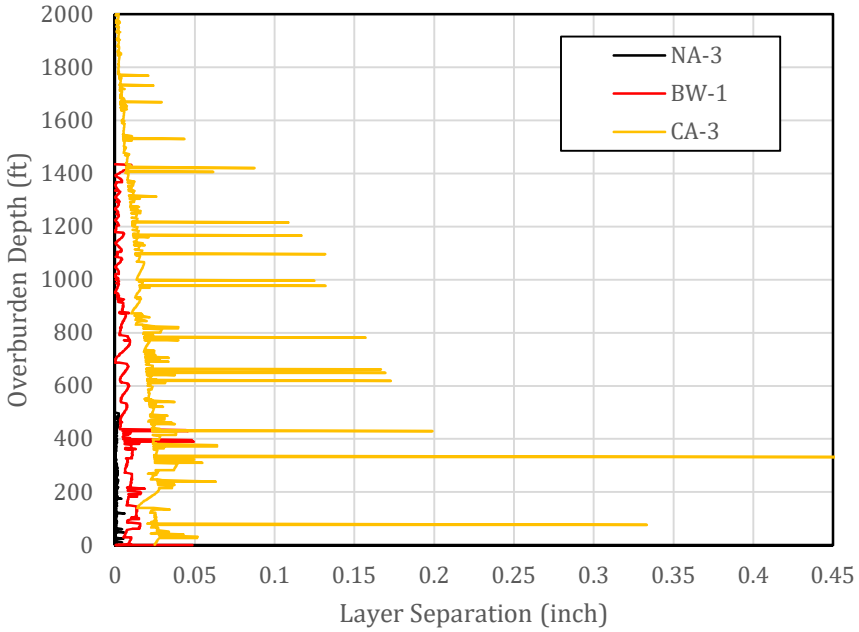

Figure 35. Separation of strong geological layers for three case study mines.

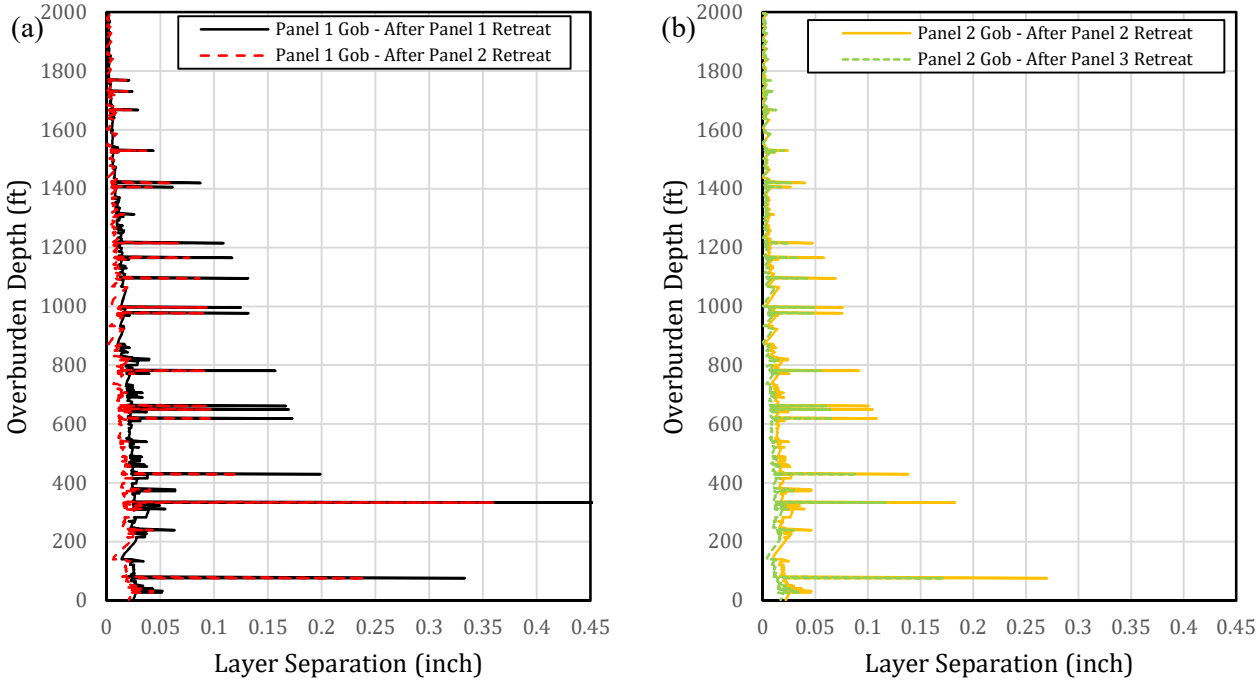

Figure 36. Separation of strong geological layers after (a) first and (b) second panel mining for mine CA-3.

Figure 36 shows the change in the overburden strata separation during the consecutive panel retreat for CA-3 mine. In Figure 36a, the black and red lines represent overburden strata separation over the first panel, after first and second panel retreat. In Figure 36b, the orange and green lines are overburden strata separations over the second panel, after second and third panel retreats. We can also see the closure of the separated strata with the consecutive panel mining.

3.4 Task 4: Development of practical loading models

The final task of this project was to develop a practical mechanistic model to allow rapid calculation of an accurate overburden response without the need to conduct a full finite-volume numerical model analyses. We used ARMPS-LAM program developed at WVU (Zhang and Heasley, 2013) as the base mechanical model, and proposed two different loading models for calibrating the strain-hardening gob of ARMPS-LAM.

As indicated in the section "*3.1 Task 1: Database development*", the field measurement database consists of three datasets, and each dataset is characterized based on the available information. The first dataset consists of 12 cases from 10 AU and 1 US longwall mines with only abutment stress measurements and geological logs with limited information. The second dataset consists of 12 cases from 12 US longwall mines with very detailed in situ measurements, geologic and operational information. The third dataset consists of 18 supplementary cases where only the mining geometry and total side abutment load were known, and not the exact stress profile or geologic information. During the development of the loading models, two different analysis methods were used: the analytical laminated overburden method and FVM.

The analytical laminated overburden method was used to analyze first dataset (with 10 AU and 1US cases) due to the nature of available information on each case in this dataset. Heasley recommended two different methods for calibrating the overburden stiffness and gob stiffness for simulating stress distribution (Heasley et al, 2010) and surface subsidence (Jian and Heasley, 2016) accurately. In addition, the laminated overburden model simulates realistic flexibility for stratified sedimentary geologies very efficiently with two overburden stiffness input parameters: elastic modulus and lamination thickness. Therefore, the laminated overburden model only requires stress profile measurements and not the detailed mechanical properties of the geological layers or subsidence profile for load analysis. Since the first data set consists of case studies with only abutment stress measurements and limited information about mechanical properties of the geologic layers, laminated overburden method is used to analyze this set.

FVM modeling methodology detailed in *section 3.2.2* works best when detailed overburden geology and mechanical properties of layers are known. In addition, verification of the method requires both subsidence and stress measurements (or at least one is measured and other should be predicted reliably). Cases in the first dataset do not have the volume of required information to use the FVM approach reliably, but the second dataset is suitable to use this approach.

Regression Analysis for Abutment Angle from analysis of first dataset with analytical laminated overburden model:

The hypothesis that there was a correlation between the stiffness of the geology and the abutment angle was tested for the first dataset. Figure 37 shows the calculated abutment angles with respect to overburden depth to panel width ratios, with the hard rock percentages as color-coded. The blue points represent the cases that have hard rock ratios were higher than 80 percent, and the yellow points represent the cases that have hard rock ratios between 50 and 80 percent. The red points represent the cases with less than 50 percent hard rock in the overlying strata. There was not any apparent significance of the percentage hard rock on the abutment angle. The only visible finding was some clustering of stronger overburden cases at lower abutment angles.

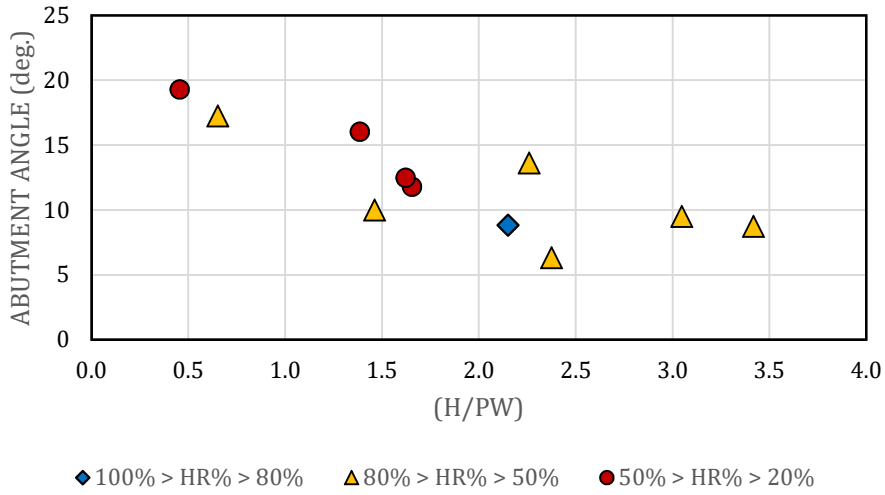

Figure 37. Abutment angles back calculated using laminated model with respect to overburden depth to panel width ratio together with hard rock percentages.

Figure 38 shows the results for the abutment angles back-calculated using the laminated model (*as explained in section 3.2.1*) together with supplementary cases. For the mines deeper than 650 ft, the abutment angle values are distributed from the maximum value of 23.4° to the minimum value of 4.7°, with the mean of 12.2°. For the mines with overburden depth less than 650 ft, the scatter is much larger, and the reason of this scatter might be related with the strong layer in the overburden geology as observed during our analysis for NA-1 and NA-2 cases (Figure 31 and Figure 33). All four cases with abutment angles higher than 30° are from Australia where thick and strong conglomerate layers are very common in the overburden geology. However due to the limited time of this project, we could not collect the required information for these cases to support this argument. Some of the variations could also be accounted for by the installation of the instrumentation, local host rock composition/strength, type of instrument and calibration errors. During the development of the loading model, it is assumed that average abutment angle of 21° is appropriate for the mines with overburden depth less than 650 due to the high success rate of ALPS and ARMPS for shallow cover cases.

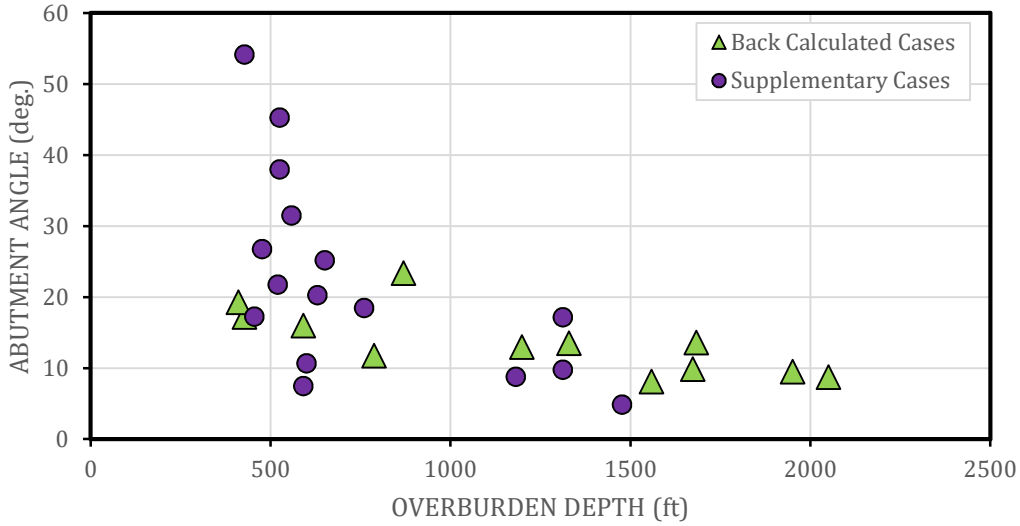

Figure 38. Determined abutment angles with respect to overburden depth.

As seen in Figure 39, there is also an apparent trend of decreasing abutment angle with increasing ratio of overburden depth to panel width (H/PW). A regression analysis to determine the abutment angle for deep cover cases (> 650 ft) was conducted. The 650 ft is selected as the limit depth, since the large data scatter occur for shallower cases. In addition, the value is reasonable to be considered as the boundary between deep and shallow mines (Mark, 2010). For the regression analysis, the H/PW ratio was found to be the most significant parameter for determining the abutment angle, and the following equation is proposed:

$$Abutment\ Angle = a \times b^{(\frac{H}{PW})} \tag{17}$$

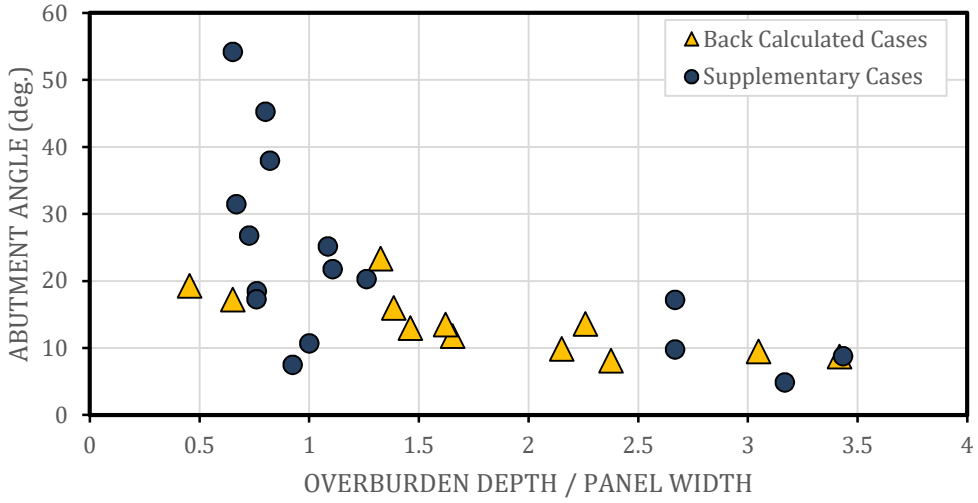

Figure 39. Determined abutment angles with respect to overburden depth to panel width ratio.

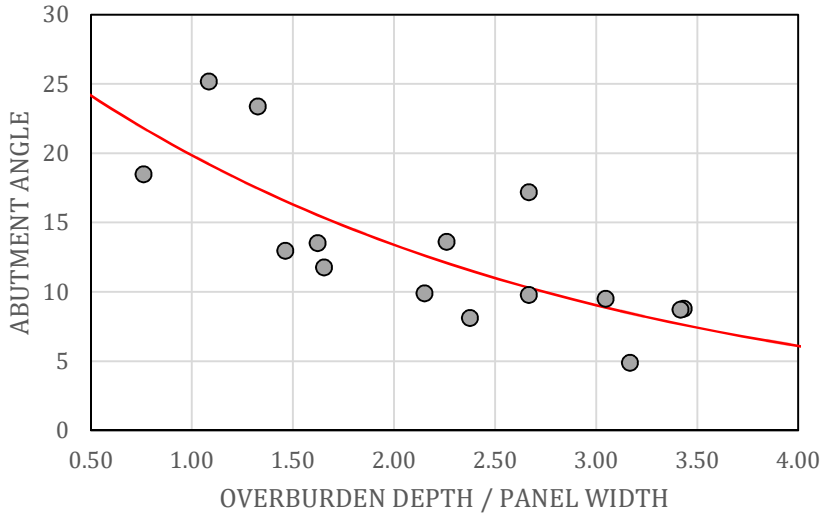

Figure 40. New abutment angle model for deep cover cases.

Table 10. Proposed abutment angle equation from analytical laminated model analysis.

Overburden Depth (H)	Abutment Angle (deg.)
H ≤ 650 ft	21°
650 ft ≤ H ≤ 2,050 ft	$29.42 \times 0.68^{(\frac{H}{PW})}$

Each data point in Figure 40 represents the cases from the first and third (supplementary) datasets where overburden depth is larger than 650 ft. Based on this field data, the proposed abutment angle determination is shown as the red line in Figure 40. When the overburden depth is less than 650 ft, a constant abutment angle of 21° is still applicable. With an overburden depth from 650 ft to 2,050 ft, an abutment angle (β) that decreases with a continuous function of the H/PW ratio is proposed (Table 10, Equation 18). This equation was derived by performing a least-square error fit to the measured abutment angles above 650 ft overburden depth. Almost all the cases deeper than 650 ft also have an H/PW ratio more than 1. The new equation should be considered applicable within the range of the case studies (0.7 < (H/PW) < 3.5).

$$Abutment\ Angle = 29.42 \times 0.68^{\left(\frac{H}{PW}\right)} \tag{18}$$

Regression Analysis for Abutment Angle from analysis of second dataset with FVM model:

For the second dataset, also there was not any statistically significant correlation between overburden loading and geology. Figure 41 shows the HR and overburden depth-to-panel width ratios of the second dataset studied in this project. In this graph, the red, orange and green horizontal dotted lines classify the weak (HR<25%), moderate (HR=35%) and strong (HR>50%) overburdens (Esterhuizen et al., 2010b). The vertical black dotted line represents the critical panel condition where case study mines on the left of this line have supercritical panels and on the right of it have subcritical panels. Overburden strength of the supercritical cases range from weak to strong. In the subcritical region, five of the six cases have strong or moderate overburden strengths. Therefore, deep and narrow panel mines in this database are generally have moderate to strong overburden strengths.

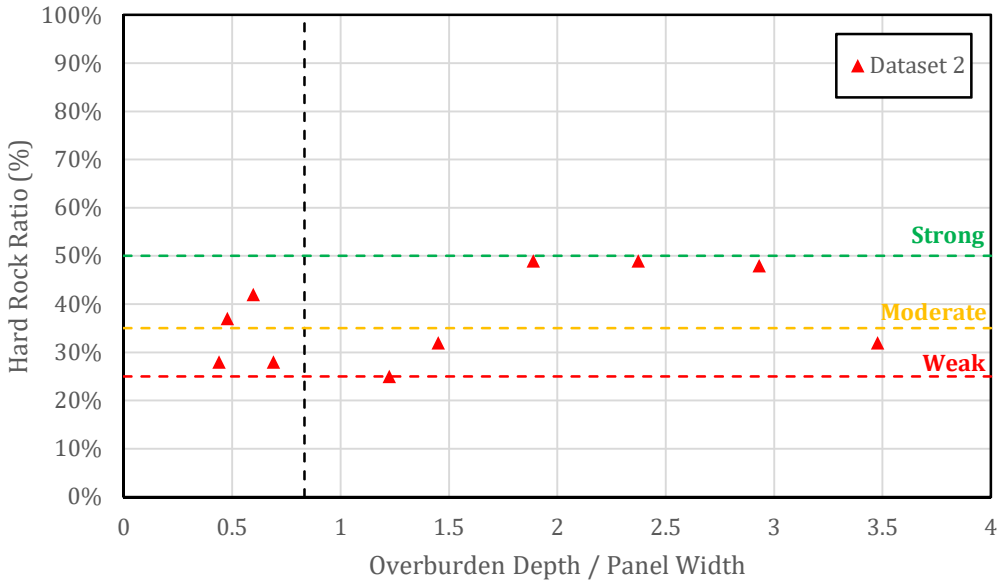

Figure 41. Second dataset HR ratio vs Overburden Depth/ Panel Width.

Figure 42 shows that there is an apparent trend of increasing abutment loads with increasing ratio of overburden depth to panel width (H/PW). This trend is analogous to the magnitudes calculated by ALPS method between H/PW ratios of 0.44 and 1.66. Therefore, for the depth to panel width ratios lower than 1.66, ALPS default abutment angle (21°) is appropriate to assume. However, after the depth to panel width ratio of 1.66, tailgate loads converge to the approximate value of 60.0%, which is a completely different trend than ALPS. Equation 19 was proposed to simulate this trend when the H/PW ratio is more than 1.66.

$$Abutment\ Angle = 34.51 \times \left(\frac{H}{PW}\right)^{-0.96} \tag{19}$$

Table 11 shows the proposed abutment angle equation from FVM analysis of the second dataset and black dotted line in Figure 42 shows the abutment angles predicted by this equation relative to overburden depth-to-panel width ratio.

Table 11. Proposed abutment angle equation from FVM model analysis.

Overburden Depth / Panel Width (H)	Abutment Angle (deg.)
H/PW ≤ 1.66	21°
H/PW > 1.66	$\beta = 34.51 \times \left(\frac{H}{PW}\right)^{-0.96}$

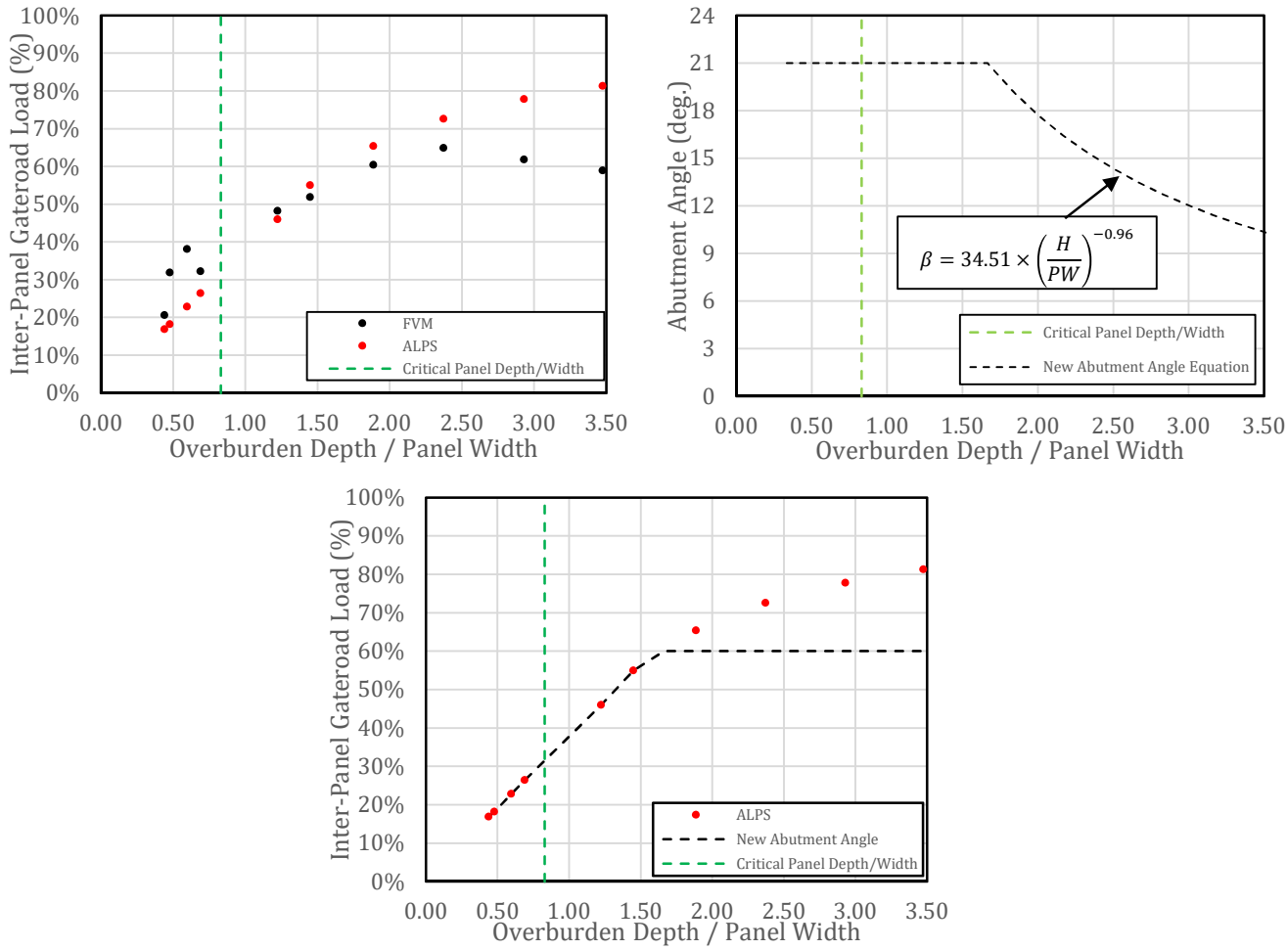

Figure 42. Proposed abutment angle equation from FVM analysis.

Testing the effectiveness of new proposed abutment angle equations with ARMPS-LAM:

Proposed abutment angle equations were programmed into ARMPS-LAM, and to confirm their applicability, the new abutment angle equations were tested on the case histories that were used for the development of the ARMPS2010 design criteria. The database used for the analysis includes the 215 deep cover case histories that utilize barrier pillars, of which 185 were successful and 33 were failed case histories. The analyses aimed to compare the classification success of the new abutment angle equations with each other, first. In the "*Research Findings and Accomplishments Section*", ARMPS-LAM classification success results were compared with ARMPS2010 design

criteria. In order to be consistent in comparison, the failure classification rate of the ARMPS2010 design criteria is matched and success classification rates of equations are compared.

Both Active Mining Zone (AMZ) and Barrier Pillar (BP) safety factor (SF) values were calculated for the same 215 cases using ARMPS-LAM. A minimum of 88% accurate failure classification is targeted for the limit SF values to be considered. That failure classification accuracy is achieved with an AMZ SF of 1.45 and BP SF of 2.2 when we implemented Equation 18 (Figure 43) and AMZ SF of 1.33 and BP SF of 2.33 for Equation 19 (Figure 44). Successful classification accuracy of 46% for Equation 18 and 52.7% for Equation 19 (Table 12) is achieved as a result of the analysis.

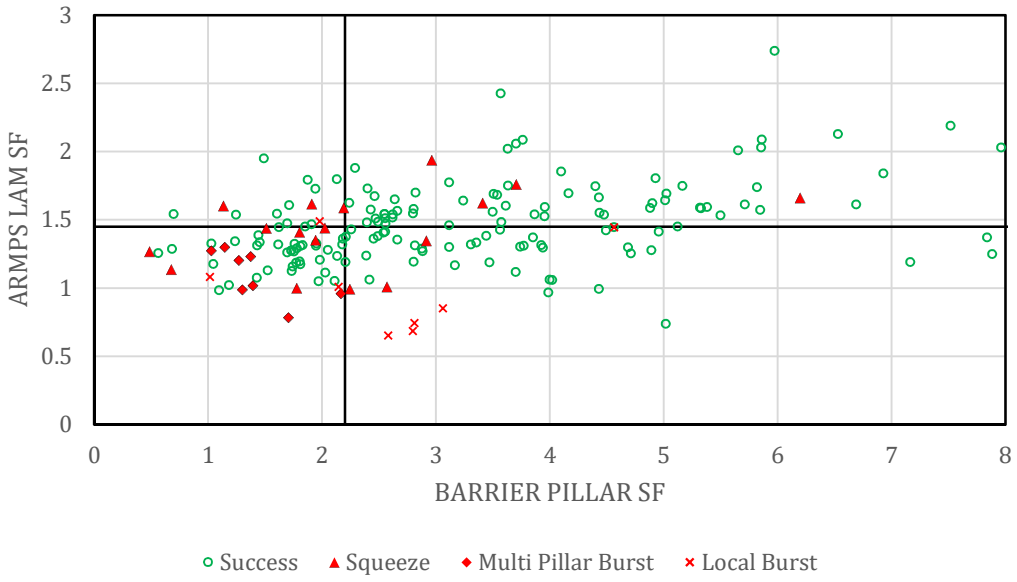

Figure 43. ARMPS-LAM classification for deep cover cases using Equation 18.

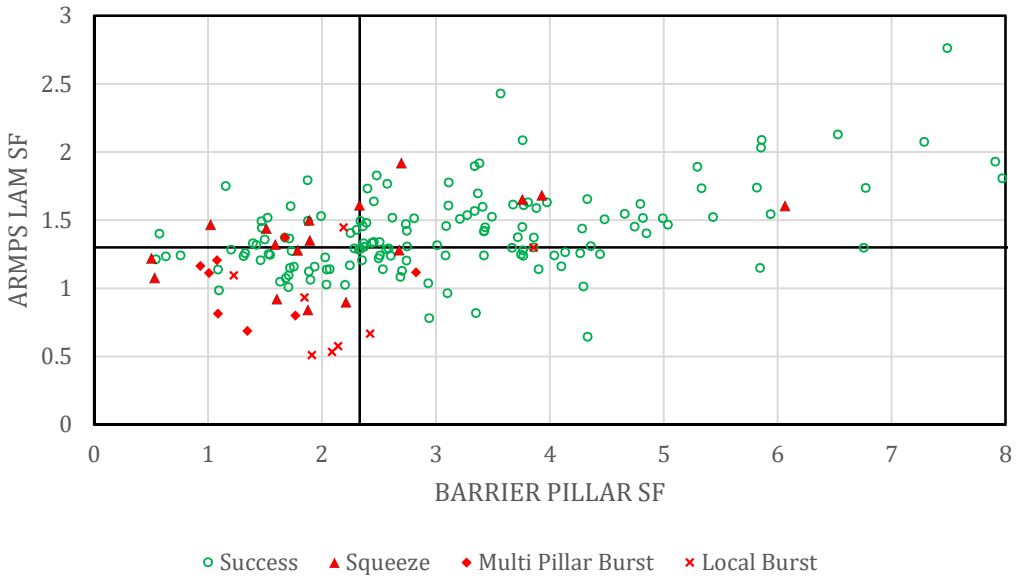

Figure 44. ARMPS-LAM classification for deep cover cases using Equation 19.

Table 12. Classification accuracies for proposed abutment angle equations.

			ARMPS-LAM Equation 18	***ARMPS-LAM Equation 19***
	No. of Cases	*Failure Classification Accuracy*	*Success Classification Accuracy*	*Success Classification Accuracy*
Deep Cover Cases with Barrier Pillar	215	87.9%	46.2%	52.7%

In the next section, "*Research Findings and Accomplishments*", classification success results presented in this section were compared with ARMPS2010 design criteria. Standard ARMPS2010 AMZ and BP stability factor to separate successful designs from unsuccessful ones is 1.5. During the analysis of ARMPS-LAM classification accuracies presented in Table 12, AMZ and BP stability factors were 1.45 and 2.2 for Equation 18 (Figure 43), and 1.33 and 2.33 for Equation 19 (Figure 44), respectively. Higher BP stability factors used to separate successful and unsuccessful cases during the analysis of ARMPS-LAM classification accuracies doesn't mean that larger barrier pillars are required for the successful design, in contrast it means that ARMPS 2010 estimates higher overburden loads on the barrier pillars compared to ARMPS-LAM.

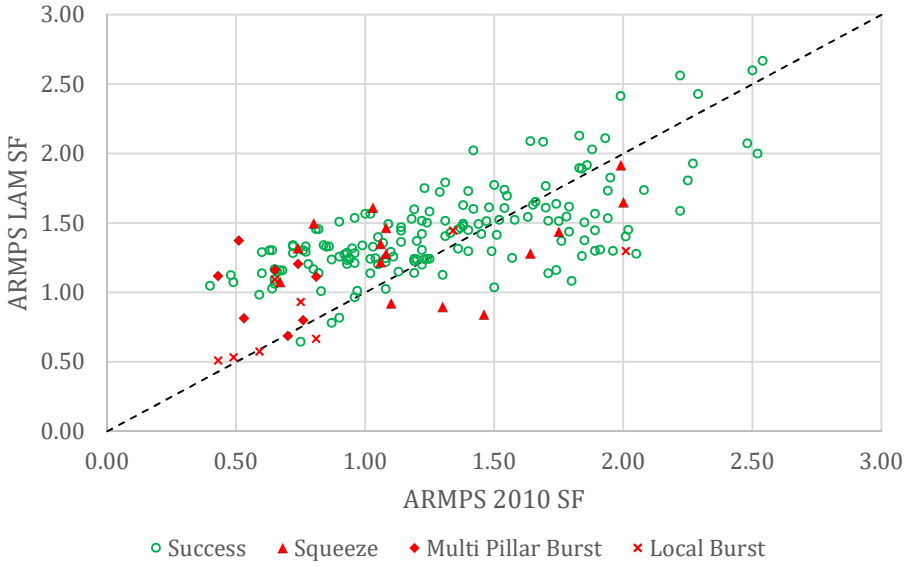

Figure 45. Comparison of AMZ safety factors calculated by ARMPS-LAM (with Equation 19) and ARMPS 2010.

Figure 45 compares the AMZ SF calculated by ARMPS-LAM with Equation 19 and ARMPS 2010. Vertical axis is the AMZ SF calculated by ARMPS-LAM and horizontal axis is the SF calculated by ARMPS 2010. Black dotted line is represented by the equation "**y=x**". Therefore, on this line, the SF calculated by ARMPS-LAM and ARMPS 2010 are equal. If any data point is below this line, the ARMPS 2010 SF is larger than ARMPS-LAM SF and vice versa for any data point above this line. Since both ARMPS 2010 and ARMPS-LAM use the Mark-Bieniawski pillar strength equation to calculate the load bearing capacity of the pillars, the AMZ load calculated by ARMPS2010 is lower than the one calculated by ARMPS-LAM for any data point below the dotted line and vice versa for any data point above this line. In Figure 45, approximately 70% of the successful and unsuccessful cases are above the dotted line which means that for the 70% of the cases, ARMPS-LAM calculates loads transferred to the AMZ less than ARMPS 2010. Therefore, for these cases overburden loads are either transferred to gob or barrier pillars.

Figure 46 compares the barrier pillar SF calculated by ARMPS-LAM with Equation 19 and ARMPS 2010. Vertical axis is the barrier pillar SF calculated by ARMPS-LAM and horizontal axis is the SF calculated by ARMPS 2010. Th eblack dotted line is represented by the equation "**y=x**". Approximately 95% of all the cases in Figure 46 are above the dotted line which indicates that ARMPS-LAM calculates overburden load on barrier pillars less than

ARMPS2010. Therefore, considering the results presented in Figure 45, for the 70% of the cases, ARMPS-LAM estimates more load on the gob and for the remaining 30% of the cases, ARMPS-LAM estimates more load on the AMZ.

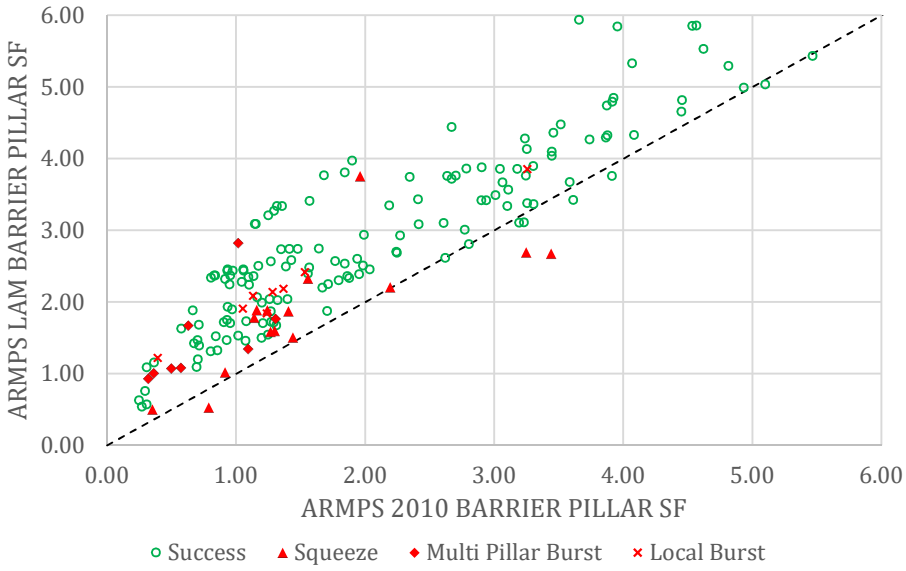

Figure 46. Comparison of barrier pillar safety factors calculated by ARMPS-LAM (with Equation 19) and ARMPS 2010.

4.0 Research Findings and Accomplishments:

The objectives of this research are (i) to understand the mechanistic behavior of the overburden under different geologic and in situ stress environments and (ii) to transfer this new mechanism to the ARMPS-LAM program and verify its effectiveness. Research findings and accomplishments are summarized by classifying them into the following two categories relating to the objectives of this research: (i) overburden loading mechanism under deep and strong cover mining and (ii) new overburden loading models.

4.1 Overburden loading mechanism under deep and strong cover mining:

An important technical accomplishment in this project is bringing a rational explanation to the lower abutment angles observed in deep mines (Colwell et al., 1999; Tulu and Heasley, 2012). To the PI's knowledge there is only one hypothesis proposed to explain this behavior by Heasley (2000). In his study, Heasley used an analytical laminated overburden model and showed that the percentage of overburden loads carried by abutments should be constant or even decrease with depth. Pursuing this hypothesis, Tulu and Heasley (2012) analyzed the field measurement data from deep Australian and USA longwall mines and proposed a new abutment angle equation that reduces the practical abutment angle with depth. In this approach, again the mechanical overburden model in LaModel was used, and the new abutment angle equation implies that as the mining depth increases, the percentage of overburden loads carried by the gob also increases. In his analysis, Heasley (2000) assumed constant overburden geology and gob input parameters for different overburden depths. In another study, Esterhuizen et al. (2010a) studied the influence of overburden geology, panel width and depth on overburden load distribution.

Esterhuizen et al. used calibrated FVM models and a ground response modeling approach to investigate the effect of depth and overburden geology on pillar loading. They calibrated the response of the FVM model with the stress and subsidence measurements from shallow and deep longwall mines (Esterhuizen et al., 2010b). Esterhuizen et al. (2010a) showed that the stress transferred to the abutments due to arching is higher for deep and narrow panels compared to shallow and wide panels which implies that percentage of overburden load carried by abutments are higher for deep and narrow panels. It is also important to note that in Esterhuizen et al., deep mines also had stiffer and stronger overburden geologies compared to shallow mines. This study falls short on explaining why lower abutment angles are observed in deep mines (Colwell et al., 1999; Tulu and Heasley, 2012).

It was found during the research documented in this report that the contradicting mechanisms proposed by Heasley (2000) and Esterhuizen et al. (2010) are missing the effect of consecutive panel mining on the response of the overburden in deep mines. Heasley's analyses with the laminated overburden model were performed on single panels. Esterhuizen et al. (2010a, 2010b) analysis also only considered up to two panels during the simulation of loads transferred to the abutments. Another weakness of the analyses was due to the simplification of the overburden geologies used during these studies. One of the fundamental assumption of the laminated overburden model is continuous vertical displacement within the overburden strata meaning that separation of the laminated layers cannot happen. Therefore, overburden rockmass properties; "elastic modulus and lamination thickness", represent the average behavior of the overburden. This is a practical and valid approach considering the extremely complex nature of the overburden geology and should be used during the design stages. However, this assumption also influenced the results of Heasley (2000) and later Tulu and Heasley (2012) analyses. Esterhuizen et al. (2010a, 2010b) simulated a more complex overburden geology during his FVM analysis, but the geology in these models was also simplified due to the impracticality of modeling each geological layer with a 3D FVM model.

Analysis of the field measurements from the 12 US longwall mines with the calibrated FVM models reveals a new understanding of the response of the strong overburden in deep mines. In deep mines, the overburden strata above the adjacent panels are influenced by the mining of the neighboring panels up to five consecutive panel mining (or more) depending on the overburden-depth to panel-width ratio. This behavior can be observed from subsidence profiles of deep and narrow panels. Figure 47 shows the subsidence profile of the deep case study mine CA-1 for mining of five successive panels. Extraction of second panel resulted in significant incremental subsidence over the first panel, and the vertical surface displacement over the first panel continued to increase during the extraction of next three panels, though at a diminishing rate. As seen in Figure 47, extraction of the second panel resulted in an

asymmetric subsidence profile and this asymmetric profile continues to be observed during the extraction of the successive panels.

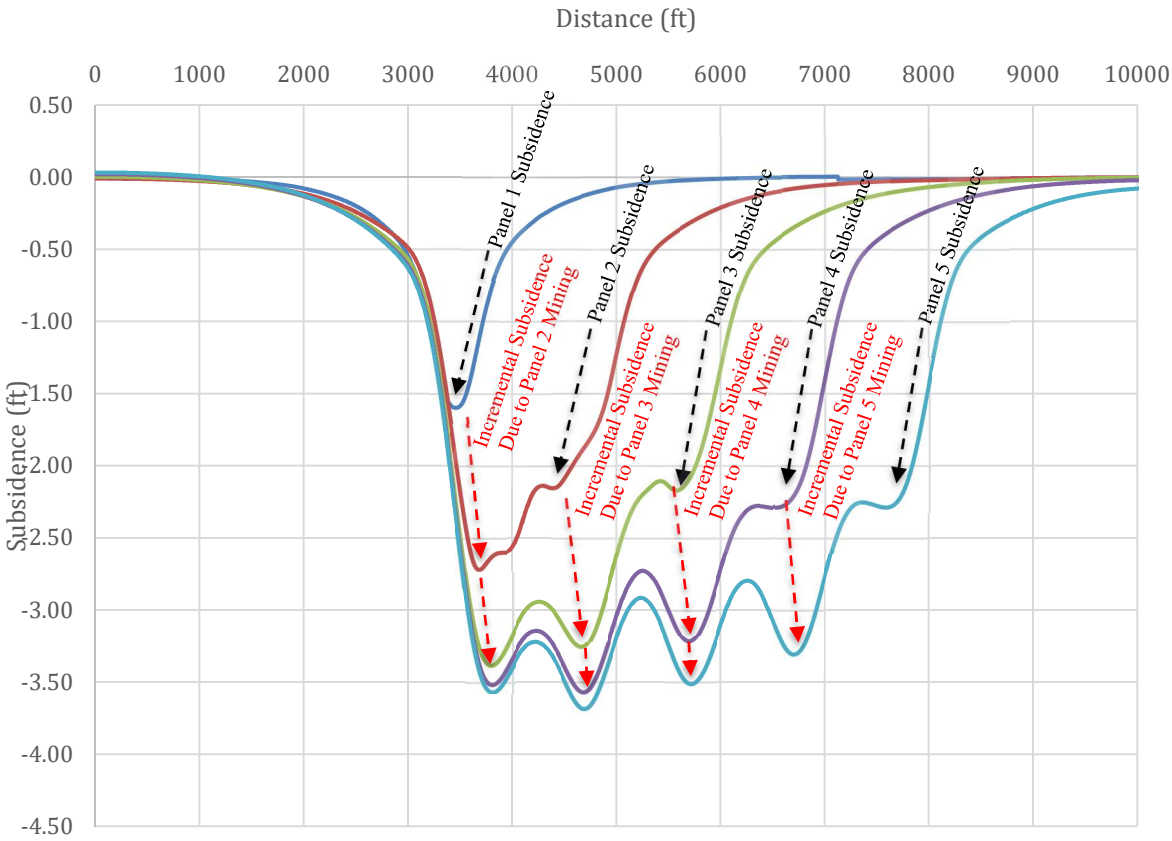

Figure 47. Subsidence profile of case study mine CA-1 up to five consecutive panel mining.

The incremental vertical displacement and the resulting asymmetric subsidence profile seen in deep and narrow panels implies that (i) gobs and pillar systems of neighboring panels in deep mines share the mining induced overburden loads for up to five panels, depending on the overburden depth to panel width ratio and (ii) the support provided to the response of the overburden by the gobs and pillar systems of the adjacent panels are not symmetric. Figure 48 shows the dimensionless overburden load distribution for mine CA-1 after the extraction of fifth panel as calculated by FVM. Analogous to the subsidence profile in Figure 47, the second panel gob has the largest and the fifth panel gob has the smallest gob loads. Similarly, inter-panel gateroads between the first and second gobs has the largest, and the fourth and fifth gobs has the smallest gateroad loads.

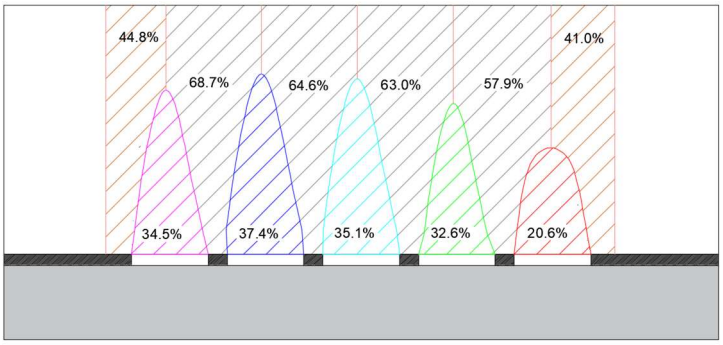

Figure 48. Dimensionless overburden load distribution of case study mine CA-1 after the extraction of panel five.

The incremental vertical displacement over the adjacent panels during the consecutive panel extraction also resulted in an increase in loads carried by the gobs of the previously extracted panels. Figure 49 shows the increase in gob loads of each panel during the successive panel extraction for CA-1. The red bar represents the gob load estimated by the ALPS method. Extraction of the first panel resulted in a lower load on its gob (black bar) when compared with ALPS method. This result is parallel to the outcome of Esterhuizen et al. (2010b), where a large portion of the overburden load is transferred to the abutments in deep and narrow panels. Extraction of the second panel resulted in large step increase in the first gob load (orange bar), analogous to the subsidence increment (Figure 47). Similar to the subsidence profile, the gob load of the first panel increases in increments (with diminishing rate) during the extraction of next four panels. These results are parallel to the hypothesis of Heasley (2000), where the overburden load carried by the gob in deep mines is higher than that estimated by ALPS.

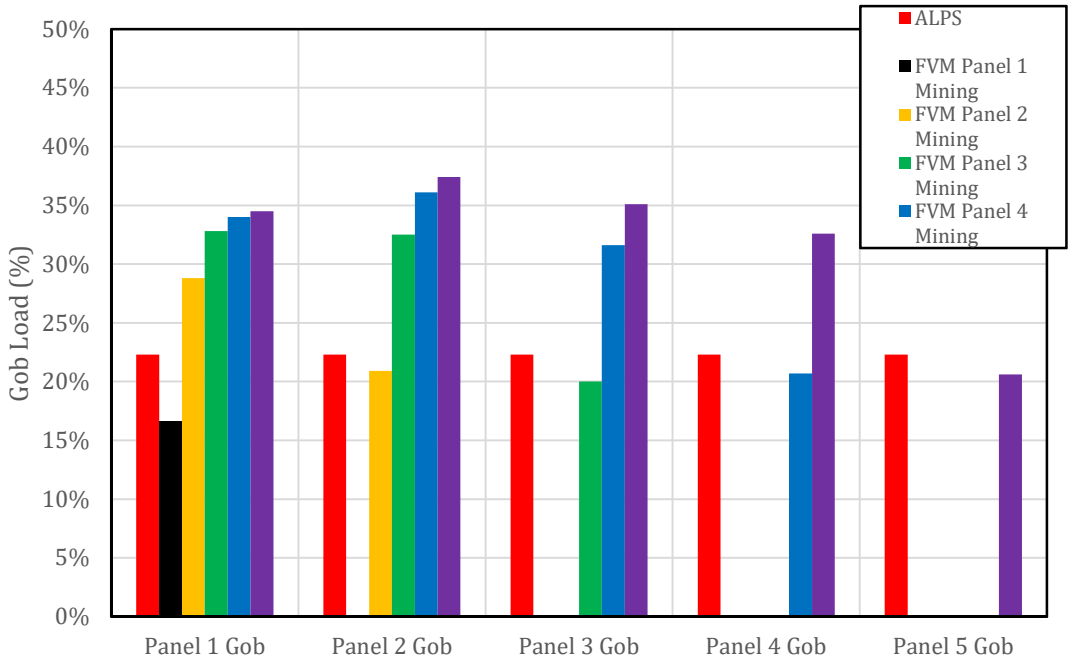

Figure 49. Dimensionless gob load distribution of case study mine CA-1 up to five consecutive panel mining.

Therefore, the FVM analysis of the deep mines (with narrow panels) indicates that the remnant structures of the prior panels provide a considerable amount of support to the overburden strata and prevents elevation of the percentage of overburden loads transferred to the active panel workings. Of course this is only possible with appropriate panel and gateroad pillar system (or barrier pillar in retreat mines) designs. This resultant load distribution on the active panel pillars during consecutive panel retreat can be simulated with LaModel if the overburden and gob input properties are calibrated accordingly.

4.2 New overburden loading models:

An important practical accomplishment in this project is the development of new overburden loading models and the ability to incorporate these models into the LaModel and ARMPS-LAM programs. Therefore, the results of this study are immediately available for the mining industry, MSHA and NIOSH to evaluate and consider for application in the ground control approval process.

The analyses in this section aimed to verify the applicability of the new abutment angle equations developed during this research by comparing them against the classification success of the ARMPS2010 design criteria and showing the effectiveness of these new approaches. In this comparison, the failure classification rates of the ARMPS2010 design criteria were matched and then the "successful" classification rates were used to compare the effectiveness of the different methods.

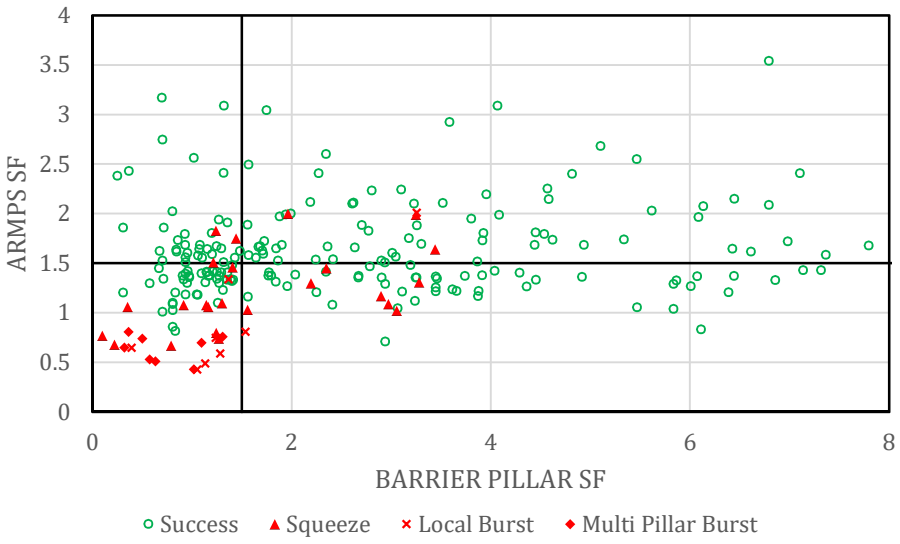

Figure 50. ARMPS2010 classification for deep cover cases.

Figure 50 shows the ARMPS classification for the 215 deep cover cases in the ARMPS database. These cases were analyzed using the default 21° abutment angle and the standard ARMPS2010 design criteria that use a value of 1.5 for both the ARMPS2010 SF and the barrier pillar stability factor (BP SF). The ARMPS2010 design criteria correctly predicted 29 of the 33 failures (88%) and 61 of the 182 successful cases (33.5%). Out of the 4 failures that were falsely predicted as successes, one of them was a local pillar burst, and the other three were pillar squeezes (Figure 50). As seen in Figures 43 and 44, both of the ARMPS-LAM methods with the new abutment angle calculations only misclassified pillar squeezes, where the ARMPS2010 design criteria misclassified a local burst failure in addition to pillar squeezes. Although pillar squeezes cause hazardous situations, the fact that they develop slowly (where collapses and bursts occur with little or no warning) makes it easier to react to the situation and abandon the area (Mark, 2010).

Table 13 compares the classification accuracies for ARMPS2010 and ARMPS-LAM method with the new proposed abutment angles. Equation 18 improves the classification accuracy of the deep cover cases by 13% and equation 19 improves the classification by 19%. These improvements are significant for the design of the deep cover mines and provides evidence to support the overburden mechanism detailed in the previous accomplishment. The major difference between the Equation 18 and 19 is that Equation 18 implies that the percentage of overburden loads carried by abutments are decreasing with depth, but equation 19 implies that they are constant with increasing depth ratio. Since equation 19 improves classification better than equation 18, it is also an important support for the hypothesis that the percentage of overburden loads distributed to the abutments stays constant or increases for deep cover mines with appropriate panel widths and gateroad or barrier pillar designs.

Table 13. Classification accuracies for ARMPS2010 and ARMPS-LAM with proposed abutment angles.

		Deep Cover Cases with Barrier Pillar	
	No. of Cases	*Failure Classification Accuracy*	*Success Classification Accuracy*
ARMPS2010	215	87.9%	33.5% (Figure 50)
ARMPS-LAM (Equation 18)			46.2% (Figure 43)
ARMPS-LAM (Equation 19)			52.7% (Figure 44)

5.0 Publication Record and Dissemination Efforts:

5.1 Presentations and papers:

1. Ph.D. student Deniz Tuncay introduced this project in 2019 SME conference student poster competition.
   Title: *Analysis of Overburden Load Transfer Mechanics using Ground Reslponse Curve Modeling Approach.*
2. Ph.D. student Deniz Tuncay presented the initial results of this project in 2019 Langwall USA Exhibition and Conference student poster contest. He also received the third place in this competition.
   Title: *Investigating Load Distribution in Longwall Mines using Ground Response Curve Modeling Approach.*
3. Ph.D. student Deniz Tuncay and I.B. Tulu (PI) published a paper introducing the initial results of this project in the ARMA 2019 conference.
   Title: *A New Abutment Angle Equation for Deep Cover Coal Mines.*
4. I.B. Tulu (PI), Deniz Tuncay (PhD students), Haozhen Zhao (PhD students) and Sena Cicek (MS student) published a paper on interim results of this project in the 2019 SME International Ground Control Conference.
   Title: *Application of eh Ground Response Curve for Understanding Overburden Load Transfer Mechanism.*
5. Ph.D. student Deniz Tuncay and I.B. Tulu (PI) published a paper in the 2019 SME International Ground Control Conference. This paper is invited to ***the 2020 SME Best of Ground Control*** session. Also, published in the ***International Journal of Mining Since and Technology***.
   Title: *Analysis of ARMPS2010 database with LaModel and an updated abutment angle equation.*
6. Ph.D. student Deniz Tuncay and I.B. Tulu (PI) will publish a paper on the results of this project in 2020 ARMA conference.
   Title: *Verification of 3D Modeling Approach for Longwall Mines with a Case Study Mine from The Northern Appalachian Coal Fields.*
7. Ph.D. student Haochen Zhao and I.B. Tulu (PI) will publish a paper on the results of this project in 2020 ARMA conference.
   Title: *Verification of Methodology to Investigation of Potential Factors Influencing Stress Redistribution at Deep Western U.S. Longwall Mines.*

5.1 A practical design software:

A major output of this project is the new overburden loading equations to simulate the overburden loads transferred to the abutments and gob. These equations have been implemented into the ARMPS-LAM software. This software and the data collected during this research have been archived in network storage system at WVU. This data and software can be made available to the Alpha Foundation upon request.

6.0 Conclusions and Impact Assessment:

The research presented in this report has produced a number of significant results that will undoubtedly raise the quality of mine design in the United States in the future, particularly for deep cover, pillar retreat and longwall mines. During this research study, a database of 40 field-monitoring cases from the USA and Australian mines was developed. 12 of these cases were from the USA coal fields: Northern Appalachia (6), Central Appalachia (3), Black Warrior (1) and the Western USA (2). This large database was analyzed with an analytical laminated overburden model and FVM modeling approaches and, a new abutment angle equation that can better simulate the distribution of the overburden loads in deep cover mines was proposed. The ARMPS-LAM program developed at WVU was used as the mechanical overburden tool and the new equation was programmed into the ARMPS-LAM program.

The Effectiveness of the new equation was tested with 215 deep cover cases from the ARMPS database. The classification accuracy of the new abutment angle equation implemented into ARMPS-LAM was compared against the accuracy of ARMPS2010. The results of this comparison show that the new loading equation together with ARMPS-LAM improves the ARMPS2010 success classification accuracy from 33.5% to 52.7%. This research project produced the following equation to predict the overburden load distribution in deep mines.

Overburden Depth (H) / Panel Width (PW)	*Abutment Angle (deg.)*
H/PW ≤ 1.66	21°
H/PW > 1.66	$\beta = 34.51 \times \left(\frac{H}{PW}\right)^{-0.96}$

The research presented in this report also offers a rational explanation for the lower abutment angles (compared to default 21^0) observed in mines deeper than 650 ft and overburden depth to panel width ratios larger than 1.66. Remnant structures (gob, barrier pillars or gateroad pillar systems) of prior panels provide considerable support to the response of the overburden strata in deep mines. The support provided by the remnant structures of the prior panels keep the percentage of overburden loads transferred to the abutments of the active panel constant when the depth to panel width ratio is larger than a threshold value (in this study, the threshold value is estimated as 1.66).

Findings of this research also indicate the importance of the size of the barrier pillars on global stability during the design of deep panels as Mark (2010) previously indicated. However, results of this study also imply that it is possible to develop safe and economical panel design by including the support provided by remnant structures of the prior panels to the design of deep cover panels rather than only increasing the barrier pillar sizes. Finally, the practical design tool and methods developed during this research are immediately available to the coal mining industry, Mine Safety and Health Administration (MSHA) and National Institute for Occupational Safety and Health (NIOSH) to evaluate and consider for application in the ground control approval process.

7.0 Recommendations for Future Work:

7.1 Better incorporating specific overburden geology into mine design

With regards to incorporating specific geology into mine design, we have demonstrated the influence of the strong beds in the overburden on the response of strata and load distribution. Although, this research project had an extensive database of field measurement cases, a statistically significant correlation between hard rock (HR) percentage and overburden loading was not found, potentially due to the similarity of the HR in the field cases. Due to the short period of this exploratory research study, we choses to use the simple HR percentage in the overburden to represent strength and stiffness of the overburden. Certainly, other, possibly more complex, stiffness calculation methods may produce better results. The results presented in section "*3.3.2*" under the title *"Mechanical Response of the Overburden"* showed that quantifying the average strength and stiffness of the overburden needs to include, not only the thickness of the strong beds, but also the relative location of the strong bed in the overburden and width of the panel. Figure 34 showed that panel depth to width ratio impacts the stiffness of the overburden significantly. In addition, the critical stress required to induce strong layer failure is proportional with the square of the layer span and inversely proportional with the square of the layer thickness (Galvin, 1981). Therefore, span of the strong layers also need to be included into the assessment of the competence of the overburden strata.

With respect to incorporating specific geology into the design, we would like to pursue using thin plate theory to compute the average strength and stiffness of the overburden by incorporating thickness, panel width and location of the bed relative to seam. Salamon et al. (1972) derived the simple elastic thin plate model to estimate the span required to break a dolerite sill. Later, Galvin (1981) improved this model by including the parting distance between coal seam and the base of the dolerite sill, the caving of the immediate roof between the dolerite layer and the coal seam, and the effect of overburden stiffness on the load applied to dolerite. We propose to apply a similar approach to calculate the average "Hard Rock Influence Factor (HRIF)" of the overburden strata. HRIF will be a function of rock type, layer thickness, panel width and the location of the layer within the overburden.

Since calculations of an average HRIF value will be either analytical, or will be solved as a boundary value problem, this new method would be transferred into a practical design tool easily. In addition, we would like to collect and compile the necessary additional data to fully analyze an additional 9 AU case studies with the FVM and full 3D LaModel. During this study, we also collected the necessary additional information from 3 active US coal mines (2 room-and-pillar and 1 longwall) and in the near future we will collect the necessary information from 3 more active longwall mines to include into the FVM analysis. With these new cases, we would like to increase the first dataset from 12 cases to 27 cases.

7.2 Improving overburden loading models by incorporating 3D panel geometries

With regards to improving overburden loading models, we have produced a new equation to predict the distribution of the overburden loads in deep mines. We programed this new equation to the ARMPS-LAM program and also tested the effectiveness of this equation with 215 deep cover cases from the ARMPS database. The new equation improved the classification accuracy by 19%.

With respect to improving loading models further, we would like to use our current datasets (with new additions) to study the 3D stress distributions to improve understanding of load concentration near the longwall tailgate T-junction split, and active panel loading condition in the retreat room-and-pillar mines. A full 3D modeling approach has recently been used to simulate three longwall mines from the USA (Klemetti et al., 2019a, Klemetti et al., 2019b, Van dyke et al., 2020). Our field measurement data sets already include the 3D load distribution data. We will use 3D FVM models and LaModel to study the influence of the specific overburden geology on the 3D load distribution near the longwall and room-and-pillar retreat face. Calibrated FVM models will be used to investigate the geology dependent mechanisms of the loading in this region. Depending on the caved, fractured and continuous strata properties, the 3D load distribution of the gob will be investigated. Results of this study will be used to improve the calibration of the strain-hardening gob properties of the LaModel to simulate geology dependent 3D load distributions near the face. Also, any new and improved loading models will be incorporate in to the ARMPS-LAM program.

In addition, we would like to investigate the influence of the barrier pillar size on the overburden load distribution for deep mines, and improve the ARMPS-LAM input to incorporate up to five consecutive panel mining into the design. The result of this research is also applicable to longwall mine gateroad stability analysis. We would like to program an "ALPS-LAM" to incorporate the new improved overburden model into the analysis of the longwall pillar stability (ALPS).

8.0 References:

Allgaier, F. (1988). Surface subsidence over longwall panels in the western united states. Dever, Colorado: U.S. Bureau of Mines.

Allgaier, F. K. (1988). Surface subsidence over longwall panels in the western united states-final results at the deer creek mine, utah. U.S. Bureau of Mines.

Agioutantis Z. and M. Karmis (2017), Quick Reference Guide and Working Examples, SDPS for Windows, version6.2J.

Building america. (n.d.). Retrieved 02 05, 2020, from https://www.uprr.com/customers/energy/coal/colorado/elkcreek.shtml

Barczak, T.M., 2017. Research developments that contributed to the landscape of longwall roof support design over the past 25 years. *Advances in Coal Mine Ground Control*, *Pages* 1-34

Bieniawski, Z.T. 1981. Improved Design of Coal Pillars for U.S. Mining Conditions. *Proceedings of the 1st International Conference on Ground Control in Mining, West Virginia University, Morgantown, WV, July, pp. 13-22*

Campoli, A., Barton, T., Van Dyke, F., and Gauna, M. (1993). Gob and gate road reaction to longwall mining in bump-prone strata. Report of Investigations 9445 (Bureau of Mines).

Colwell, M., R. Frith and C. Mark. 1999. Analysis of Longwall Tailgate Serviceability (ALTS): A Chain Pillar Design Methodology for Australian Conditions. *In Proceedings of the Second International Workshop on Coal Pillar Mechanics and Design, NIOSH: IC 9448, pp. 33-48.*

Dolinar, D.R., 2003, August. Variation of horizontal stresses and strains in mines in bedded deposits in the eastern and midwestern United States. In *Proceedings of the 22nd International Conference on Ground Control in Mining, Morgantown, WV* (pp. 178-185).

Esterhuizen, E., C. Mark and M. Murphy. 2010a. The Ground Response Curve and Its Impact on Pillar Loading in Coal Mines. *In Proceedings of the 3rdInternational Workshop on Coal Pillar Mechanics and Design, U.S. NIOSH, pp. 123-131.*

Esterhuizen, E., Mark, C. and Murphy, M.M. 2010b. July. Numerical model calibration for simulating coal pillars, gob and overburden response. *In Proceeding of the 29th international conference on ground control in mining, Morgantown, WV* (pp. 46-57).

Esterhuizen, G.S. and Tulu, I.B., 2015, November. Rapid Assessment of Roof Stability in Coal Mine Entries Based on the Outcome of Validated Numerical Models. In *49th US Rock Mechanics/Geomechanics Symposium*. American Rock Mechanics Association.

Frith, R. and Reed G. (2017). "Coal Pillar Design When Considered As An Overburden Reinforcement Rather Than Suspension Problem." In: *Proceedings of the 36th International Conference on Ground Control in Mining*. Morgantown, WV: West Virginia University, pp. 1–11.

Galvin, James Maurice. "The mining of South African thick coal seams: rock mechanics and mining considerations." PhD diss., 1981.

Galvin, J. M. 2010. The UNSW Pillar Design Methodology and Considerations for Using This and Other Empirical Pillar System Design Approaches. *In Proceedings of the 3rdInternational Workshop on Coal Pillar Mechanics and Design, U.S. NIOSH, pp. 19-29.*

Galvin, J.M., 2016. Ground engineering-principles and practices for underground coal mining. *Springer.*

Heasley, K.A. 1998. Numerical Modeling of Coal Mines with a Laminated Displacement-Discontinuity Code. *Ph.D. Dissertation, Colorado School of Mines, May.*

Heasley, K.A., M.M. Sears, I.B. Tulu, C.H. Calderon-Arteaga, and L.W. Jimison II. 2010 Calibrating the LaModel Program for Deep Cover Pillar Retreat Coal Mining. *Proceedings of the 3rd International Workshop on Coal Pillar Mechanics and Design, Morgantown WV, July 26, pp. 47-57.*

Hoek E, Brown ET. Underground excavations in rock. *London: Inst. Min. Metallurgy*; 1980. p. 527.

Karmis, M., Jarosz, A. and Agioutantis, Z., 1989. Predicting subsidence with a computer. *Coal*, *26*(12), pp.54-61.

Klemetti, T., Van Dyke, M., Tulu, I., Tuncay, D., Wickline, J., & Compton, C. (2019a). Longwall Gateroad Yield Pillar Response and Model Verification - A Case Study. 53rd US Rock Mechanics/Geomechanics Symposium. New York City.

Klemetti, T., Van Dyke, M., Tulu, I., & Tuncay, D. (2019b). A Case Study of the Stability of a Non-typical Bleeder Entry System at a U.S. Longwall Mine. Proceedings of the 38th International Conference on Ground Control in Mining. Morgantown WV.

Klemetti, T., Van Dyke, M., & Tulu, I. (2018). Deep cover bleeder entry performance and support loading: A case study. International Journal of Mining Science and Technology, 85-93.

Mark, C. and F.E. Chase. 1997. Analysis of Retreat Mining Pillar Stability. *Paper in New Technology for Ground Control in Retreat Mining: Proceedings of the NIOSH Technology Transfer Seminar. NIOSH IC 9446, pp. 17-34.*

Mark, C., 2010. ARMPS 2010: Pillar Design for Deep Cover Retreat Mining. *In Proceedings of the Second International Workshop on Coal Pillar Mechanics and Design, NIOSH, pp. 106-122* .

Mark, C., 1992. Analysis of Longwall Pillar Stability (ALPS): an update. *In Proceedings of the Workshop on Coal Pillar Mechanics and Design. BuMines IC 9315, pp. 238-249.*

Mohamed, K.M., Tulu, I.B. and Murphy, M.M., 2016, July. Numerical model calibration for simulating coal ribs. In *Proceedings of the 35th International Conference on Ground Control in Mining. Morgantown, WV, University of West Virginia* (pp. 289-298).

MSHA. (2007). Report of Investigation for Fatal Underground Coal Burst Accidens in Crandall Canyon Mine . Department of Labor Mine Safety and Health Adminstration.

MSHA. (2019, March). *Accident Injuries Data Set.* Retrieved from https://arlweb.msha.gov/OpenGovernmentData/OGIMSHA.asp

MSHA. (2020). Mine Data Retrieval System. Retrieved 02 05, 2020, from https://www.msha.gov/mine-data-retrieval-system

Pappas DM, Mark C. (1993). Behavior of simulated gob material. U.S. Bureau of Mines. RI 9458.

Peng, S.S. (2008). *Coal Mine Ground Control.* 3rd edition, Department of Mining Engineering, West Virginia University, 750 pp.

Salamon, M. D. G. "Rock mechanics problems associated with longwall trials in South Africa." In *Paper to be presented to the 5th International Strata Control Conference*, pp. 1-21. 1972.

Salamon MDG (1990). Mechanism of caving in longwall coal mining. *In: Proceedings of the 21th U.S. rock mechanics symposium*, Denver CO. A.A. Balkema; p.161–8.

Su, D. W. H., G. J. Hasenfus, and L. A. Stull. (2014). Ground control design considerations for reducing longwall-induced stress and seismicity associated with massive sandstone under deep cover. Englewood, CO: Society for Mining, Metallurgy, & Exploration.

Tulu, I., Esterhuizen, G., Gearhart, D., Klemetti, T., Mohamed, K., & Su, D. (2018). Analysis of global and local stress changes in a longwall gateroad. International Journal of Mining Science and Technology, 127-135.

Tulu IB, Heasley KA. (2012). Investigating abutment load. *In: Proceedings of the 31st international conference on ground control in mining*. Morgantown: West Virginia University p. 1-10.

USGS. (2004). U.S. Geological Survey Fact Sheet 2004-3092. Retrieved 01/31/2020 https://pubs.usgs.gov/fs/2004/3092/fs2004-3092.html

USGS. (2020, January). National Coal Resources Data System Web Map. Retrieved from https://eerscmap.usgs.gov/ncrds2/

Van Der Merwe, J. N. (2006). "Beyond Coalbrook: Critical review of coal strata control developments in South Africa." In: *Proceedings of the 25th International Conference on Ground Control in Mining*. Morgantown, WV: West Virginia University, pp. 335–346.

Van Dyke, M., Klemetti, T., Tulu, I., Tuncay, D., (2020). Moderate cover bleeder entry and standing support performance in a longwall mine: a case study. 2020 SME annual Meeting and Exhibit. Phoenix, AZ: Society for Mining, Metallurgy, & Exploration

Yang, Jian ; Heasley, Keith A (2016). Calibrating LaModel for Subsidence. *35th International Conference on Ground Control in Mining*

Zhang, P. and Heasley, K.A., 2013. Initial results from implementing a laminated overburden model into ARMPS. In *Proceedings of the 32nd International Conference on Ground Control in Mining. Morgantown, WV: West Virginia University* (pp. 239-247).

Zipf RK (2007). Numerical modeling procedures for practical coal mine design. *Proceedings of the international workshop on rock mass classification in underground mine design*, NIOSH IC 2007;9498:153–62.

9.0 Appendices:

9.1 Field Measurement Database

During the database development task, field monitoring database with total of 40 cases from 40 mines were developed. Cases in the database categorized into three datasets based on available information. The first dataset consists of 12 longwall mine cases that have the full side abutment measurements and geological logs from 11 different mines (10 Australian and 1 US mines). Second dataset consist of 12 cases from 12 different US longwall mines that have the either stress measurements, subsidence measurement or both, detailed geological logs, overburden map, mine map and other operational parameters. Third dataset consists of 18 supplementary cases from 6 US and 12 Australian mines that only have magnitude of the measured loads and basic operational parameters.

9.1.1 Dataset-1 Australian Mines

AU1 Mine: The AU1 mine's coal seam varies in thickness from 5.9 to 8.9 ft. The overlying strata mostly consists of sandstone and laminate units. Enough information was not available to construct a representative stratigraphic column, however; the geologic formations that were present in the immediate roof were known. The depth of cover around the instrumentation site is approximately 870 ft. The chain pillars are developed on 148-ft × 328-ft centers with a 16.7-ft entry width and the panel is 673 ft wide. The immediate floor is strong with minimum slaking potential. There were no stratigraphic data to determine the hard rock percentage of the overlying strata.

AU2 Mine: The AU2 mine operates with a seam thickness from 9.5 to 13.8 ft, and the seam thickness is approximately 11.8 ft at the monitoring site. The stratigraphic sequence can be seen in Figure 2. A sandstone and siltstone unit overlies the coal seam. A thick clay unit overlies a clay/sand sequence followed by a varying thickness of basalt. The overburden depth above the instrumentation site is around 410 ft. The panel width is 920 ft and the chain pillars are on 115-ft × 427-ft centers with 16.4 ft entry widths. The hard rock ratio is calculated as 48% for this mine.

AU3 Mine: The seam thickness for the AU3 mine varies from 11 to 13 ft, and a typical stratigraphic column near the instrumentation site is presented in Figure 2. The seam is overlain mostly by sandstone with a couple of bands of siltstone and claystone. The hard rock percentage is calculated as 57%. The depth of cover is approximately 427 ft, and the panel void width is 673 ft. The chain pillars are on 98-ft × 410-ft centers with 17-ft-wide roadways. There is a 3.3-ft thick clayey siltstone underlying the coal seam that deteriorates when exposed to water and traffic, so 1.7 ft of coal is left for maintaining good roadway conditions. Below the clayey siltstone, the lithology continues with strong layers of sandstone, shale, mudstone and siltstone.

AU4 Mine: At the AU4 mine, 15.7 ft of coal is extracted. The overlying strata consists of layers of generally competent and strong layers of shale, sandstone, conglomerate, volcanic tuff and coal seams (Figure 1). The depth of cover varies from 490 to 660 ft where it is approximately 590 ft at the instrumentation site. The 444-ft-wide longwall panels are designed with 102 ft × 335 ft center chain pillars with 16.4 ft wide roadways. The hard rock ratio is around 33%. The floor of the seam mostly consists of sandstone with occasional thin shale units in some areas.

AU5 Mine: The seam extracted at the AU5 mine is relatively flat and 8.2 ft in thickness. Overlying the seam, there is a 984-ft-thick sequence of major sandstone and shale units. That sequence is overlain by a massive sandstone of 525 to 590 ft of thickness. Figure1 has the visual representation of the stratigraphic column; however, it is generated from the description of the geology in a report without a core log. The overburden is approximately 1,560 ft above the instrumentation site and can be considered 71% hard rock. The 673-ft-wide panels are supported by 138-ft × 335-ft center chain pillars, and the roadway width is approximately 15.7 ft. The immediate floor is around 3.3 ft of carbonaceous siltstone underlain by a strong sandstone.

AU6 Mine: The coal seam at the AU6 mine is 21.3-ft thick, but the development thickness is 10.5 ft. Immediately overlying the seam is a competent volcanic tuff layer of 4.9-ft thickness. Sequence of shale and sandstone layers follow with some minor coal seams. There is a very strong sandstone/conglomerate unit lying 50-60 ft above the roof (Figure 1). The depth of cover varies from 720 to 920 ft with 787 ft adjacent to the instrumentation site with

around 23% hard rock. The 492-ft-wide panels are separated by chain pillars on 115-ft centers with 16-ft-wide roadways. The immediate floor is 13-ft-thick shale underlain by inter-bedded sandstones and shales.

AU7 Mine: The AU7 mine operates at a depth of cover of 1,330 ft with a variable seam thickness from 5.9 to 12 ft. The panel widths are 656 to 820-ft wide (rib to rib), and they are supported by 158-ft-wide chain pillars, which have 17-ft-wide nominal cut-throughs at 328-ft centers. The overlying strata mostly consist of sandstone intermixed or interbedded with siltstone (Figure 1) that produced about a 21% hard rock ratio.

AU8a-b Mine: Two sets of measurements were taken from the AU8 mine. The depth of cover changes from 1,640 to 1,755 ft. The seam thickness varies from 16.4 to 21.7 ft. The overlying strata mostly consists of thick sandstone layers and siltstone giving a 72% and 95% hard rock ratio, respectively (Figure 1). The immediate floor and roof have conglomerate units. The measurements are taken next to two different panels that are 745- and 778-ft wide. Chain pillars are 148 ft wide with 16.4 ft wide entries for the 745-ft-wide panel and for the 778-ft-wide panel, the chain pillars are 197-ft-wide with 20-ft-wide entries

AU9 Mine: The depth of cover for the AU9 mine typically ranges from 984 to 1,148 ft. A sandy soil cover of 3 to 16-ft depth overlies a low to very low strength, highly weathered sandstone on the surface. Highly competent and massive sandstone units exist between depths of 165 to 655 ft (Figure 1). The panel extracted adjacent to the instrumentation site is 820-ft wide with an extraction height of 22 ft, and the chain pillars are 141 ft wide, rib to rib with 16.4-ft-wide roadways. The hard rock ratio is calculated as 61%.

9.1.2 Dataset-2 The USA Longwall Mines

Northern and Cetral Appalachian longwall mines:

Mine NA-1: The first northern Appalachian longwall mine (Mine NA-1) studied in this work is in South West Pennsylvania. The mine operated in the Pittsburgh coal seam. According to the Mine Safety and Health Administration (MSHA) data retrieval system (MSHA, 2020), the mine produced approximately 6.77 and 6.42 million tons of coal in 2017 and 2018, respectively. Figure A1 shows the outline of the panels near the study site. The depth of cover around the studied area is around 650 ft. In previous operations, the panel widths were around 800ft where currently the mine is operating panel widths more than 1500ft. The chain pillar system is 3-entries with 80ft wide pillars and 16 ft wide entries. The mining height is approximately 6.5 ft.

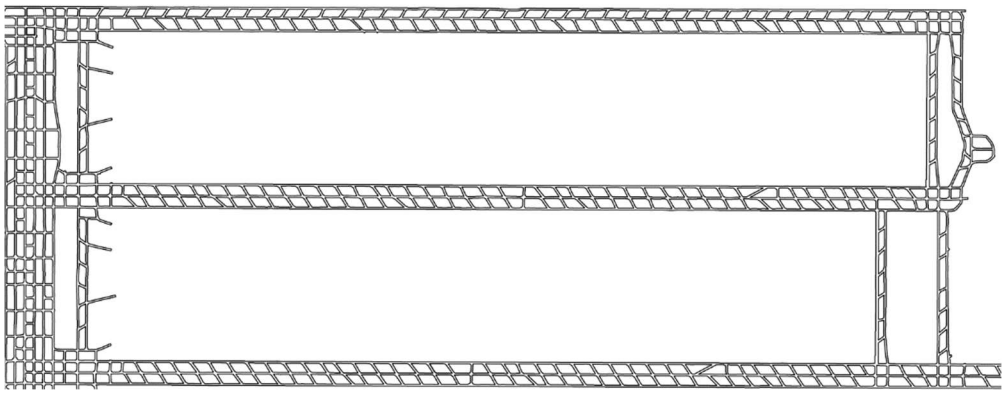

Figure A1. Northern Appalachian mine NA-1.

Mine NA-2: The second northern Appalachian longwall mine (Mine NA-2) studied in this work is in Northern West Virginia. The mine operated in the Pittsburgh seam. Figure A2 shows the outline of the panels near the study site. The depth of cover around the study area is about 700 ft. The studied longwall panel is roughly 1170 ft wide and the gateroad system is a three entry with approximately center-to-center, 115 and 100-ft-wide chain pillars with approximately 16 ft wide entries. The mining height is approximately 7.5 ft. The immediate roof generally consisted of shale, rider coal, claystone, and sandstone or limestone, and the floor was claystone or shale.

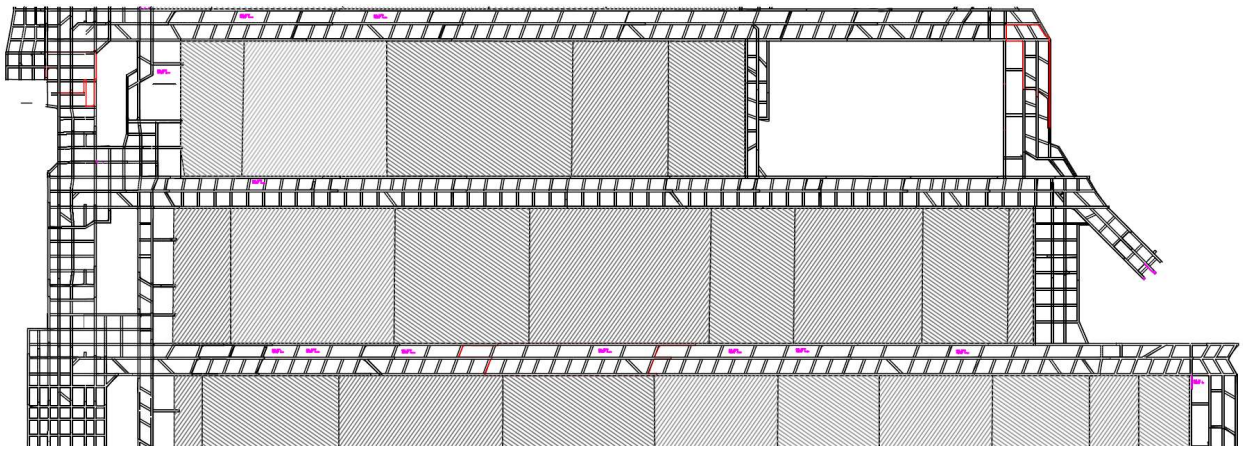

Figure A2. Northern Appalachian mine NA-2.

Mine NA-3: The third northern Appalachian longwall mine (Mine NA-3) studied in this work is in Northern West Virginia. The mine operated in the Middle Kittanning coal bed. According to the Mine Safety and Health Administration (MSHA) data retrieval system (MSHA, 2020), the mine produced approximately 3.38 and 3.44 million tons of coal in 2017 and 2018, respectively. Figure A3 shows the outline of the panels near the study site (Tulu et al., 2018). The depth of cover throughout the mine ranges from 500 to 750 ft, and the typical depth is about 520 ft. The longwall panels are roughly 1200 ft wide by 8000 ft long. The gateroad system is a three entry with approximately center-to-center, 100-ft-wide chain pillars with approximately 20 ft wide entries. The mining high is approximately 7 ft.

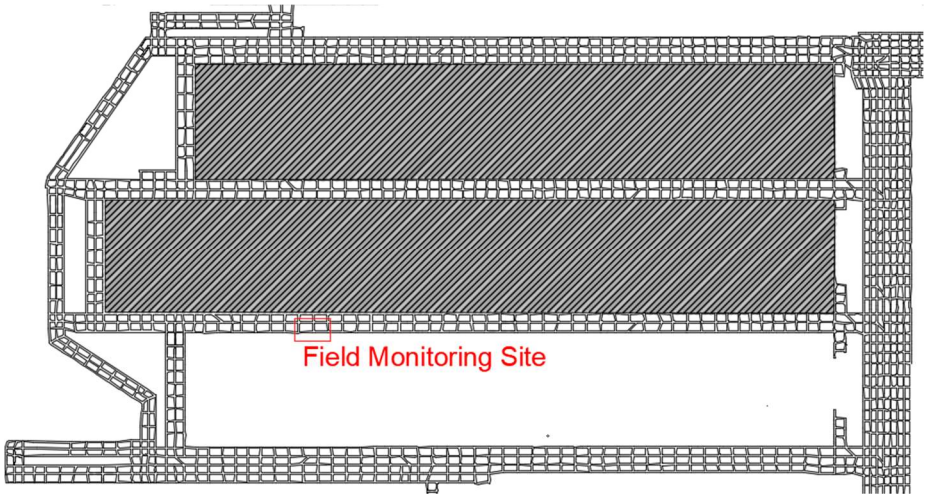

Figure A3. Northern Appalachian mine NA-3 (modified from Tulu et al., 2018).

Based on the in-mine mapping, as well as available exploration drillhole data, the geologic conditions are typical for the Allegheny Formation. The Middle Kittanning coal bed that is mined is overlain by dark gray to carbonaceous clay shale. The clay shale grades upward to gray sandy shale, dark gray sandy shale, or gray sandstone. The gray sandy silt shale and dark gray sandy silt shale beds vary in grain size and sand content, based on their proximity to the laterally correlative gray sandstone beds.

Mine NA-4: The fourth northern Appalachian longwall mine (Mine NA-4) studied in this work is in Southwestern Pennsylvania. The mine operated in the Lower Kittanning coal bed. Figure A4 shows the outline of the panels near the study site. The depth of cover around the studied area is 650 ft and the longwall panel is roughly 600 ft wide by 2725 ft long. The gateroad system is a three entry with approximately rib-to-rib, 80-ft-wide and 60-ft-wide chain pillars with approximately 20 ft wide entries. The mining high is approximately 4 ft.

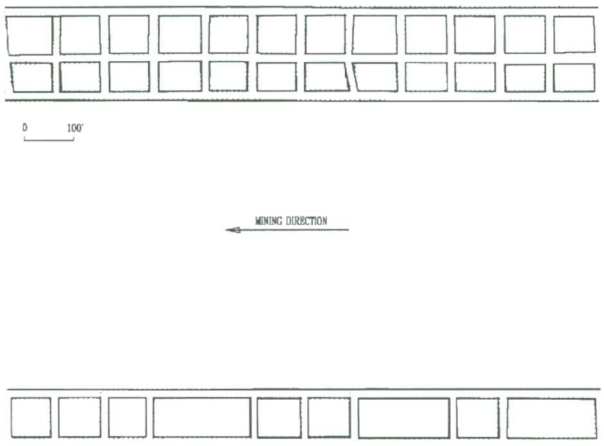

Figure A4. Northern Appalachian mine NA-4.

Mine NA-5: The fifth northern Appalachian longwall mine (Mine NA-5) studied in this work is located on the border between North Central West Virginia and South Western Pennsylvania, mining the Pittsburgh coal bed. Figure A5 shows the outline of the panels near the study site (Van Dyke et al., 2020). The depth of cover at this mine ranges from 400-ft to about 1400 ft. The longwall panels near the study site are 1100-ft-wide and are 12000 ft long. The gateroad consists of a small and a large pillar with center to center 90-ft and 165-ft-wide. The entry and crosscuts in the gateroads are 18-ft-wide. The mining height is around 7 ft.

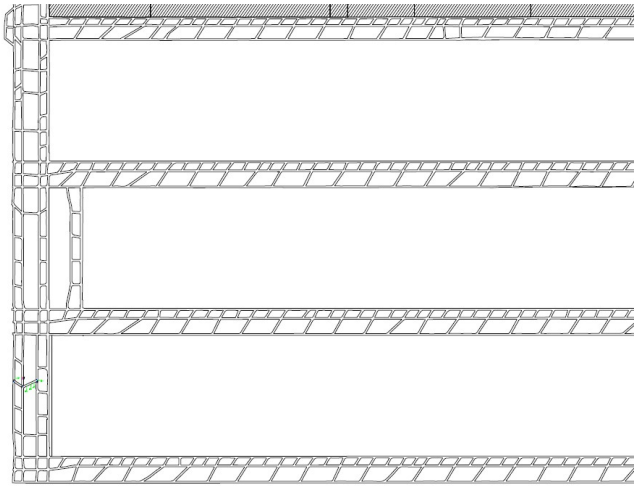

Figure A5. Northern Appalachian mine A5 (modified from Van Dyke et al., 2020).

Mine NA-6: The sixth northern Appalachian longwall mine (Mine NA-6) studied in this work is in South West Pennsylvania. The mine operated in the Pittsburgh coal seam. Figure A6 shows the outline of the panels near the study site. The depth of cover around the studied area is around 690 ft and the longwall panel is roughly 1000 ft wide. The chain pillar system is 3-entries with rib-to-rib 85-ft-wide pillars and 17 ft wide entries. The mining height is approximately 6.5 ft.

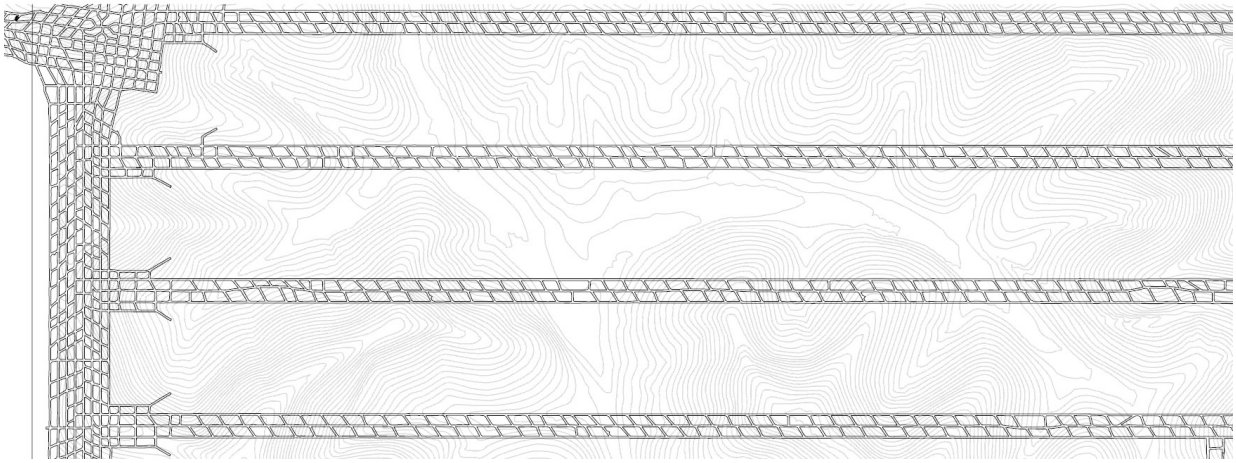

Figure A6. Northern Appalachian mine NA-6.

Mine CA-1: The first, central Appalachian longwall mine (Mine CA-1) studied in this work is in Virginia. The mine operates in the Pocahontas No.3 coal bed. The mine produced approximately 4.9 million tons of low-vol met coal in 2017. Figure A7 shows the outline of the panels near the study site (Klemetti et al., 2018). The depth of cover throughout the mine ranges from 1200 to 2300 ft. The longwall panels are roughly 700 ft wide by 10000 ft long. The gateroad system is a four entry with approximately center-to-center, 50-ft-wide yield pillars and 174-ft-wide abutment pillars with approximately 18 ft wide entries. The mining height is approximately 5.5 ft on average for the studied panel. The typical roof geology consists of silty to sandy shales, sandstones, and coal. Shales usually dominate the bolted horizon followed by a sandstone with an inconsistent shale parting before reaching the Pocahontas No. 4 coal seam (Klemetti et al., 2019a).

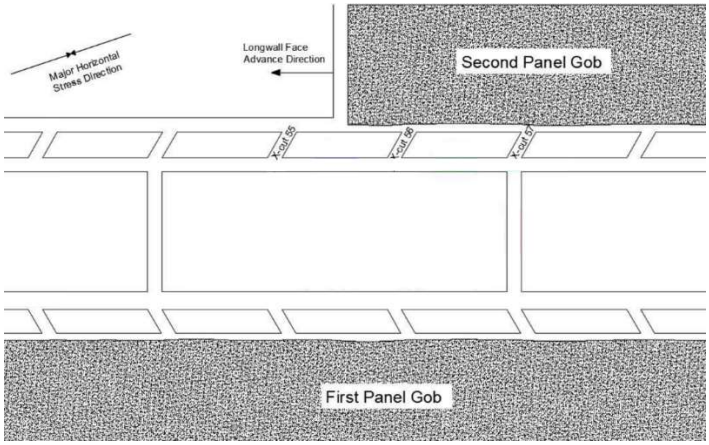

Figure A7. Central Appalachian mine CA-1 (modified from Klemetti et al., 2018).

Mine CA-2: The second central Appalachian longwall mine (Mine CA-2) studied in this work is in southern West Virginia. The mine operated in the Pocahontas No. 3 coal bed. Figure A8 shows the outline of the panels near the study site. Overburden depth around the study area ranged from 447 to 645 ft. The longwall panel studied is 800 ft wide by 5300 ft long. The gateroad system is a four entry with approximately rib-to-rib, 105-ft-wide center pillars and 40 ft-wide side pillars with approximately 16 ft wide entries. The mining high is approximately 4.2 ft. Based on drill logs provided, the rocks in the overburden strata are classified into the following four types: sandstone, shaly sandstone, shale and sandy shale, and coal.

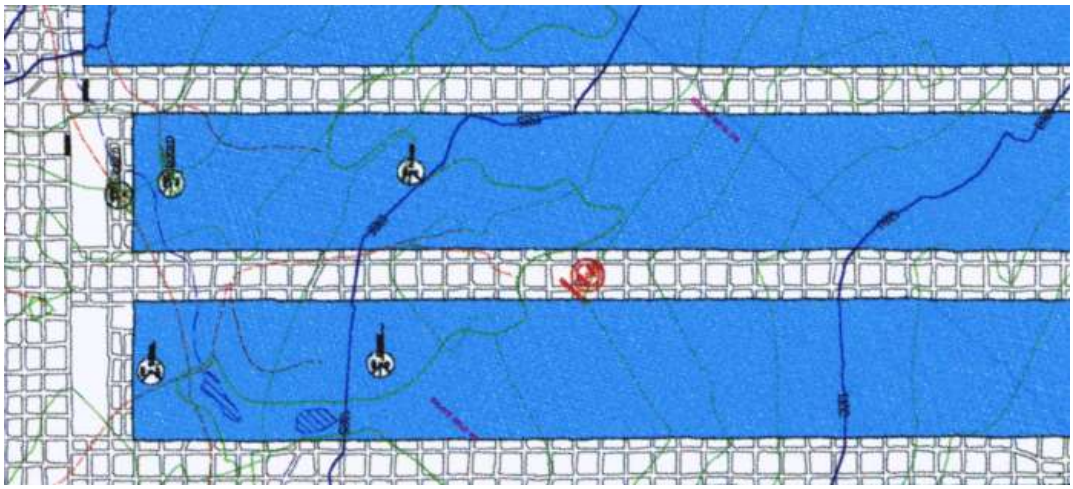

Figure A8. Central Appalachian mine CA-2 (modified from the mine closure map).

Mine CA-3: The third, central Appalachian longwall mine (Mine CA-3) studied in this work is located in Virginia. The mine operated in the Pocahontas No. 3 coal bed. Figure A9 shows the outline of the panels near the study site (Campoli et al., 1993). The depth of cover throughout the mine ranges from 1200 to 2200 ft, and the depth around the studied area is about 2085 ft. The longwall panels are roughly 600 ft wide by 6000 ft long. The gateroad system is a four entry with approximately center-to-center, 40-ft-wide yield pillars and 165-ft-wide abutment pillars with approximately 20 ft wide entries. The mining height averages approximately 5.5 ft.

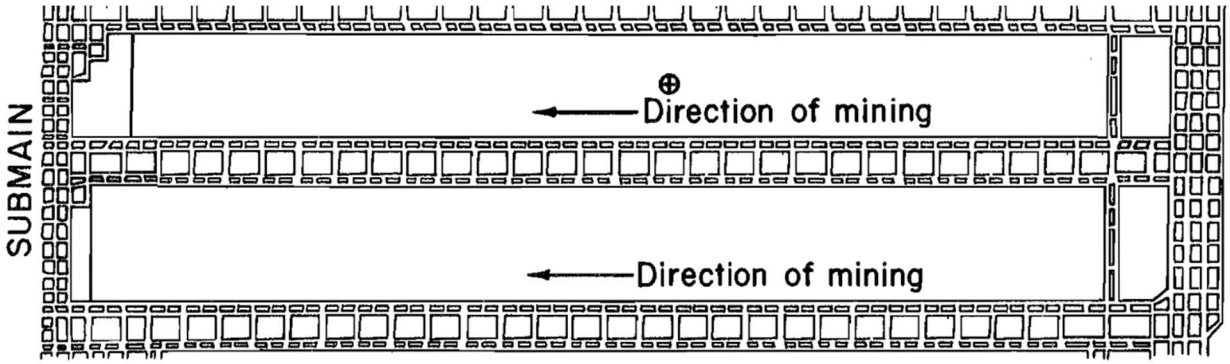

Figure A9. Central Appalachian mine site (modified from Campoli et al., 1993*).*

Mine-wide, the Pocahontas No. 3 Coalbed is under overburden ranging from 1,200 to 2,200 ft in thickness and the coalbed dips 1° from east to west. The immediate roof, in the south end of the mine, consists of a widely jointed siltstone overlain by a very stiff, massive sandstone. Minewide, the siltstone ranges from a maximum thickness of 110 ft down to being nonexistent. The massive sandstone in the main roof varies from a maximum thickness of 450 ft to a minimum of 135 ft (Campoli et al., 1993).

Black Warrior Basin longwall mine:

Mine BW-1: The Black Warrior Basin longwall mine (Mine BW-1) studied in this work is in Alabama. The mine operated in the Blue Creek coal seam. According to the Mine Safety and Health Administration (MSHA) data retrieval system (MSHA, 2020), the mine produced approximately 4.86 and 5.60 million tons of coal in 2017 and 2018, respectively. Figure A10 shows the outline of the panels near the study site (Klemetti et al., 2018). The depth of cover throughout the mine ranges from 1100 to 2200 ft. The longwall panels are roughly 1000 ft wide by 7000

ft long. The gateroad system is a four entry with approximately center-to-center, 40-ft-wide yield pillars and 165-ft-wide abutment pillars with approximately 20 ft wide entries. The mining high is approximately 7.9 ft.

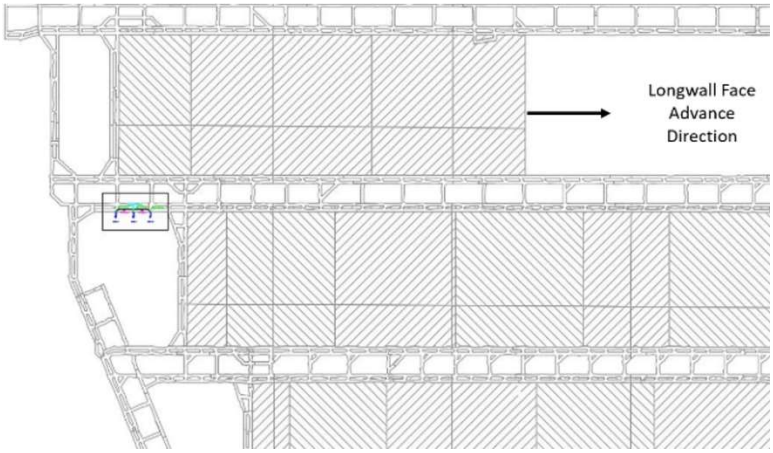

Figure A10. Black Warrior Basin mine site (modified from Klemetti et al., 2019).

The Blue Creek seam that is mined is overlain by a shale parting that follows the Mary Lee seam. The two seams can be separated by as much as 25 ft, but when the Mary Lee seam is within 3 ft of the Blue Creek seam, both seams are mined simultaneously. The local roof geology consists of silty shale and sandstones. The sandstone is thinly bedded to laminated with shale, with shale and coal streaks in the upper and lower extents (Klemetti et al., 2019).

Western US longwall mines:

Mine W1: The first western longwall mine studied in this work is located in the Emery County, Utah. The mine was operated in the Hiawatha coal seam at a depth of 2000 ft (US Bureau of Mines, 1988). Four entries were developed through the Main West North Barrier beneath overburden ranging from 1,500 to 2,240 ft (MSHA, 2007). At Mine W1, extraction height averages 8.8 ft and the width of panel is 550 ft. No previous mining had been conducted above this mine. The longwall panels were roughly 775 ft wide by 4,540 ft long in west part of mine. Single yield pillar applied between the panel in Mine W1, the dimension of pillar is 35 by 108 ft.

The local roof geology consists of sandstones and siltstones. Sandstones and interbeds of siltstones, sandstones, and mudstones are the predominant units. The total percentage of sandstone in the overburden is between 35 and 45 percent including all thin beds and laminations. There is a 100 ft thick limestone bed at the surface, following about 400 ft siltstone and sandstone layers.

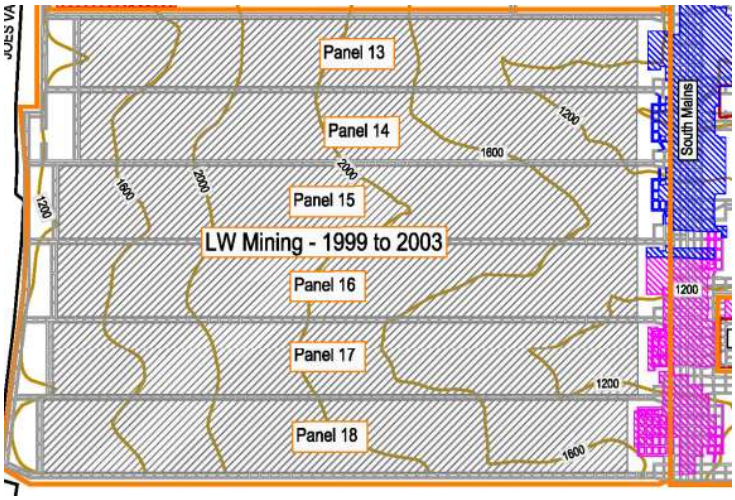

Figure A11. Western US W1 mine site (MSHA report, 2007)

Mine W2: The second western longwall mine studied in this work is located on the Wasatch Plateau in central Utah. The surface elevation of this mine averages 9,100 ft, and the topography is generally rolling, with a maximum ground slope of 45 percent. Mine W2 operated in the Blind Canyon coal seam. Panel 5E was developed using three entries; the remaining three panels were developed with two entries. The pillar size in Mine W2 is 32 by 82 ft with 20 ft wide entries. Dimensions of the mined panels are roughly 500 by 2,500 ft. The average depth of cover over the four panels was 1,500 ft (US Bureau of Mines, 1988).

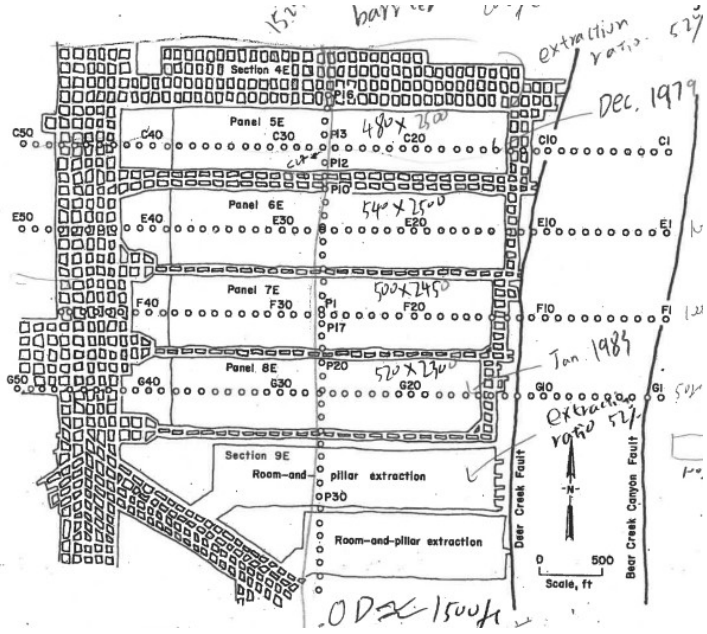

Figure A12. Western US W2 mine site (US Bureau of Mine, 1988)

The generalized overburden stratigraphy for Mine W2 was determined from company drill logs. Sandstones and interbeds of siltstones, sandstones, and mudstones are the predominant units. The total percentage of sandstone in the overburden is 45 percent, with 35 percent occurring in thick beds. The Fault is located near the east end of the study panels; however, there are no faults crossing the panels (US Bureau of Mine, 1988).

Mine W3: The third western longwall mine studied in this work, located near Somerset in Gunnison County, Colorado, annually produces approximately 6 million tons of high-quality steam coal (Building America, 2019). Mine W3 has used a three-entry abutment pillar design for all gateroads. There are several different types of pillar designs applied in Mine W3 depending on the support needs, including 73 by 180 ft, 100 by 180 ft and 170 by 180 ft. The length of panels range from 7000 ft to 9000 ft, and the width of panel is roughly 780 ft. The coalfield is exposed at a few localities and is buried to a depth of as much as 2,500 ft. The average extraction thickness in Mine W3 is 8ft. The average overburden depth in right part is about 2000 ft and left part is about 1500 ft in Mine W3.

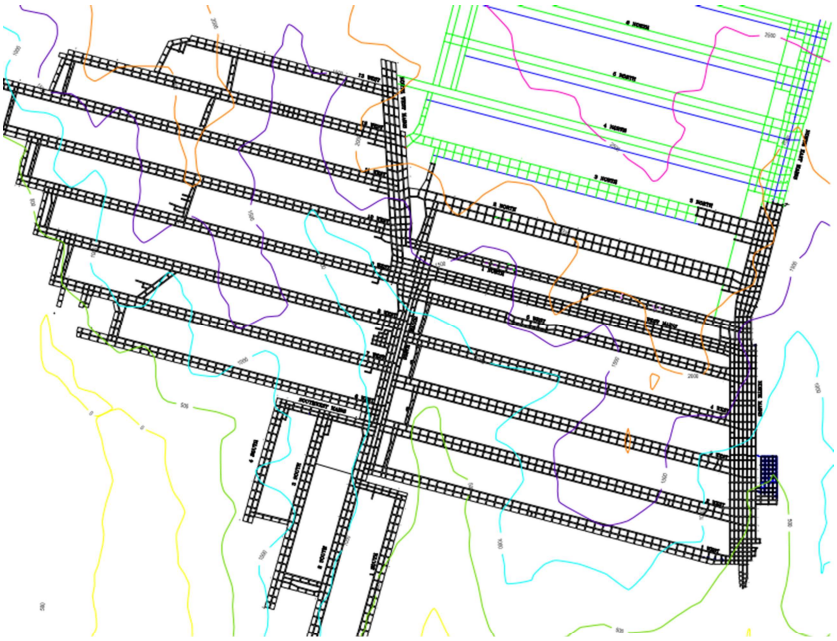

Figure A13. Western US W3 mine site

The generalized overburden stratigraphy for Mine W3 was determined from a consulting company report. Sandstones and interbeds of siltstones, sandstones, and shale are the predominant units. However, there are some mudstone layers occurred in the roof and floor, which causes the floor heave problem in Mine W3.

9.2 Model verification

Mine NA-1 (Figure A14) is a shallow mine with typical overburden depth of 647 ft and panel width of 1391 ft. To simulate the subsidence and mining induced stress distribution, cross-section AA' was approximated with the FVM model geometry shown in Figure A14, and total of 74 layers are modeled including the seam level and the bottom filler layers, resulting in 628,000 total number of elements. Three mining steps were simulated for Mine NA-1; development, Panel-1mining and Panel-2 mining. Since the Panel-1 is in supercritical loading condition, influence of Panel-1 mining on Panel-2 headgate is negligible.

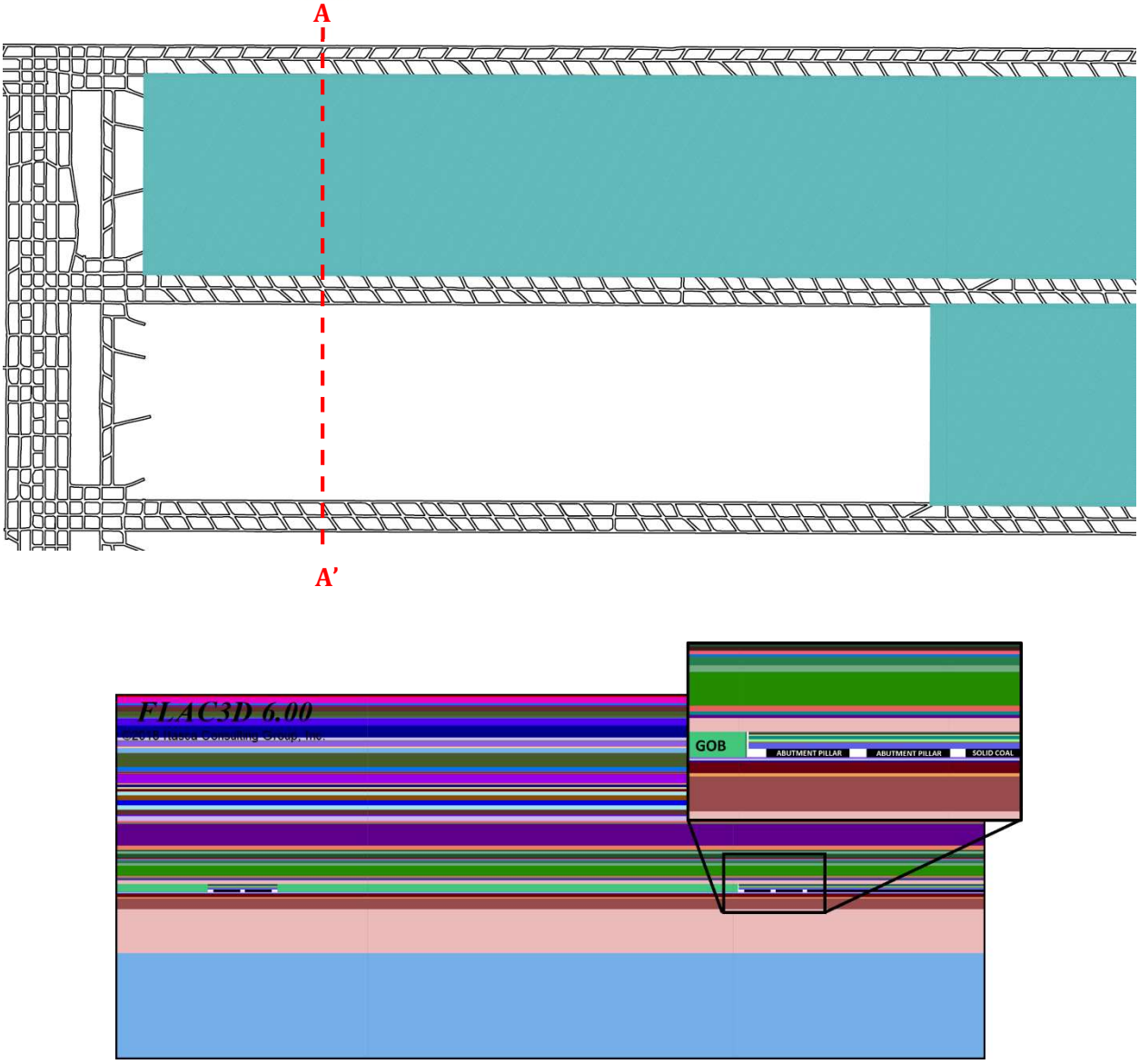

Figure A14. FVM model geometry for mine NA-1.

FVM Model Results and Verification with Field Monitoring: After, each case study mine model was solved, stresses and displacements computed by the model at the instrument locations were queried and compared with the field monitoring results, initially for model verification. Figure A15 shows the surface subsidence approximated by the model and measured in the field for the mine NA-1. The model approximated maximum subsidence of the first panel to be 4.77 ft compared to the measurements of 4.88 – 5.11 ft. Figure A16 shows the abutment stress distribution approximated by the FVM.

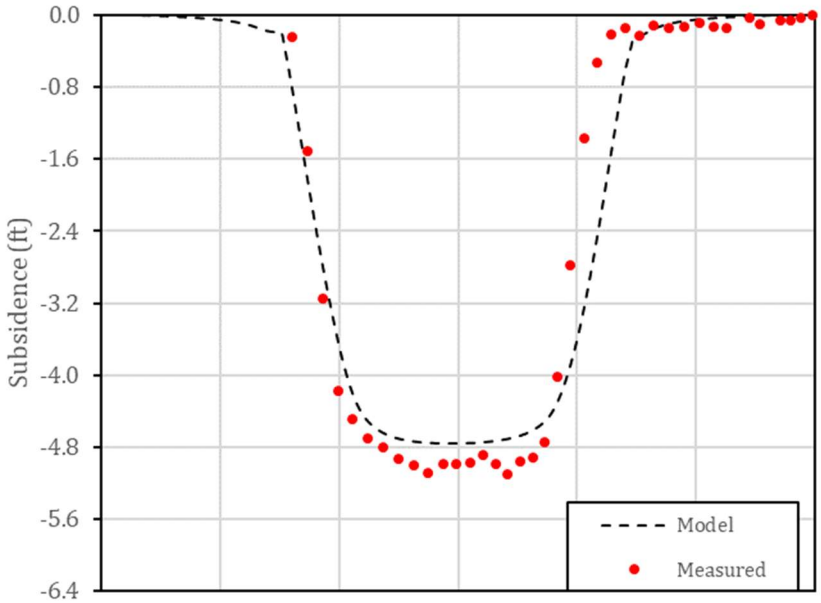

Figure A15. Comparison of model calculated and field measured surface subsidence for Mine NA-1.

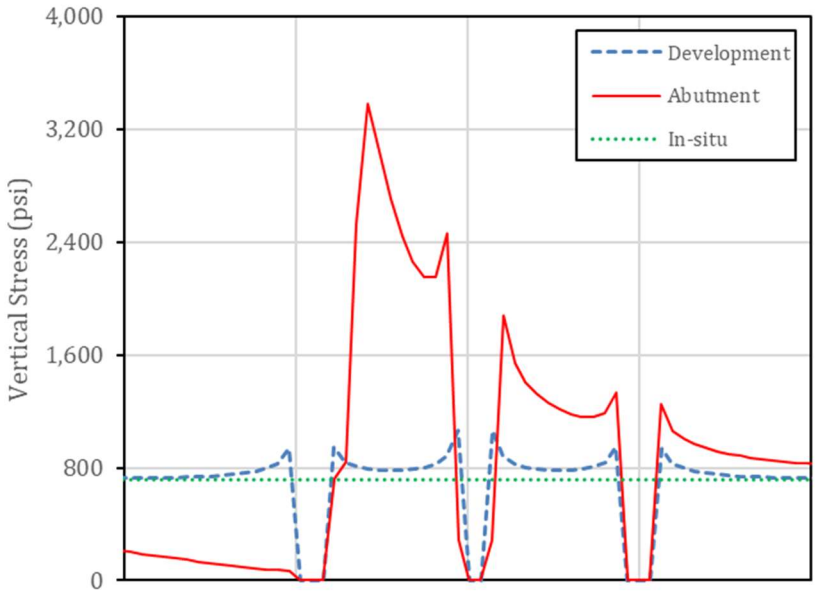

Figure A16. Comparison of the modeled and measured stresses in the abutment pillars for Mine NA-1.

Mine NA-2 (Figure A17) is a shallow mine with typical overburden depth of 700 ft and panel width of 1171 ft. To simulate the subsidence and mining induced stress distribution, cross-section AA' was approximated with the FVM model geometry shown in Figure A17, and total of 66 layers are modeled including the seam level and the bottom filler layers, resulting in 662,000 total number of elements. Three mining steps were simulated for Mine NA-2; development, Panel-1 mining and Panel-2 mining. Since the Panel-1 is in supercritical loading condition, influence of Panel-1 mining on Panel-2 headgate is negligible.

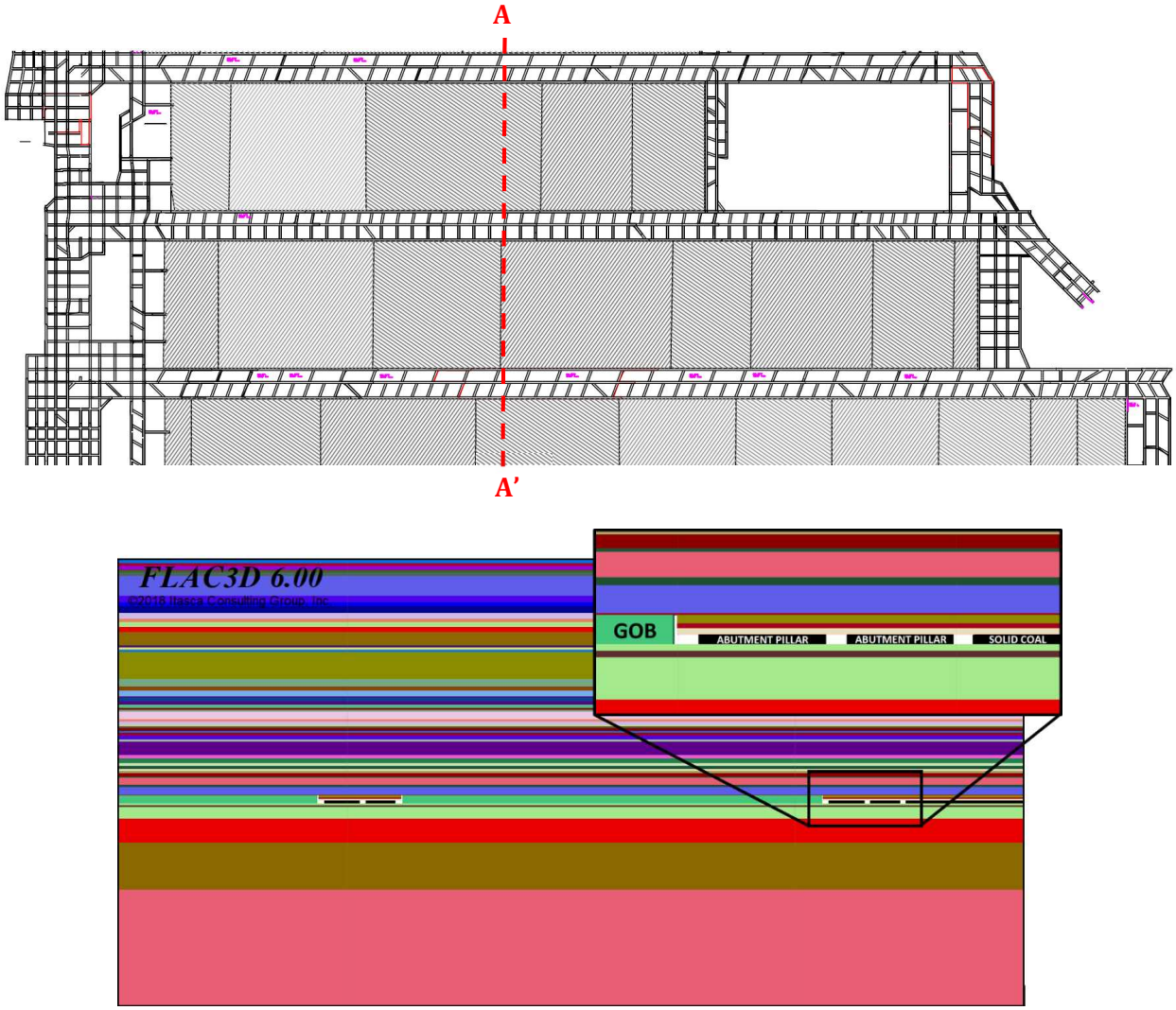

Figure A17. FVM model geometry for mine NA-2.

FVM Model Results and Verification with Field Monitoring: After, each case study mine model was solved, stresses and displacements computed by the model at the instrument locations were queried and compared with the field monitoring results, initially for model verification. Figure A18 shows the surface subsidence approximated by the model and obtained by empirical tools (SDPS) for the mine NA-2. The model approximated maximum subsidence of the first panel to be 4.51 ft compared to the 4.24 ft obtained by the empirical method. Figure A19 shows the abutment stress distribution approximated by the FVM model for mine NA-2.

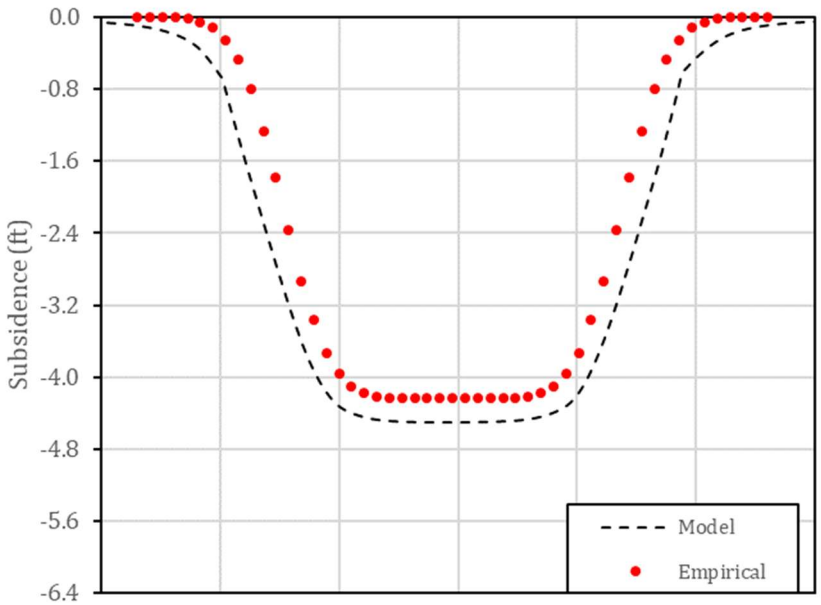

Figure A18. Comparison of model calculated and field measured surface subsidence for Mine NA-2.

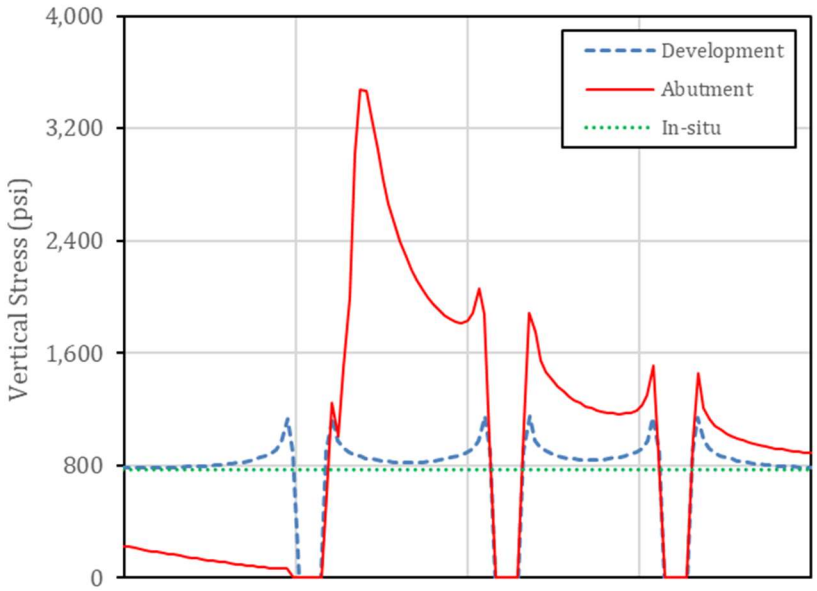

Figure A19. Comparison of the modeled and measured stresses in the abutment pillars for Mine NA-2.

Mine NA-3 (Figure A20) is a shallow mine with typical overburden depth of 520 ft and panel width of 1200 ft. To simulate the subsidence and mining induced stress distribution, cross-section AA' was approximated with the FVM model geometry shown in Figure A20, and total of 100 layers are modeled including the seam level and the bottom filler layers, resulting in 860,000 total number of elements. Three mining steps were simulated for Mine NA-3; development, Panel-2 mining and Panel-3 mining. Since the Panel-1 is more than 1300 ft away from the instrumented portions, influence of Panel-1 mining on measurements is negligible.

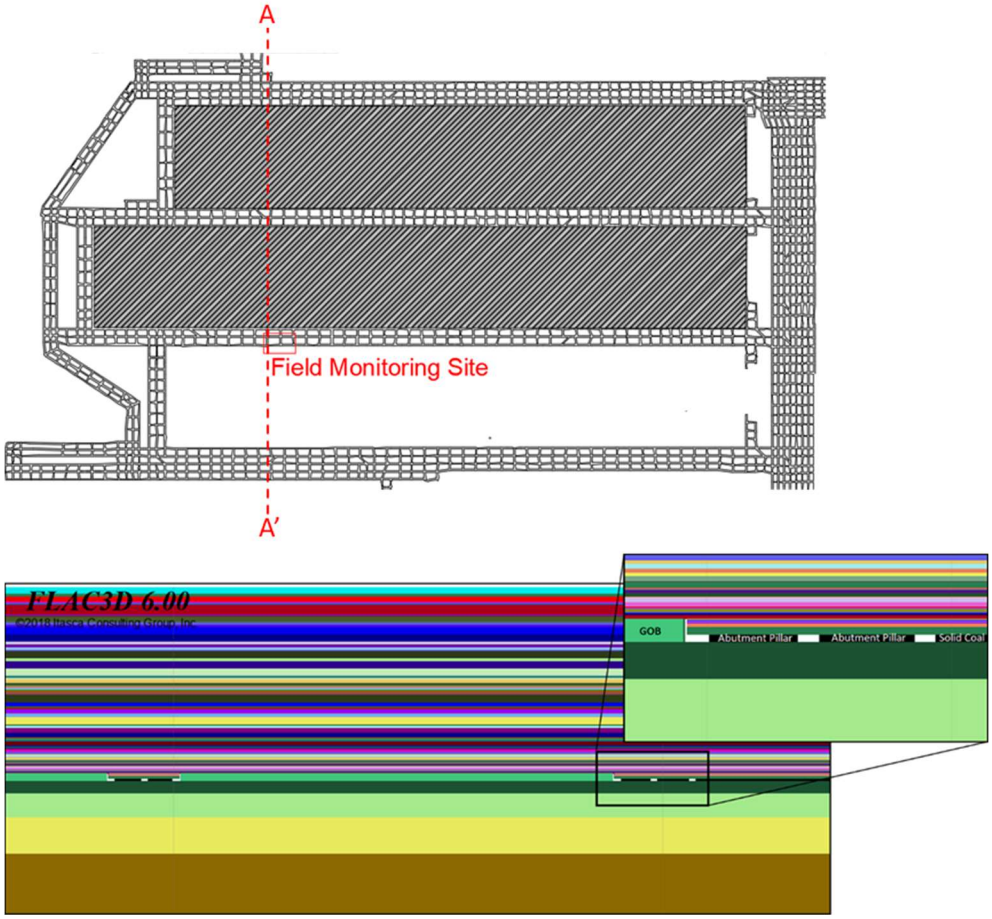

Figure A20. FVM model geometry for mine NA-3.

FVM Model Results and Verification with Field Monitoring: After, each case study mine model was solved, stresses and displacements computed by the model at the instrument locations were queried and compared with the field monitoring results, initially for model verification. Figure A21 shows the surface subsidence approximated by the model and measured in the field for the mine NA-3. The model approximated maximum subsidence of the first panel to be 3.85 ft compared to the measurements of 3.84 – 3.93 ft.

Figure A22 shows the abutment stress distribution approximated by the FVM model and measured by the Borehole Pressure Cells (BPC) for case study mine NA-3. The model approximated abutment stresses at the BPC locations are within 2% - 10% of the field values. Although there are inconsistencies between the measured and modeled stresses, the general trend is similar and within reasonable accuracy. Some of the variations could be accounted for the installation of the instrumentation, local coal composition/strength and calibration errors.

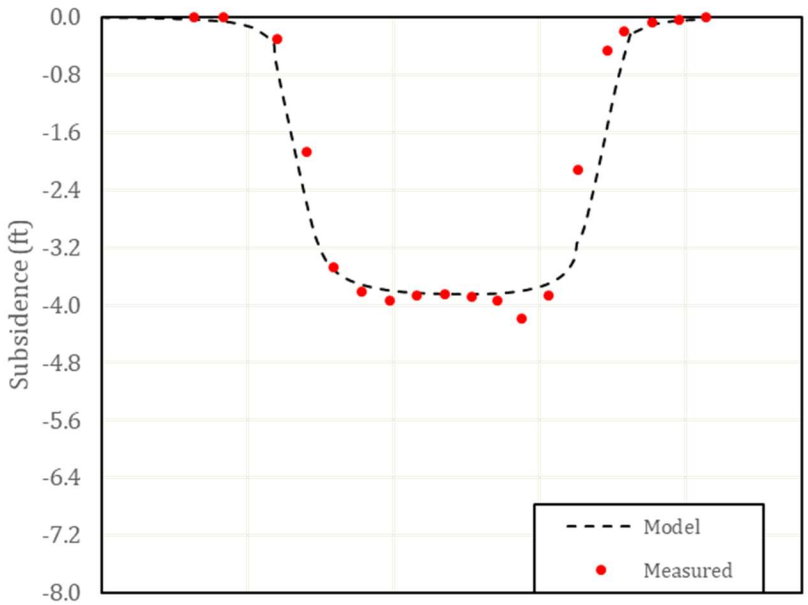

Figure A21. Comparison of model calculated and field measured surface subsidence for Mine NA-3.

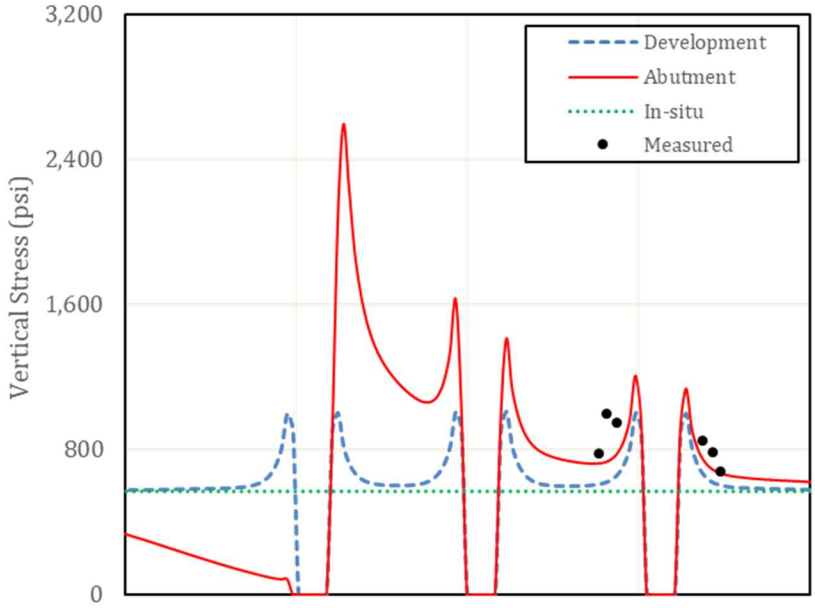

Figure A22. Comparison of the modeled and measured stresses in the abutment pillars for Mine NA-3.

Mine NA-4 (Figure A23) is a shallow mine with typical overburden depth of 650 ft and panel width of 590 ft. To simulate the subsidence and mining induced stress distribution, cross-section AA' was approximated with the FVM model geometry shown in Figure A23, and total of 33 layers are modeled including the seam level and the bottom filler layers, resulting in 424,000 total number of elements. Three mining steps were simulated for Mine NA-4; development, Panel-1 mining and Panel-2 mining.

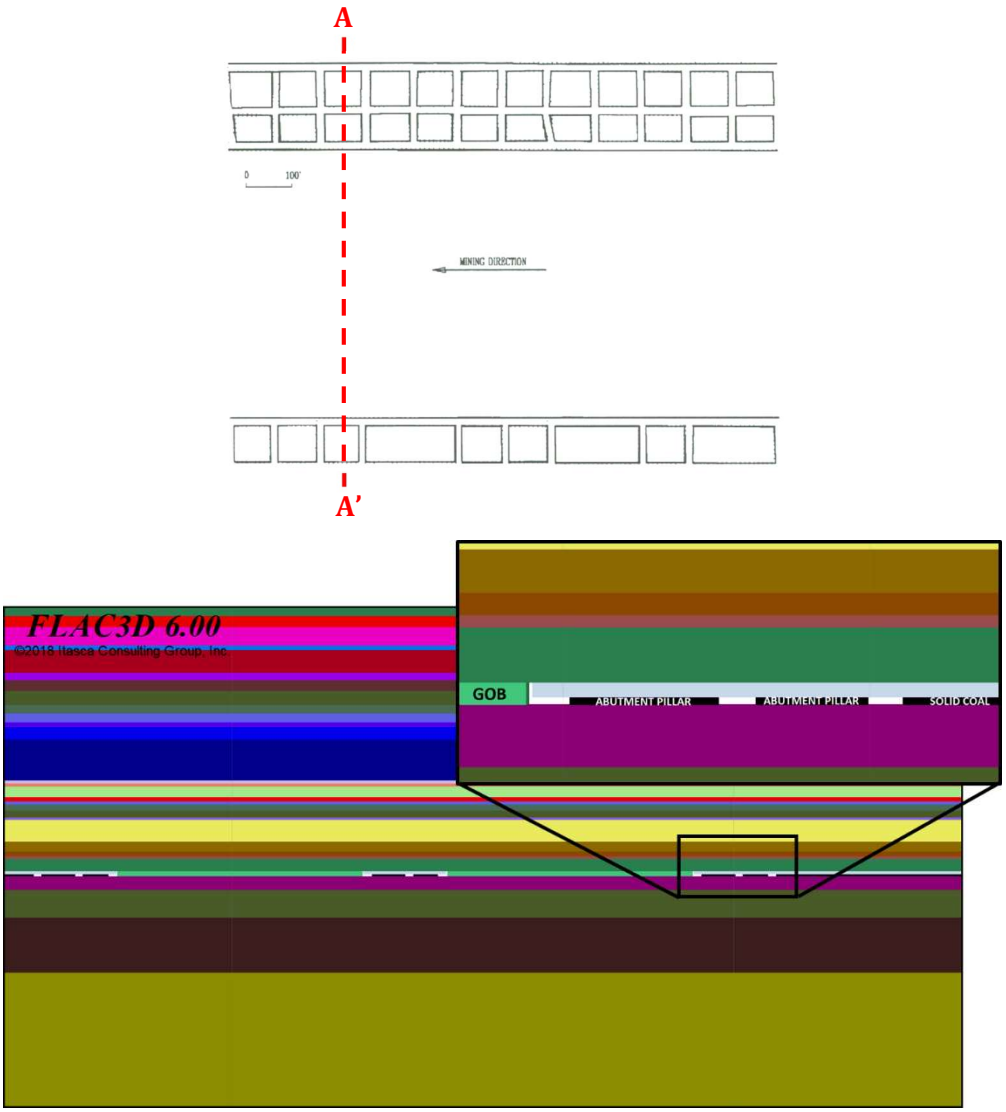

Figure A23. FVM model geometry for mine NA-4.

FVM Model Results and Verification with Field Monitoring: After, each case study mine model was solved, stresses and displacements computed by the model at the instrument locations were queried and compared with the field monitoring results, initially for model verification. Figure A24 shows the surface subsidence approximated by the model and measured in the field for the mine NA-4. The model approximated maximum subsidence of the first panel to be 1.49 ft compared to the measurements of 1.4 – 1.5 ft. Figure A25 shows the abutment stress distribution approximated by the FVM of the mine NA-4.

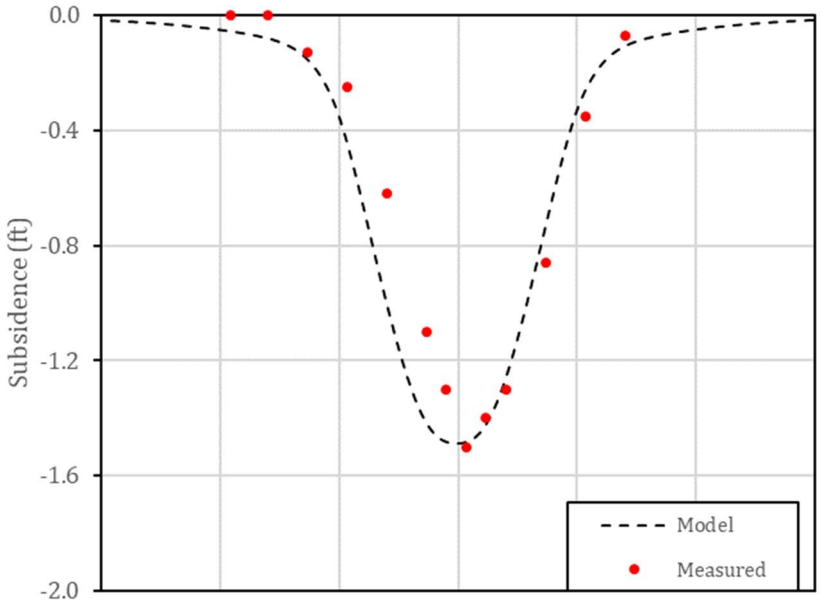

Figure A24. Comparison of model calculated and field measured surface subsidence for Mine NA-4.

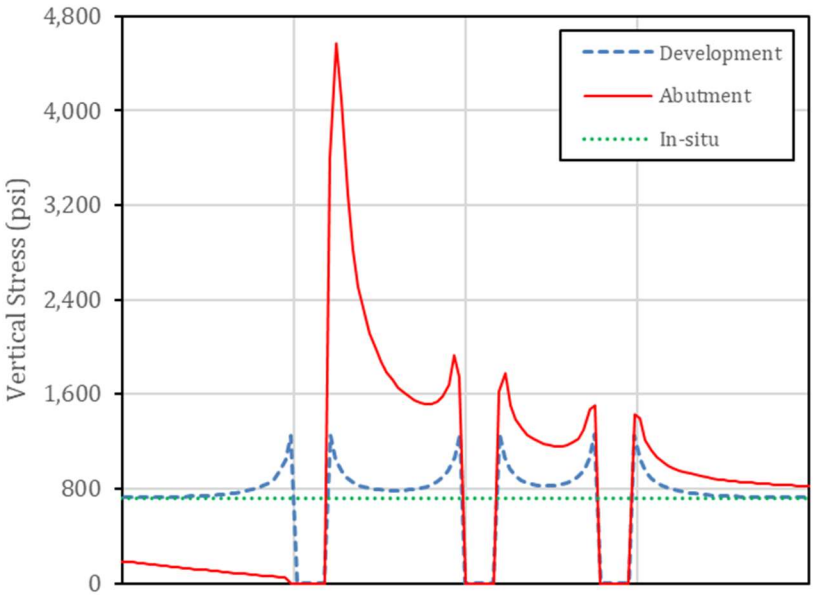

Figure A25. Comparison of the modeled and measured stresses in the abutment pillars for Mine NA-4.

Mine NA-6 (Figure A26) is a shallow mine with typical overburden depth of 690 ft and panel width of 1000 ft. To simulate the subsidence and mining induced stress distribution, cross-section AA' was approximated with the FVM model geometry shown in Figure A26, and total of 75 layers are modeled including the seam level and the bottom filler layers, resulting in 393,000 total number of elements. Three mining steps were simulated for Mine NA-6; development, Panel-1 mining and Panel-2 mining. Since the Panel-1 is in supercritical loading condition, influence of Panel-1 mining on Panel-2 headgate is negligible.

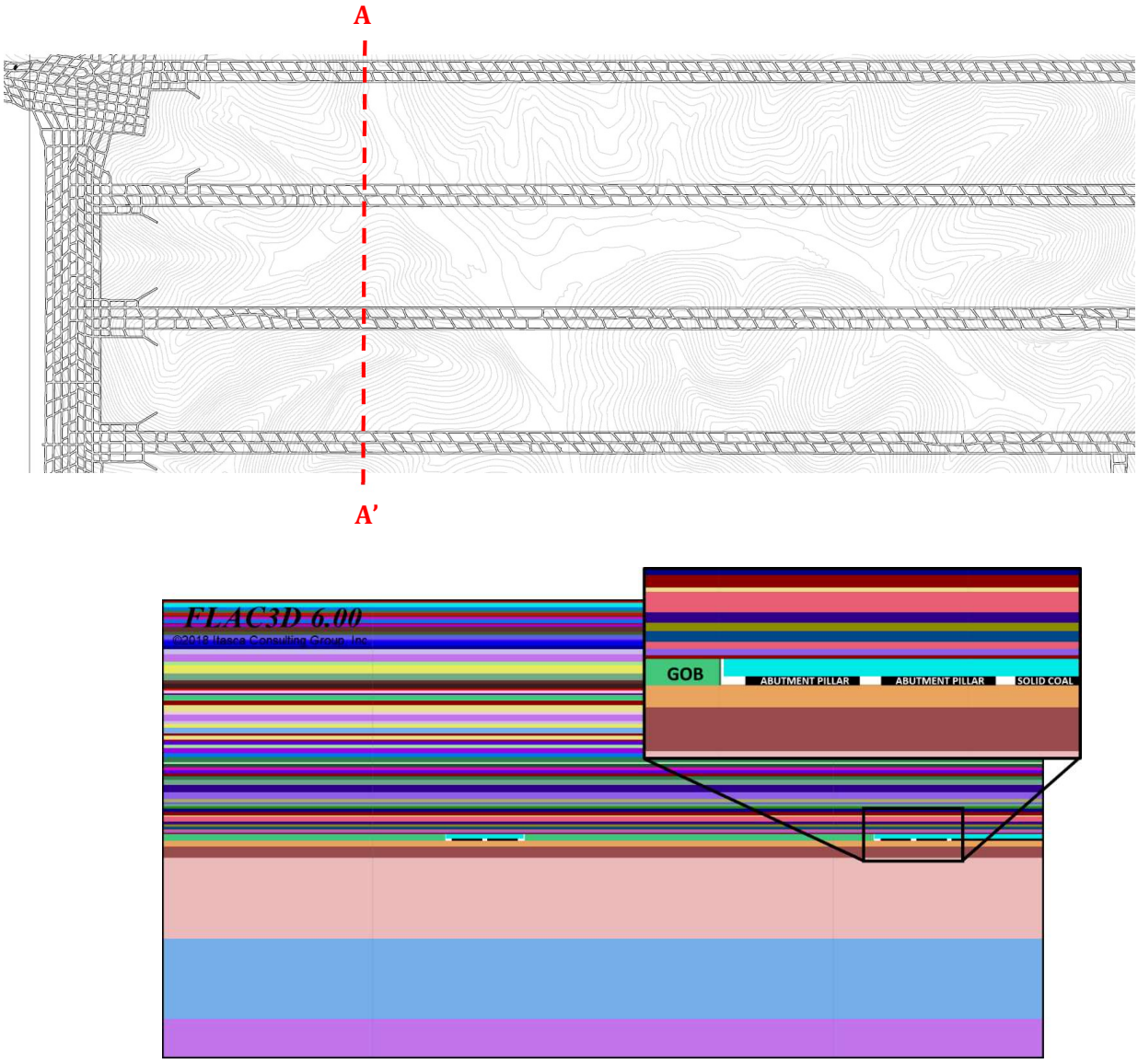

Figure A26. FVM model geometry for mine NA-6.

FVM Model Results and Verification with Field Monitoring: After, each case study mine model was solved, stresses and displacements computed by the model at the instrument locations were queried and compared with the field monitoring results, initially for model verification. Figure A27 shows the surface subsidence approximated by the model and measured in the field for the mine NA-6. The model approximated maximum subsidence of the first panel to be 3.86 ft compared to the measurements of 3.96 ft.

Figure A28 shows the abutment stress distribution approximated by the FVM model for case study mine NA-6.

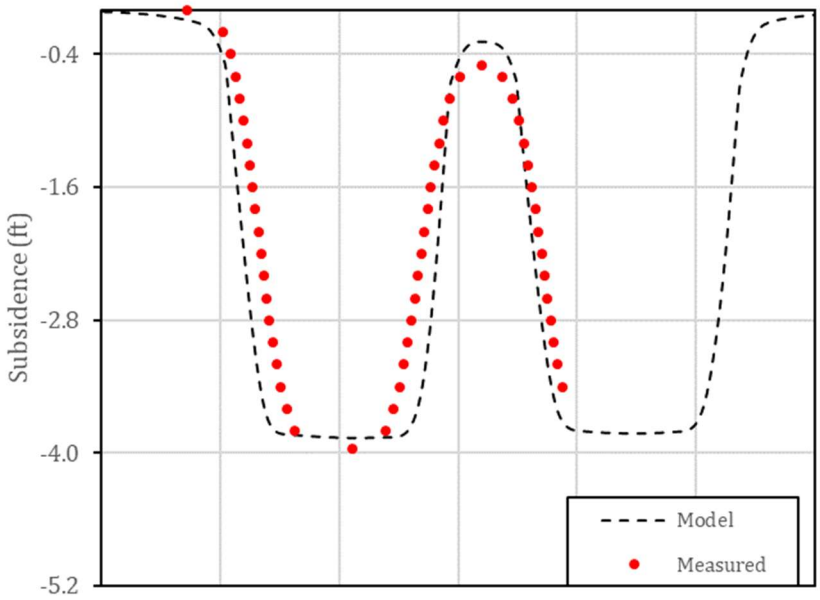

Figure A27. Comparison of model calculated and field measured surface subsidence for Mine NA-6.

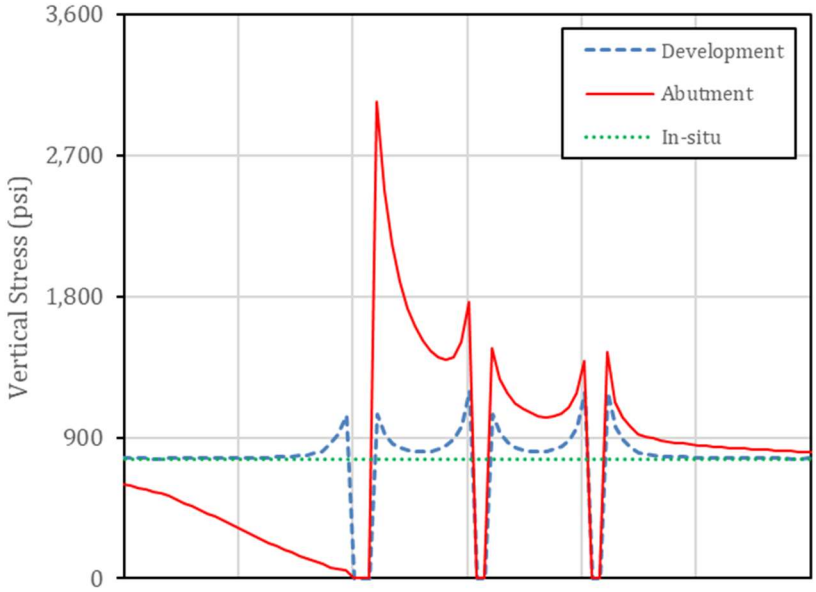

Figure A28. Comparison of the modeled and measured stresses in the abutment pillars for Mine NA-6.

Mine CA1 (Figure A29) is a deep mine with typical overburden depth of 2057 ft and panel width of 700 ft. To simulate the subsidence and mining induced stress distribution, the FVM model geometry shown in Figure A29 was created, and total of 142 layers are modeled including the seam level and the bottom filler layers, resulting in 1,092,800 total number of elements. Six mining steps were simulated for Mine CA1.

Figure A29. FVM model geometry for Mine CA1

FVM Model Results and Verification with Field Monitoring: After, each case study mine model was solved, displacements computed by the model at the instrument locations were queried and compared with the field monitoring results, initially for model verification. Figure A30 respectively shows the surface subsidence profile approximated by the model for the mine CA1 after first two panels mined and all four panels mined. The model approximated maximum subsidence after the first two panels mined to be 2.65 ft compared to the measurements of 2.45 ft. The subsidence profile and maximum subsidence after all four panels mined are not available.

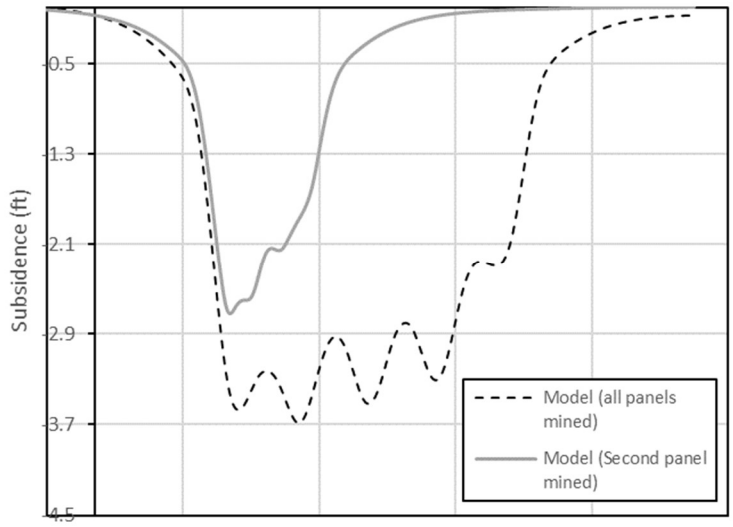

Figure A30. Comparison of model calculated and field measured surface subsidence for Mine CA1

Figure A31 shows the abutment stress distribution approximated by the FVM model. The stress measurement in this mine not available.

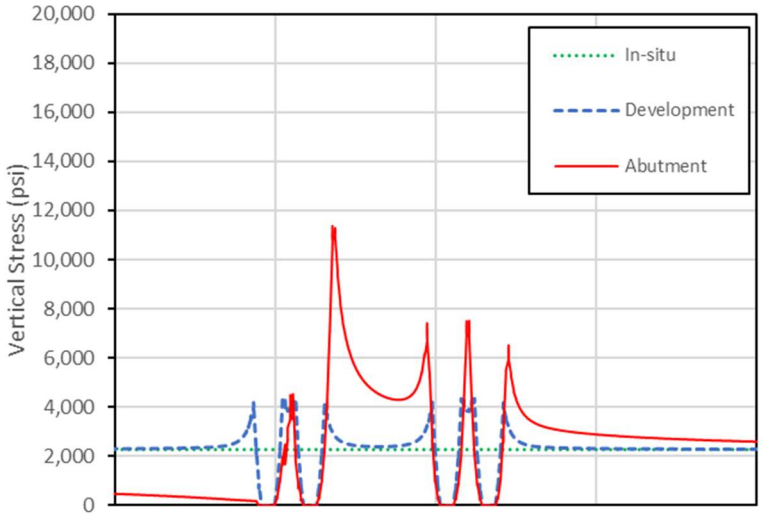

Figure A31. Comparison of the modeled and measured stresses in the abutment pillars for Mine

Mine CA-3 (Figure A32) is a deep cover mine with typical overburden depth of 2086 ft and panel width of 600 ft. To simulate the subsidence and mining induced stress distribution, cross-section AA' was approximated with the FVM model geometry shown in Figure A32, and total of 232 layers are modeled including the seam level and the bottom filler layers, resulting in 2,580,000 total number of elements. Six mining steps were simulated for Mine CA-3; development, and Panel-1 through Panel-5 mining. Since Mine CA-3 is a deep cover mine, five consecutive panels are modeled for possible influence of previous panels on the stresses.

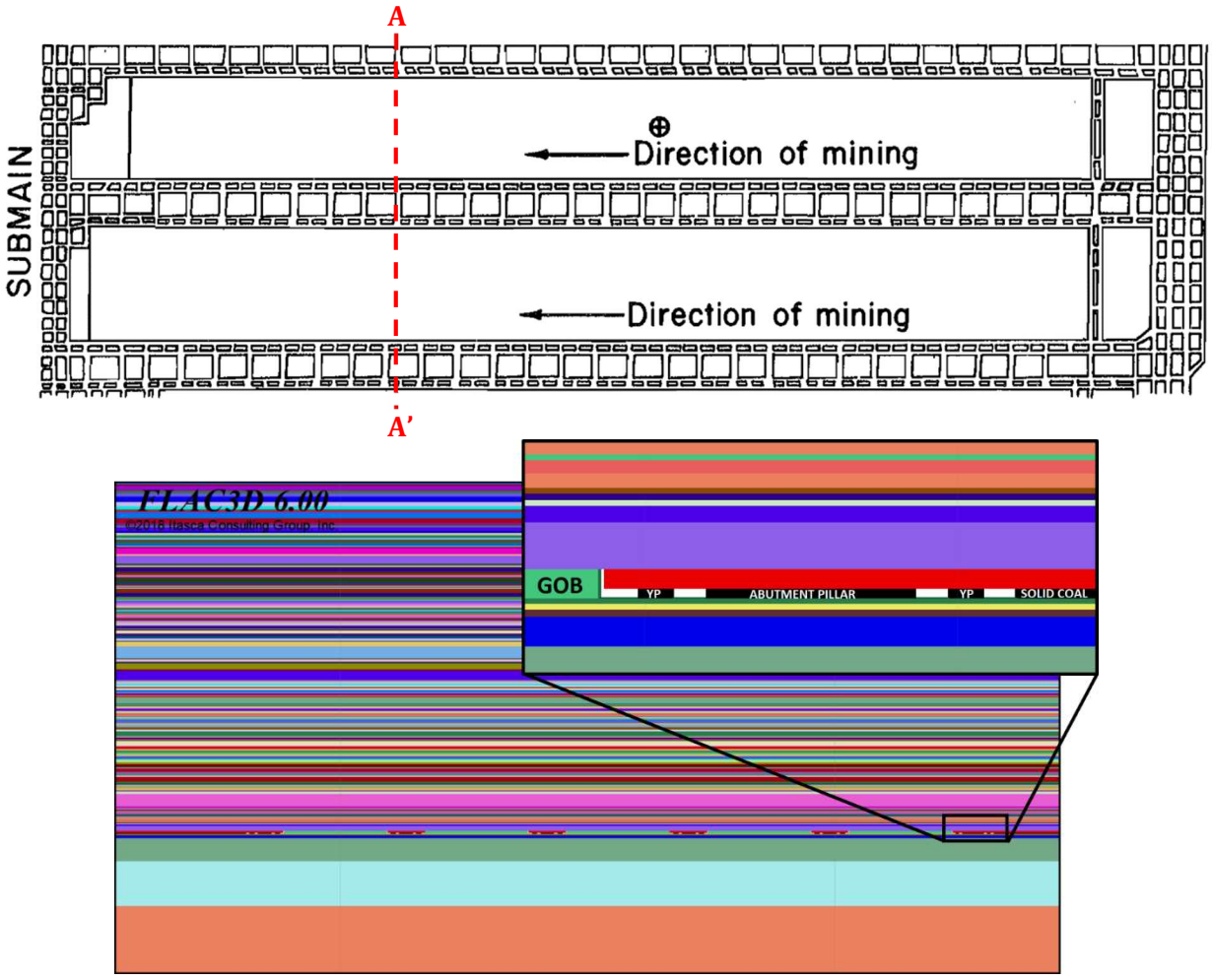

Figure A32. FVM model geometry for mine CA-3.

FVM Model Results and Verification with Field Monitoring: After, each case study mine model was solved, stresses and displacements computed by the model at the instrument locations were queried and compared with the field monitoring results, initially for model verification. Figure A33 shows the surface subsidence approximated by the model for 5 consecutive panels for mine CA-3. The model approximated maximum subsidence of the first panel to be 0.84 ft. According to the study conducted by Su et al. (2014), another central Appalachian mine with similar geology but a wider panel (700 ft) shows around 1.4 ft subsidence

Figure A34 shows the abutment stress distribution approximated by the FVM model and measured by the Borehole Pressure Cells (BPC) for case study mine CA-3. The model approximated abutment stresses at the BPC locations are significantly lower than the field values. Although there are inconsistencies between the measured and modeled stresses, the general trend is similar and variations could be accounted for the installation of the instrumentation,

local coal composition/strength and calibration errors. When back-calculated, the measured stresses amount to extremely high abutment loads that might also suggest those errors.

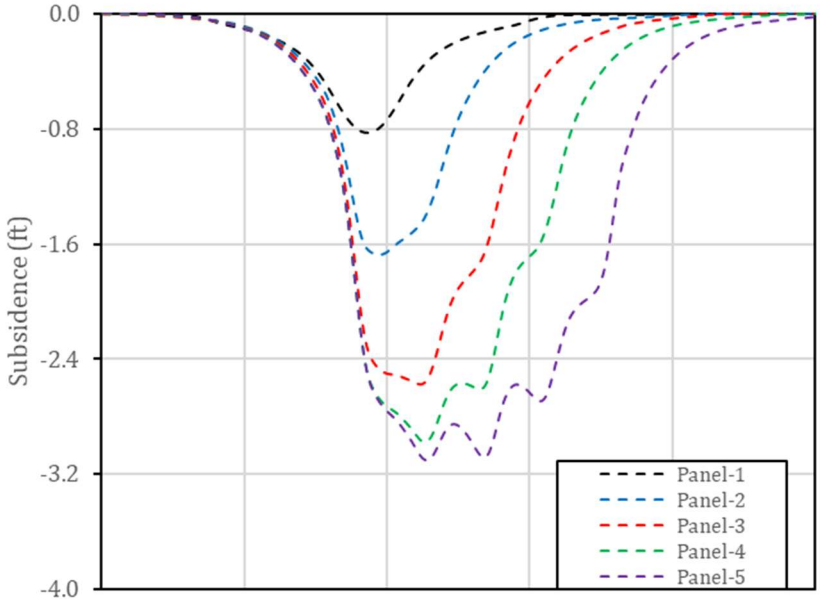

Figure A33. Comparison of model calculated and field measured surface subsidence for Mine CA-3.

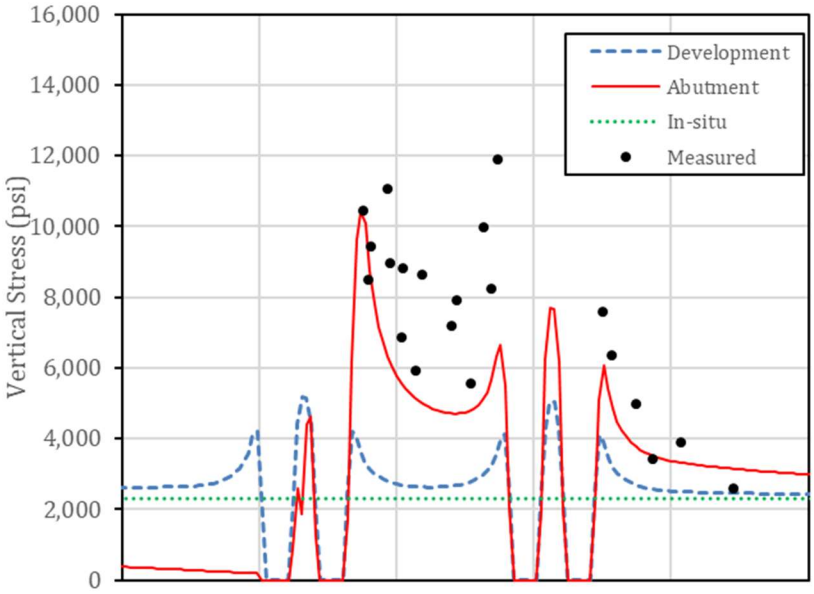

Figure A34. Comparison of the modeled and measured stresses in the abutment pillars for Mine CA-3.

Mine W1 (Figure A35) is a deep mine with typical overburden depth of 2000 ft and panel width of 775 ft. To simulate the subsidence and mining induced stress distribution, cross-section AA' was approximated with the FVM model geometry shown in Figure A35, and total of 145 layers are modeled including the seam level and the bottom filler layers, resulting in 859,125 total number of elements. Six mining steps were simulated for Mine W1; development, Panel-13 mining, Panel-14 mining, Panel-15 mining, Panel-16 mining and Panel-17 mining.

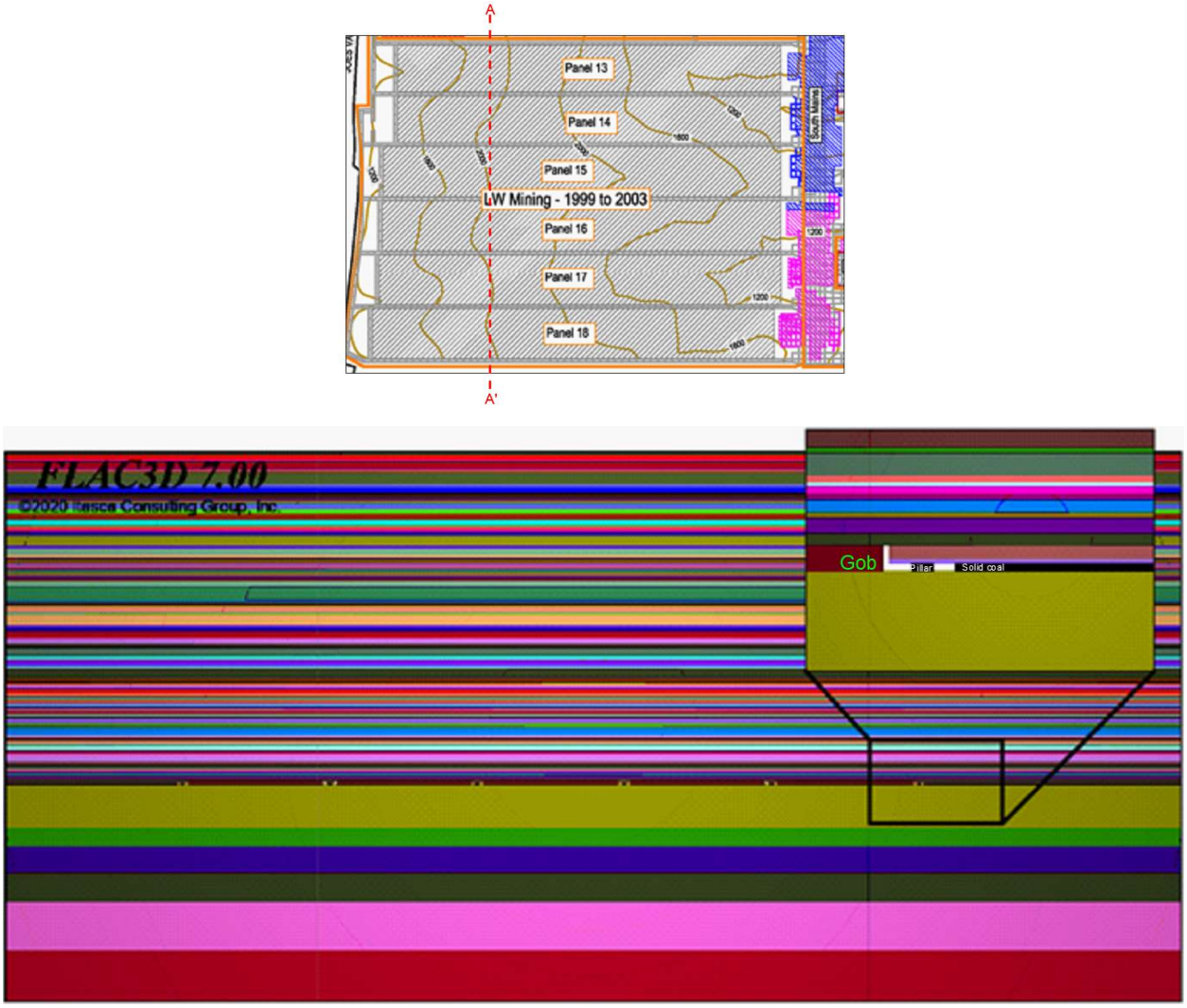

Figure A35. FVM model geometry for Mine W1

FVM Model Results and Verification with Field Monitoring: After, each case study mine model was solved, displacements computed by the model at the instrument locations were queried and compared with the field monitoring results, initially for model verification. Figure A36 shows the surface subsidence approximated by the model and measured in the field for the mine W1 after Panel-13 and Panel-14 mined. The model approximated maximum subsidence of the first panel to be 4.13 ft compared to the measurements of 3.95 to 4.10 ft.

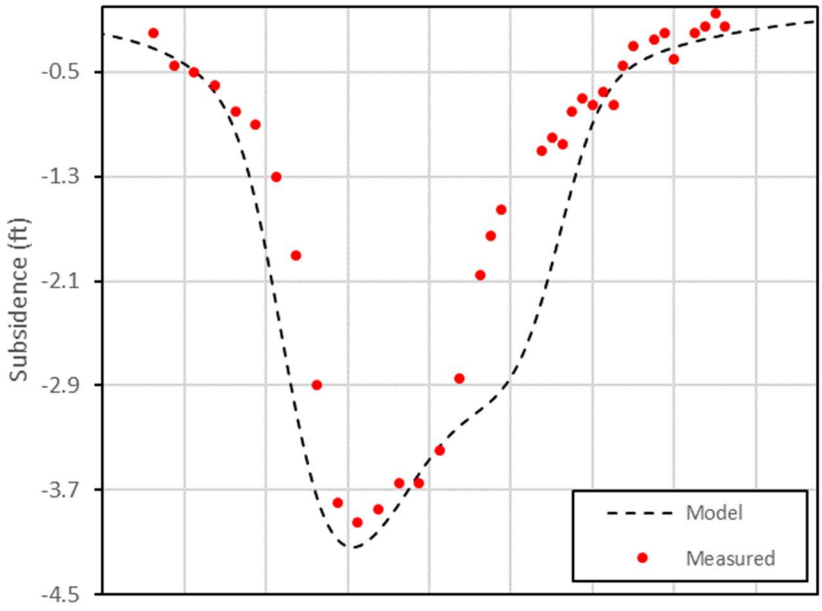

Figure A36. Comparison of model calculated and field measured surface subsidence for Mine W1

Figure A37 shows the abutment stress distribution approximated by the FVM model. The stress measurement in this mine not available.

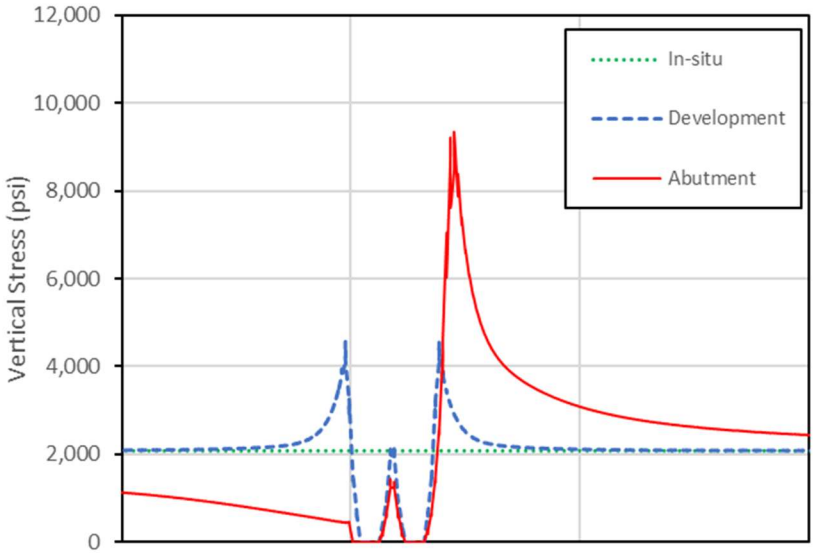

Figure A37. Comparison of the modeled and measured stresses in the abutment pillars for Mine W1

Mine W2 (Figure A38) is a deep mine with average overburden depth of 1500 ft and panel width of 500 ft. To simulate the subsidence and mining induced stress distribution, cross-section AA' was approximated with the FVM model geometry shown in Figure A38, and total of 53 layers are modeled including the seam level and the bottom filler layers, resulting in 1,036,750 total number of elements. Five mining steps were simulated for Mine W2; development, Panel-5E mining, Panel-6E mining, Panel-7E mining and Panel-8E mining.

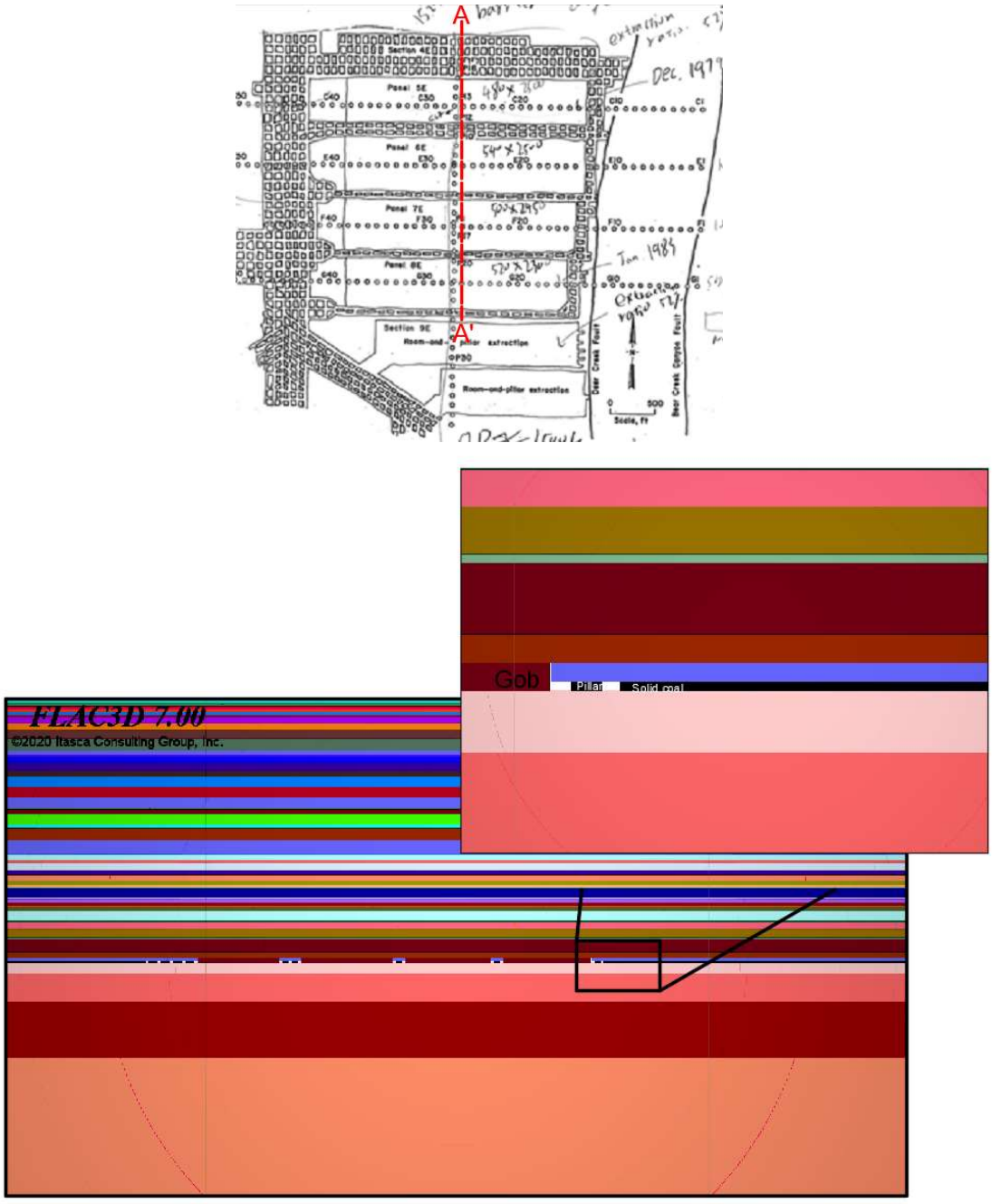

Figure A38. FVM model geometry for Mine W2

FVM Model Results and Verification with Field Monitoring: After, each case study mine model was solved, displacements computed by the model at the instrument locations were queried and compared with the field monitoring results, initially for model verification. Figure A39 shows the surface subsidence approximated by the

model and measured in the field for the mine W2. The model approximated maximum subsidence of the first panel to be 6.15 ft compared to the measurements of 5.75 ft. Even if there are some differences in maximum subsidence and subsidence profile, the general trend is similar and within reasonable accuracy.

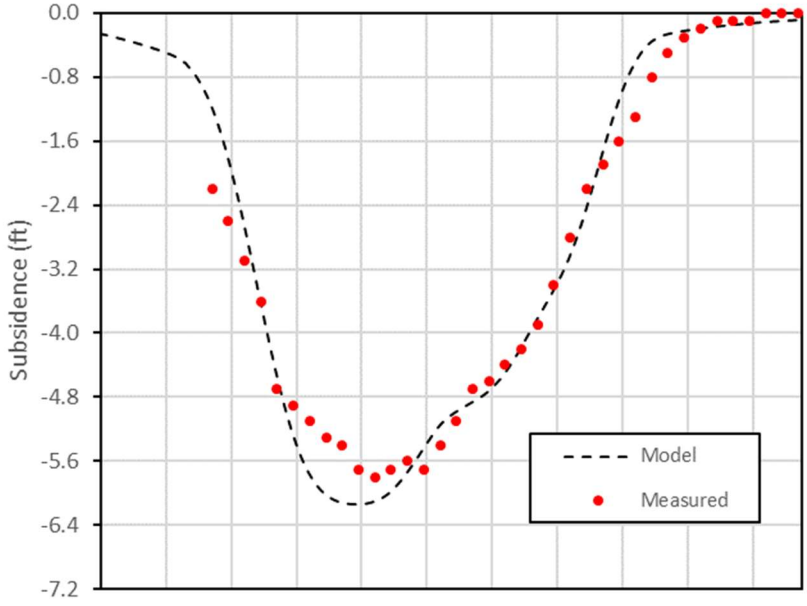

Figure A39. Comparison of model calculated and field measured surface subsidence for Mine W2

Figure A40 shows the abutment stress distribution approximated by the FVM model. The stress measurement in Mine W2 not available.

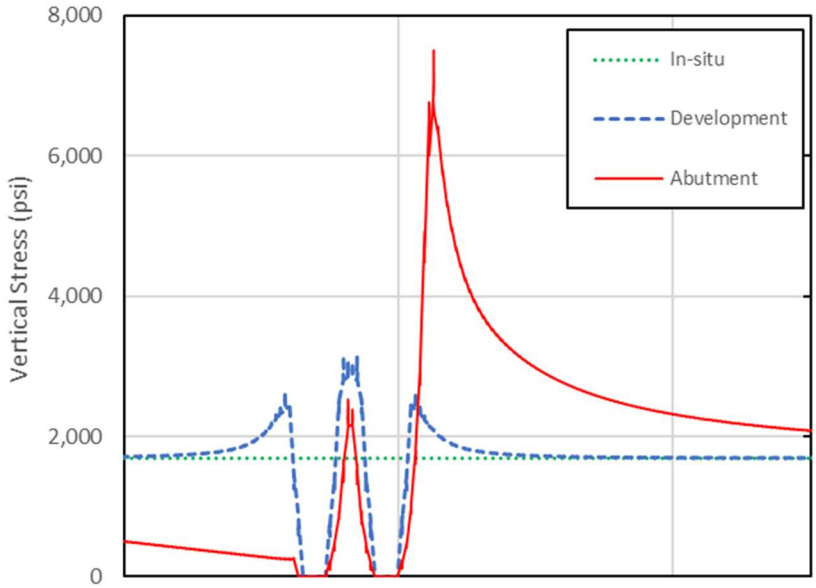

Figure A40. Comparison of the modeled and measured stresses in the abutment pillars for Mine W2

Mine W3 (left) (Figure A41) is a deep mine with average overburden depth of 1487 ft and panel width of 788 ft. To simulate the subsidence and mining induced stress distribution, cross-section AA' was approximated with the FVM model geometry shown in Figure A41, and total of 70 layers are modeled including the seam level and the bottom filler layers, resulting in 759,607 total number of elements. Five mining steps were simulated for Mine W3 (left); development, Panel-9west mining, Panel-10west mining, Panel-11west mining and Panel-12west mining.

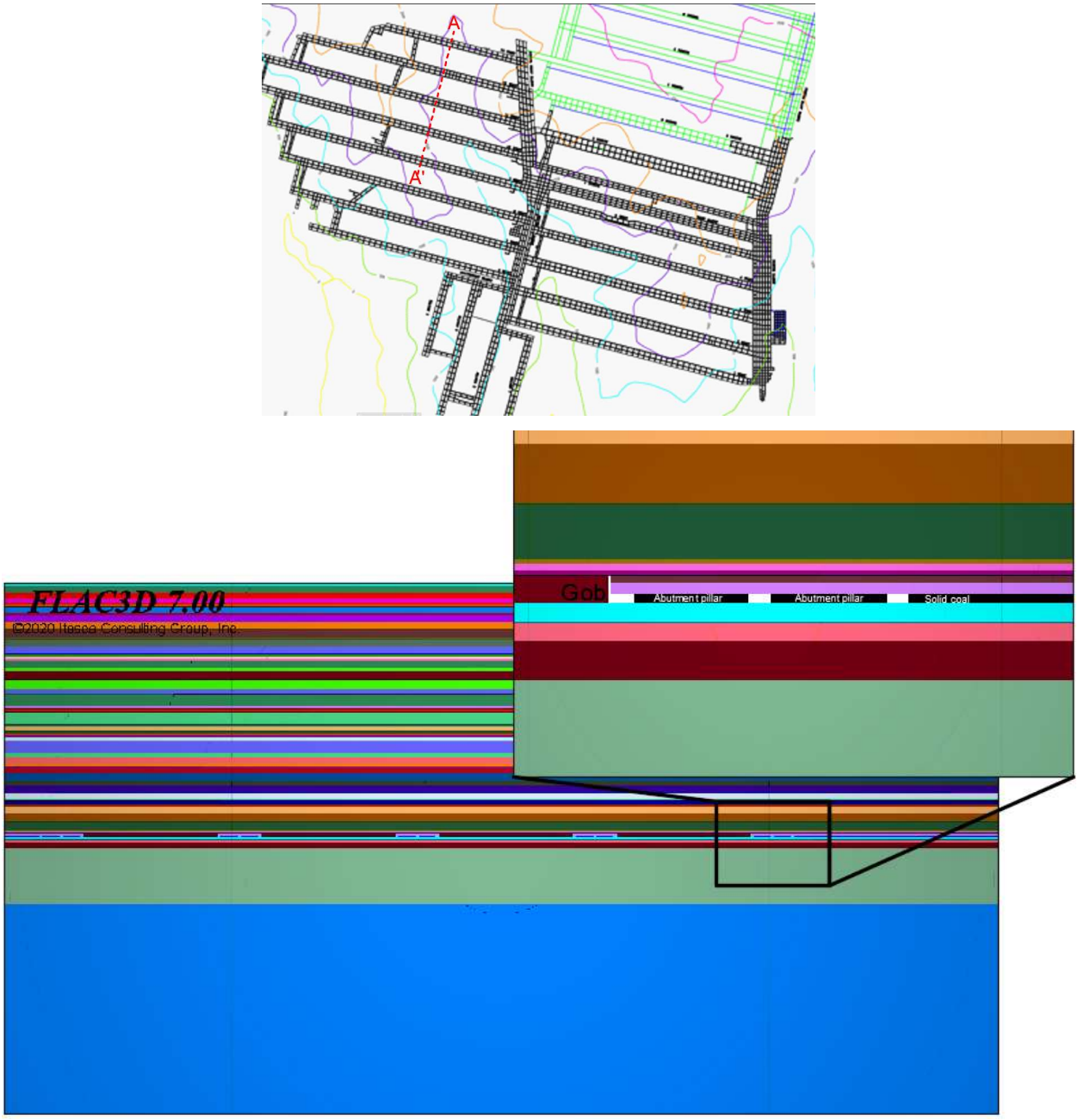

Figure A41. FVM model geometry for Mine W3 (left)

FVM Model Results and Verification with Field Monitoring: After, each case study mine model was solved, stresses and displacements computed by the model were queried. Figure A42 shows the surface subsidence approximated

by the model for the Mine W3 (left). The model approximated maximum subsidence of mine is 2.35ft. The surface subsidence measurement is not available in Mine W3 (left).

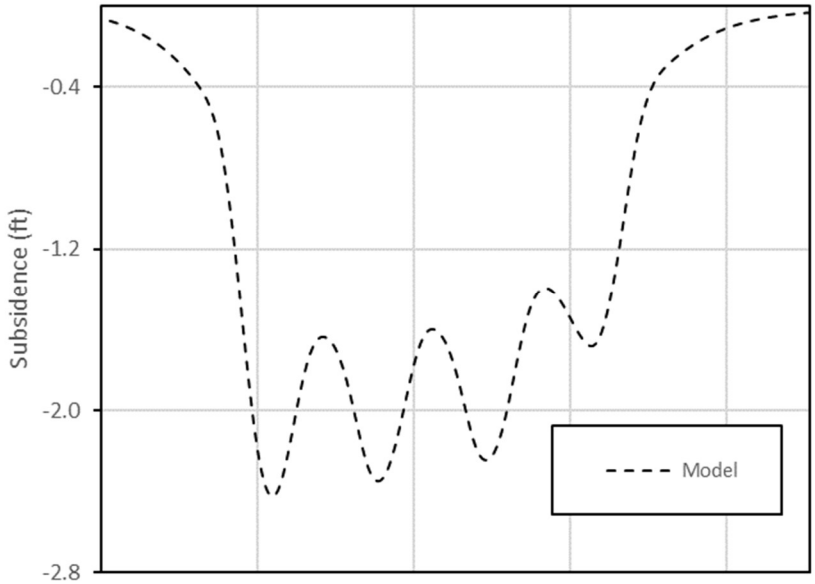

Figure A42. Comparison of model calculated and field measured surface subsidence for Mine W3(left)

Figure A43 shows the abutment stress distribution approximated by the FVM model and measured by the Borehole Pressure Cells (BPC) for case study mine W3 (Left). Although there are inconsistencies between the measured and modeled stresses, the general trend is similar and within reasonable accuracy. Some of the variations could be accounted for the installation of the instrumentation, local coal composition/strength and calibration errors.

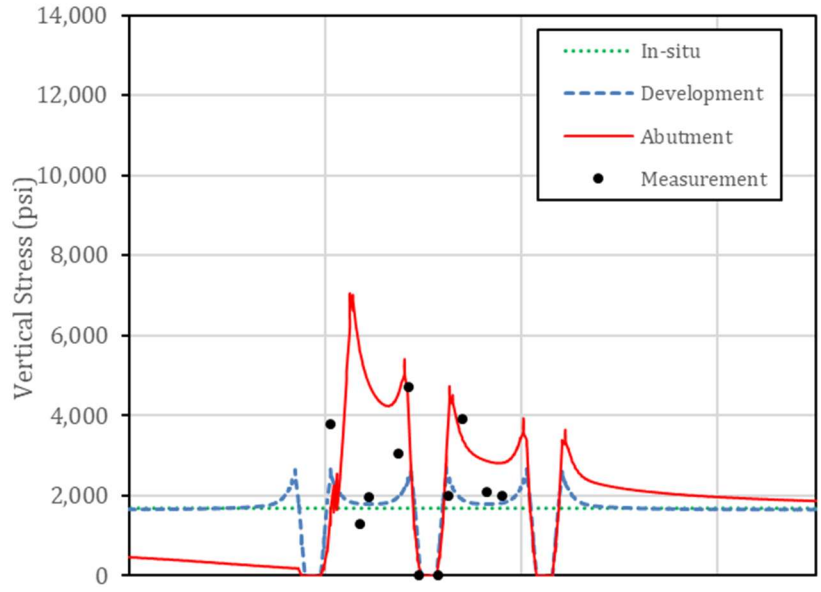

Figure A43. Comparison of the modeled and measured stresses in the abutment pillars for Mine W3 (left)

Mine W3 (right) (Figure A44) is a deep mine with average overburden depth of 1978 ft and panel width of 834 ft. To simulate the subsidence and mining induced stress distribution, cross-section AA' was approximated with the FVM model geometry shown in Figure A44, and total of 89 layers are modeled including the seam level and the bottom filler layers, resulting in 941,625 total number of elements. Five mining steps were simulated for Mine W3 (right); development, Panel-1north mining, Panel-2north mining, Panel-3north mining and Panel-4north mining.

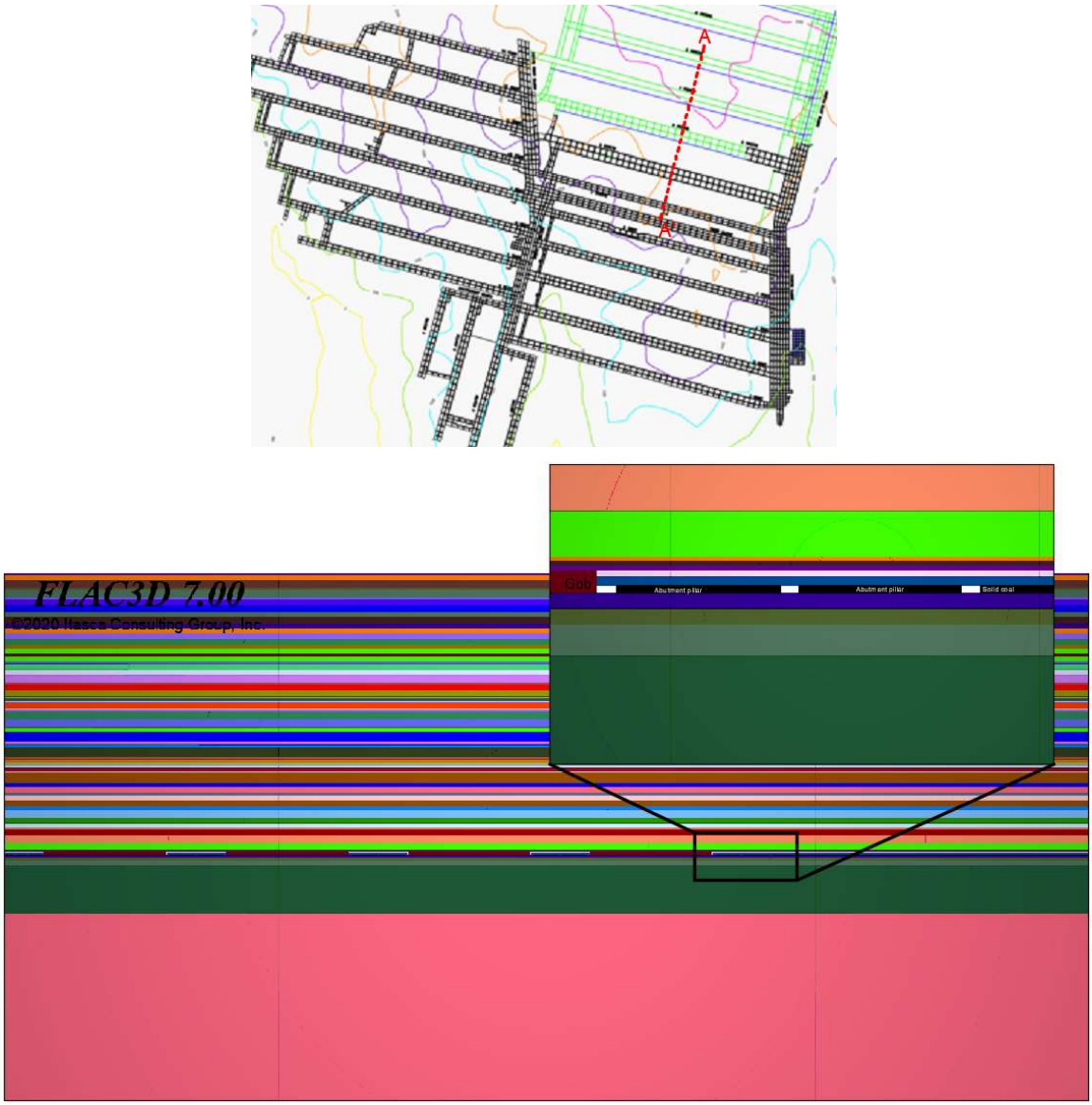

Figure A44. FVM model geometry for Mine W3 (right)

FVM Model Results and Verification with Field Monitoring: After, each case study mine model was solved, stresses and displacements computed by the model were queried. Figure A45 shows the surface subsidence approximated by the model for the Mine W3 (right). The model approximated maximum subsidence of mine is 2.16ft. The surface subsidence measurement is not available in Mine W3 (right).

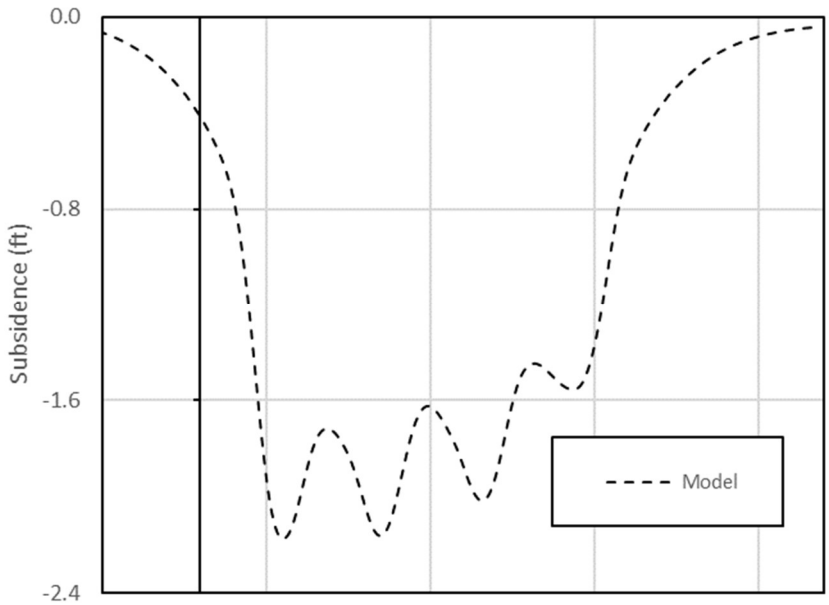

Figure A45. Comparison of model calculated and field measured surface subsidence for Mine W3(right)

Figure A46 shows the abutment stress distribution approximated by the FVM model and measured by the Borehole Pressure Cells (BPC) for case study mine W3 (Right). Although there are inconsistencies between the measured and modeled stresses, the general trend is similar and within reasonable accuracy. Some of the variations could be accounted for the installation of the instrumentation, local coal composition/strength and calibration errors.

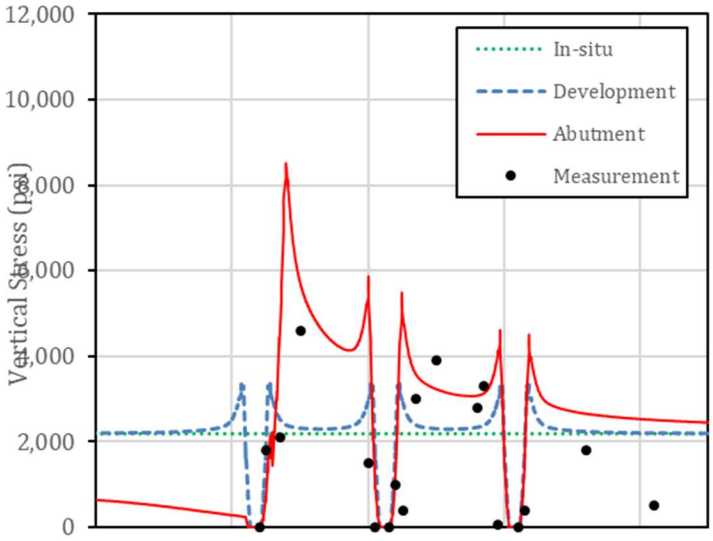

Figure A46. Comparison of the modeled and measured stresses in the abutment pillars for Mine W3 (right)